

HIGGS BOSON PRODUCTION IN
HADRON-HADRON COLLIDERS

By

Christopher James Glosser

A DISSERTATION

Submitted to
Michigan State University
in partial fulfillment of the requirements
for the degree of

DOCTOR OF PHILOSOPHY

Department of Physics and Astronomy

2001

ABSTRACT

HIGGS BOSON PRODUCTION IN HADRON-HADRON COLLIDERS

By

Christopher James Glosser

The Higgs boson is the last remaining component of the Standard Model of Particle Physics to be discovered. Within the context of the Standard Model, the Higgs boson is responsible for the breaking of the $SU_L(2) \times U(1)$ gauge symmetry and provides a mechanism for the generation of the masses of the corresponding gauge bosons, the W^\pm and the Z . In addition, this same mechanism provides masses for the leptons and quarks via Yukawa couplings. Therefore, the discovery and subsequent study of the Higgs boson and its properties is of the highest priority in particle physics today.

The dominant production mechanism for Higgs bosons in hadron-hadron colliders is via gluon-gluon fusion, in which gluons fuse via a virtual top quark to produce a Higgs. At the Large Hadron Collider, which has a center of mass of approximately 14 TeV, one expects 4000-40000 of these particles to be produced via this process in one year of running. At leading order in Quantum Chromodynamics (QCD), the process $gg \rightarrow H$ produces a Higgs with no momentum component transverse to the beam axis. Higgs bosons of non-trivial transverse momentum may be produced if the Higgs recoils against one or more emitted partons.

In this work we seek to compute precisely the rate at which these Higgs particles are produced as a function of the transverse momentum and the rapidity at the Large Hadron Collider. This calculation is carried out to next leading order in the QCD strong coupling α_s . In particular, this calculation includes the dominant

gluon-initiated mechanism, which is responsible for the majority of the cross section. We work in the infinite top mass approximation, and argue that this is very precise in the domain of applicability.

We find an increase in the cross section by a factor of 1.9 - 2.0 in the intermediate transverse momentum range, where this theory applies. We also find that the renormalization scale dependence is much reduced in our calculation as compared to the leading order prediction.

I would like to dedicate this work my parents, Natalie Miller and Donn Miller, and to my friend Kelly R. Carmichael, for their unending support and encouragement.

I would like to dedicate this work to the memory of James W. Glosser, who instilled a love and passion for science in his son, and hence made this work possible.

ACKNOWLEDGMENTS

I would like to acknowledge the following people. Carl R. Schmidt, for his useful advice and guidance, Tim Tait for his interesting topical discussions, Tom Rockwell and Jim Amundson for their endless patience with me in computer matters, Wu-Ki Tung, Chien-Peng Yuan, Csaba Balazs, Pavel Nadolsky, Hung-Jian He for their physics input, and finally, Jim Linnemann for his mentorship.

Contents

List of Tables	x
List of Figures	xii
1 Introduction: The Standard Model of Particle Physics	1
1.1 Yang-Mills Gauge Theory	2
1.2 The Standard Model	7
1.2.1 Spin 1 Gauge Bosons	7
1.2.2 Spin 1/2 Fermions	8
1.3 Electroweak Symmetry Breaking	10
1.3.1 The Higgs Boson	12
1.3.2 The Masses of the W and Z Bosons	13
1.3.3 Fermion Masses and the CKM Matrix	14
2 The Higgs Boson: Phenomenological Overview	18
2.1 Vacuum Stability and Triviality	19
2.2 Electroweak Precision Data and the Rho Parameter	20
2.3 Phenomenology at Colliders	21

2.3.1	Width and Branching ratios	21
2.3.2	Cross Sections	23
3	Perturbation Theory	26
3.1	Divergences and Regularization Schemes	27
3.1.1	Divergences	27
3.1.2	Historical Regularization Schemes	28
3.1.3	Dimensional Regularization	28
3.2	Renormalization	31
3.2.1	Modified Minimal Subtraction	32
3.3	Quantum Chromodynamics	33
3.3.1	The Naive Parton Model	33
3.3.2	Perturbative Quantum Chromodynamics: Improved Parton Dynamics	35
3.4	Helicity Amplitudes and Color Ordering	39
4	The Higgs Boson Cross Section and Transverse Momentum Spectrum: Leading Order Calculation	41
4.1	The Gluon Fusion Cross Section	42
4.2	Low Energy Effective Lagrangian	46
4.3	The Leading Order p_{\perp} spectrum in the large m_{top} limit	48
4.3.1	Kinematics and Notation	49
4.3.2	Analytic Procedure	50

4.3.3	Numerical Procedure and Results	52
5	The Higgs Boson Transverse Momentum Spectrum: Gluonic Radiative Corrections	56
5.1	Notational Conventions	58
5.2	Cross Section at NLO	60
5.3	Angular Integration of Real Emission Piece	61
5.3.1	$gg \rightarrow Hgg$	62
5.4	Extraction of Soft Divergences and Collinear Renormalization	68
5.5	Virtual Contribution	70
5.6	Cancellation of Soft Singularities and Renormalization of Ultraviolet Singularities	71
5.7	Numerical Procedure and Results	72
5.7.1	p_{\perp} Spectrum and the K Factor	73
5.7.2	Rapidity Spectrum	77
5.7.3	Small p_{\perp} Behavior	78
6	Conclusions	81
A	Matrix Elements	83
A.1	Helicity Amplitudes	84
A.2	Real Contributions	85
A.2.1	$H \rightarrow ggg$	86
A.2.2	$H \rightarrow gggg$	87

A.3	Virtual	88
A.3.1	$H \rightarrow ggg$	88
B	Formulas for Angular Integration	90
B.1	General Expression for terms of the form $\frac{1}{S_{13}^m S_{23}^m}$	90
B.2	Expressions for terms of the form $\frac{1}{S_{13}^n S_{123}^m}$	92
C	Results of Angular Integration	95
C.1	Expression for Regular Pieces of $H \rightarrow gggg$ Matrix element	95
C.1.1	$m(1^-, 2^+, 3^+, 4^+)$	97
C.1.2	$m(3^-, 4^+, 1^+, 2^+)$	99
C.1.3	$m(1^-, 3^+, 2^+, 4^+)$	101
C.1.4	$m(3^-, 2^+, 4^+, 1^+)$	102
D	Formulas for Cross Sections	104
D.1	Expression for a $2 \rightarrow 2$ Cross Section	104
D.2	Evaluating the Convolutions	105
D.2.1	Evaluating Terms With “+” Functions	107
	References	107

List of Tables

1.1	Gauge Boson Properties	7
1.2	Fermion Properties	8
1.3	Fermion Quantum Numbers	10

List of Figures

2.1	Higgs Width vs Mass	21
2.2	Higgs Branching Ratios	23
2.3	Higgs production rates at the LHC	25
4.1	Feynman Diagram for Higgs Production through Gluon Fusion	43
4.2	Comparison of the infinite quark mass approximation with the $m_{\text{top}} = 174$ GeV calculation.	44
4.3	Feynman diagrams for Higgs production in the large m_{\perp} limit.	50
4.4	Comparison of the exact leading-order p_{\perp} spectrum with the effective theory calculation.	53
4.5	The Higgs p_{\perp} spectrum at leading order	54
5.1	Variation of the p_{\perp} spectrum with scale	74
5.2	Scale dependence at $p_{\perp} = 50\text{GeV}$	75
5.3	K factor at the LHC ($\sqrt{S} = 14 \text{ TeV}$)	76
5.4	NLO Higgs p_{\perp} spectrum at the LHC ($\sqrt{S} = 14 \text{ TeV}$) for various values of the Higgs rapidity, y_H	77

5.5	Rapidity Spectrum at the LHC ($\sqrt{S} = 14$ TeV). The dotted lines are the leading order calc, and the solid lines are the NLO calc.	78
5.6	Rapidity dependence of the K factor ($\sqrt{S} = 14$ TeV)	79
5.7	Small p_{\perp} dependence of the cross section, $y_H = 0$	80

Chapter 1

Introduction: The Standard Model of Particle Physics

The Standard Model (SM) of Particle Physics is the most stringently tested theoretical description of the world in which we live. It has succeeded in describing all subatomic phenomenology seen to date, to an incredible degree of accuracy [1]. However, even with all of the successes of the SM, a number of theoretical questions remain. Of these the most crucial is the mechanism in which the electroweak symmetry is broken. Over the past twenty years or so, a number of different methods have been proposed to generate this symmetry breaking. All models using a perturbative approach to this symmetry breaking require at least one additional scalar electroweak isospin doublet. The phenomenological manifestation of this scalar is generically dubbed a “Higgs boson.”

In order to understand why such a field is necessary, a pedagogical review of the Standard Model and its gauge theory is beneficial. From this discussion, we will come to understand the role of the Higgs field in maintaining gauge invariance, as well as understanding some of the theoretical problems that a lone Higgs doublet generates.

It is crucial to understand the experimental signatures of the Higgs with the next generation of high energy experiments. As the current phenomenological understanding of the Higgs is plagued with large theoretical uncertainties, new calculations are required to improve the present predictions. With the discovery of the Higgs and a detailed theoretical and experimental description of its properties, we will gain our first insight into the question of electroweak symmetry breaking.

1.1 Yang-Mills Gauge Theory

The entire dynamics of the SM is the result of a particular manifestation of *Yang Mills gauge theory* [2], which was inspired by General Relativity. In Yang-Mills gauge theory, we note that measurable quantities are proportional to the absolute square of a complex field, and thus the general theory should be invariant under a general phase transformation. That is, we may demand that the fermion field $\Psi(x_\mu)$ be invariant under the transformation

$$\Psi(x_\mu) \rightarrow \exp(i\alpha)\Psi(x_\mu). \quad (1.1)$$

Since from quantum mechanics, we know that all observables are computed from expectation values of some differential operator, it is quite trivial to see that these observables will remain unchanged under this phase rotation. This invariance is known as a *global gauge symmetry*.

Now, we may require that the theory be invariant under a *local gauge symmetry*, in which the phase parameter is a function of the space time co-ordinates x_μ , by making the replacement

$$\alpha \rightarrow \alpha(x_\mu). \quad (1.2)$$

A typical fermion Lagrangian is of the form

$$L_F = \bar{\Psi}(x_\mu)(i\cancel{\partial} - m)\Psi(x_\mu). \quad (1.3)$$

It is quite trivial to see that the Lagrangian is not invariant under such a transformation, since the derivative in the kinetic energy may act directly on the $\alpha(x_\mu)$. However, if we replace the derivative with

$$D_\mu = \partial_\mu + igA_\mu(x) \quad (1.4)$$

and demand that the field A_μ transform as

$$A_\mu(x) \rightarrow A_\mu(x) + \frac{1}{g}\partial_\mu(\alpha(x_\mu)), \quad (1.5)$$

we see that the latter term cancels the anomalous term resulting from the differentiation of the phase. The phase parameter $\alpha(x)$ is, in this case, a scalar function of the space-time variables. This is known as an *abelian gauge symmetry*.

Now, we wish to know what will happen if we give the fermion field some gauge index, i , and demand that it transform under a local gauge symmetry

$$\Psi_i(x) \rightarrow [\exp(i\alpha^a(x_\mu)T^a)]_{ij} \Psi_j(x), \quad (1.6)$$

where we imagine that $\Psi_i(x)$ transforms under some gauge group G . The matrices T^a are the gauge group generators of some representation of the gauge group G . This is an example what is commonly called a *non-abelian gauge transformation*. Again, it is trivial to see that kinetic terms in the Lagrangian will be spoiled by this transformation. One then notes that the kinetic terms may be rescued, provided that

the conventional kinetic term $i\partial_\mu$ is replaced with the so-called *covariant derivative*,

$$[D_\mu]_{ij} = \partial_\mu \delta_{ij} + igT_{ij}^a A_\mu^a(x). \quad (1.7)$$

This expression is completely analogous to equation (1.4). The *gauge field* $A_\mu^a(x)$ is required to transform under the gauge transformation as

$$T_{ij}^a A_\mu^a(x) \rightarrow [e^{i\alpha^b(x_\mu)T^b}]_{ik} \left\{ T_{kl}^a A_\mu^a(x) - \frac{1}{ig} \partial_\mu \delta_{kl} \right\} [e^{i\alpha^c(x_\mu)T^c}]_{lj}^\dagger \quad (1.8)$$

in order to cancel the term coming from the differentiation of the phase in the kinetic term. After making the replacement $\partial \rightarrow D$, we find that the covariant fermion Lagrangian for a non-abelian gauge theory,

$$L_{GF} = \bar{\Psi}(x_\mu)(i\not{D} - m)\Psi(x_\mu), \quad (1.9)$$

is completely invariant under the transformation (1.6).

In order to have nontrivial dynamics, kinetic terms for the gauge fields must be introduced. These kinetic terms must satisfy the following properties:

- They must be gauge invariant.
- The resultant quantum theory must be renormalizable.¹
- There must be one term which is quadratic in ∂_μ .

All of these constraints are satisfied by the tensor $F_{\mu\nu}^a$, where

$$T^a F_{\mu\nu}^a = \frac{1}{ig} [D_\mu, D_\nu] \quad (1.10)$$

¹ It is possible to construct models with “higher dimension operators” which are not renormalizable in the conventional sense. The divergent loop terms are then cut off at some arbitrary scale at which new physics comes into play. These theories are beyond the scope of the discussion, however, as they do not play a role in conventional Standard Model dynamics.

$$= T^a \{ \partial_\mu A_\nu^a - \partial_\nu A_\mu^a - g f^{abc} A_\nu^b A_\mu^c \}, \quad (1.11)$$

which allows us to write down a kinetic term for the gauge fields,

$$L_{GF} = -\frac{1}{4} \text{Tr}[F_{\mu\nu} F^{\mu\nu}]. \quad (1.12)$$

Note that a general gauge field is self-interacting because of the self-coupling term proportional to f_{abc} in the tensor $F_{\mu\nu}^a$.²

So far, everything is completely consistent, although we have been considering only the classical limit of the theory. If we wish to consider a Quantum Field Theory, in which the fields themselves consist of discrete numbers of excitations, we must be more careful in order to ensure that the unitarity of the S-matrix is not violated. There are two different procedures for quantizing a field theory, the *canonical* approach and the *path integral*³ approach. After naive quantization of the theory, one finds that quantum corrections apparently spoil the unitarity of the S-matrix, for particular gauge choices. In order to compensate, one then adds ghost fields (scalar fields that obey fermion statistics) to cancel the non-unitary terms in the Lagrangian.

While this may seem ad-hoc, the ghost terms may be derived using an explicit gauge fixing constraint in the path integral in what is known as Fadeev-Popov gauge fixing, in which the ghost terms are generated spontaneously when the gauge in the path integral is fixed [4]. Consider the path integral for a non-abelian field A_μ^a ,

$$\int \mathcal{D}A \exp [iS[A]] = \int \mathcal{D}A \exp \left[-\frac{i}{4} \int d^4x \left((G_{\mu\nu}^a)^2 \right) \right]. \quad (1.13)$$

This path integral infinitely overcounts the field configurations, since it sums over

² It should also be noted that a CP violating term $-\frac{1}{4} \text{Tr}[\epsilon_{\mu\nu\rho\sigma} F_{\rho\sigma} F_{\mu\nu}]$ is also consistent with the listed conditions. Again, this is beyond the scope of the discussion

³For an introduction to the path integral, a field theory text such as reference [3] is useful.

the gauge “copies” that represent the same physics. To remove this overcounting, we must establish a gauge choice by constraining the field A through some functional relationship $F[A] = 0$. This is known as fixing the gauge. As an example, the familiar Lorentz gauge is fixed through the constraint $F[A] = \partial_\mu A^{a\mu} = 0$.

To fix our choice of gauge, we begin by inserting an expression for 1 into the path integral,

$$1 = \int \mathcal{D}\alpha \delta(F[A_\alpha]) \text{Det} \left[\frac{\partial F[A_\alpha]}{\partial \alpha} \right], \quad (1.14)$$

where

$$A_\alpha^{a\mu} = A^{a\mu} + \frac{1}{g} D_\mu \alpha^a. \quad (1.15)$$

We may freely change variables in the path integral from $A \rightarrow A_\alpha$. Since the integration measure $\mathcal{D}A$ and the action $S[A]$ are gauge invariant, everything in the path integral now is a function of A_α and therefore we may, without loss of generality, remove the label α . The resulting expression is

$$\int \mathcal{D}A \exp[iS[A]] = \left(\int \mathcal{D}\alpha \right) \int \mathcal{D}A \exp[iS[A]] \delta(F[A]) \text{Det} \left[\frac{\partial F[A]}{\partial \alpha} \right], \quad (1.16)$$

where the term $\int \mathcal{D}\alpha$ contributes an infinite overall constant to the normalization.

The factor $\text{Det} [\partial F[A]/\partial \alpha]$ can be evaluated by introducing the ghost field. It is instructive to work this out explicitly for the Lorentz gauge. Since the gauge field varies infinitesimally as $(A^\alpha)_\mu^a - (A^0)_\mu^a \approx \frac{1}{g} D_\mu \alpha^a$, the determinant may be rewritten;

$$\text{Det} \left[\frac{\partial F[A_\alpha]}{\partial \alpha} \right] = \text{Det} \left[\frac{1}{g} \partial^\mu D_\mu \right] \quad (1.17)$$

$$= \int \mathcal{D}c \int \mathcal{D}\bar{c} \exp \left[i \int d^4x \bar{c} (-\partial^\mu D_\mu) c \right], \quad (1.18)$$

where the c is an anti-commuting scalar field⁴, and therefore a ghost. We have thus

⁴Anticommuting fields become *Grassman variables* in the path integral representation.

Boson	Symbol	Mass(GeV)	Charge	Color	Isospin
gluon	g	0	0	Adjoint	No
photon	γ	0	0	No	No
W	W_{\pm}	80.41	$\pm e$	No	Yes
Z	Z	91.187	0	No	Yes

Table 1.1: Gauge Bosons

generated the Fadeev-Popov ghost term as a result of rigorously fixing the gauge. The c fields are indeed ghosts, and have no asymptotic states. They do, however, contribute as closed loops in diagrams. Moreover, the infinite gauge repetitions have been systematically eliminated in the path integral, and the gauge has been fixed.

1.2 The Standard Model

The Standard Model is, in essence, a Yang-Mills gauge theory, consisting of three “copies” of fermions, called flavors, interacting with a set of gauge bosons dictated by the direct product of groups $\mathbf{G} = \mathbf{SU}_C(3) \times \mathbf{SU}_I(2) \times \mathbf{U}_Y(1)$. As was seen before, for each of these symmetries we may associate a dynamical gauge field. Therefore, there is a gluon field G_{μ}^a that interacts with the SU(3) “color” quantum number, A Weak Boson field W_{μ}^i that interacts with the isospin quantum number (I), and an abelian field B_{μ} that interacts with the Hypercharge (Y).

1.2.1 Spin 1 Gauge Bosons

Since the Electroweak symmetry is broken, we will observe admixtures of its fields, W_{μ}^i and B^{μ} , in nature. The 4 fields combine into two electric charge eigenstates, W_{\pm} , a massive chargeless boson, the Z , and a massless chargeless boson, the photon γ . A list of the general properties of these particles may be found in Table 1.1

Fermion	Symbol	Mass(GeV)	Charge	Color
electron	e	.000511	$-1e$	Singlet
muon	μ	.106	$-1e$	Singlet
tau	τ	1.78	$-1e$	Singlet
electron neutrino	ν_e	$< 15 \times 10^{-9}$	0	Singlet
muon neutrino	ν_μ	$< .00017$	0	Singlet
tau neutrino	ν_τ	$< .0182$	0	Singlet
up	u	.001 to .005	$\frac{2}{3}e$	Triplet
charm	c	1.15 to 1.35	$\frac{2}{3}e$	Triplet
top	t	175	$\frac{2}{3}e$	Triplet
down	d	.003 to .009	$-\frac{1}{3}e$	Triplet
strange	s	.075 to .170	$-\frac{1}{3}e$	Triplet
bottom	b	4.0 to 4.4	$-\frac{1}{3}e$	Triplet

Table 1.2: Standard Model Fermions

1.2.2 Spin 1/2 Fermions

There are three different generations of fermions. The first generation consists of the electron, the electron neutrino, the up quark and the down quark. The second consists of the muon, the muon neutrino, the charm quark, and the strange quark. The third generation consists of the tau, the tau neutrino, the top quark and the bottom quark.

The particles of different generations may be grouped into subsets of particles which are indistinguishable, save their masses and Yukawa couplings (with the Higgs). These are known as *families*. For instance, an electron, muon and tau have exactly the same isospin and charge characteristics, and hence belong to the same family. Table 1.2 organizes the various known fermions by their family⁵.

Since the left and right handed components couple differently to the electroweak sector of the theory, it is beneficial to list the separate components and their

⁵The masses in Table 2 were obtained from reference [1]. The quark masses are the so-called “current-quark masses.”

transformation properties in a separate table. The lepton doublets contain a left handed, -1 charge piece, which is “isospin down” (this refers to the eigenvalues of the σ_3 matrix), and a charge zero component that has “isospin up”, to be identified with the e, μ, τ (former) and their respective neutrinos (latter). We then arrange the components into isospin doublets,

$$L_L = \begin{pmatrix} (\nu_e)_L \\ e_L \end{pmatrix}, \quad (1.19)$$

with identical expressions for the remaining two families. The Hypercharge (Y) may be computed directly from the charges and the isospin eigenvalue, using the formula $Q = I + \frac{Y}{2}$ (the charge here is in units of e). We find that the left-handed $e, \mu, \tau, \nu_e, \nu_\mu,$ and ν_τ have a hypercharge of -1, while the right-handed $e, \mu,$ and τ have a hypercharge of -2.

We also arrange the left-handed quarks into an isospin doublet

$$Q_L = \begin{pmatrix} u_L \\ d_L \end{pmatrix}. \quad (1.20)$$

The left-handed quarks transform just as the left-handed leptons do under $\mathbf{SU}_I(2)$, and have a hypercharge $Y = \frac{1}{3}$. This, of course, implies that both components have nontrivial interactions with the electromagnetic field. The right-hand components of the up and down type components have hypercharges of $\frac{4}{3}$ and $-\frac{2}{3}$ respectively. Again, these may be computed directly from the charge formula, $Q = I + \frac{Y}{2}$.

All quark species transform as triplets in the fundamental representation of the $\mathbf{SU}_C(3)$ color force, while all leptons transform as singlets, and thus do not interact strongly. That is, each of the quark components may be written as a three component

Fermion	Q	I	Y	Color
L_L	$(-1,0)$	Doublet	-1	Singlet
Q_L	$(+2/3,-1/3)$	Doublet	1/3	Triplet
u_R	$+2/3$	Singlet	4/3	Triplet
d_R	$-1/3$	Singlet	-2/3	Triplet
l_R	-1	Singlet	-2	Singlet

Table 1.3: Fermion Quantum Numbers

spinor,

$$Q = \begin{pmatrix} Q_r \\ Q_g \\ Q_b \end{pmatrix}, \quad (1.21)$$

where Q may be any of the quark fields, Q_l , u_r or d_r . The leptons do not couple to the color sector and hence are all singlets under $\mathbf{SU}_C(3)$. The quantum numbers of the standard model particles are conveniently summarized in Table 1.3.

One may notice that, in dividing terms up into left and right-handed states, and by demanding that these states transform differently under the various gauge groups, that terms which mix the left and right handed terms are expressly forbidden. Since mass terms do exactly this, they are forbidden in (Unbroken) Electroweak gauge theory. Thus we must break the Electroweak gauge symmetry somehow in order to have a realistic model of the Standard Model Particles.

1.3 Electroweak Symmetry Breaking

The most glaring problem with the current particle physics phenomenology is the existence of massive particles. Electroweak gauge invariance forbids hard mass terms of the form $\mu^2 B^2$, which is obviously not invariant under a gauge transformation $B \rightarrow B + \partial A$. Also, the left and right-handed fermions, which transform differently

under $SU_I(2)$ and $U_Y(1)$, seem to preclude the existence of any mass terms for the fermions, since mass terms mix the right and left-handed components, once again spoiling gauge invariance.

We wish to introduce these terms in a gauge invariant way. The first clue is that we must somehow include three additional degrees of freedom, one for each additional spin state of the three massive bosons. This seems to indicate that another field is necessary to compensate for the additional degrees of freedom.

The general way to break the electroweak symmetry is through *spontaneous symmetry breaking*. To spontaneously break a symmetry, one introduces a field with a vacuum state which is not invariant under the symmetry in question. One then expands the field around this vacuum. Since the kinetic energy terms in the Lagrangian of this field will, in general, contain covariant derivatives (which in turn contain couplings to the fields W,Z), expanding the field around its *vacuum expectation value* (VEV), will introduce mass terms for the gauge bosons.

If we also allow the field to interact with fermions via a fermion-antifermion-scalar interaction known as a *Yukawa coupling*, we find that we have also spontaneously generated masses for the fermions. The mass of this field which we have introduced can be arbitrary (at least at tree level) in the SM. We therefore have a theoretical answer to all inconsistencies in the Standard Model.

A scalar field which has these properties is generically dubbed a *Higgs field*. In the SM, the Higgs is a complex isospin doublet, so that it transforms under both the hypercharge and isospin rotations. Since this introduces four degrees of freedom, there is one left over degree of freedom after the Electroweak symmetry is broken. The phenomenological consequence of this is the existence of a massive, chargeless scalar called the *Higgs Boson*.

One final caveat concerns the quark masses. The quark masses are not as well

defined as those of the other fermions, and so they must be treated with some care. Masses in a quantum field theory are basically due to the self coupling of the field. These, like other couplings in the theory are affected by the renormalization process. Since most masses in the SM are measurable parameters (that is, not predefined by the theory), particle masses are generally empirically defined as being the masses in the absence of other forces. The problem is of course that the quarks are confined inside hadrons and mesons, and thus are never “free particles” in the classic sense. For a quark, this limit never exists, so the idea of a “rest mass” is poorly defined. Quarks that have large Yukawa couplings to the Higgs may still have a rest mass defined, as long as it is larger than the strong coupling scale, Λ_{QCD} .

1.3.1 The Higgs Boson

To begin our discussion of the Higgs field, we write down the conventional Lagrangian for a standard model Higgs boson. It is

$$L_H = (D_\mu \Phi)^\dagger (D^\mu \Phi) - \lambda \left(|\Phi|^2 - \frac{v^2}{2} \right)^2, \quad (1.22)$$

where Φ is complex scalar isospin doublet, and thus has hypercharge +1. The covariant derivative in this case is

$$[D_\mu]_{ij} = \partial_\mu \delta_{ij} + \frac{ig_2}{2} \sigma_{ij}^i W_\mu^i(x) + \frac{ig_1}{2} \delta_{ij} B_\mu^a(x), \quad (1.23)$$

where we include both the isospin field W_μ^i as well as the hypercharge field B_μ . Now, we parameterize the isoscalar doublet as

$$\Phi = \frac{1}{\sqrt{2}} \begin{pmatrix} \phi_1 + i\phi_2 \\ v + \phi_3 + i\phi_4 \end{pmatrix}; \quad (1.24)$$

or, writing this as a gauge rotation,

$$\Phi = \exp(-i\frac{\sigma_i}{2}\theta_i(x)) \begin{pmatrix} 0 \\ \frac{v+H(x)}{\sqrt{2}} \end{pmatrix}. \quad (1.25)$$

The dynamical field $H(x)$ is the Higgs boson field. We see that for a particular gauge choice (commonly called the *unitary gauge*), we may eliminate three degrees of freedom. These degrees of freedom will show up as the necessary third degree of freedom for each of the gauge fields W_μ^i, B_μ , leading to the rather quaint analogy that the gauge fields have “eaten” three of the components of the Higgs doublet, leaving the Higgs boson field as an undiscovered dynamical field.

1.3.2 The Masses of the W and Z Bosons

As a consequence of choosing the field Φ to have a nontrivial vacuum, numerous phenomenological characteristics of the SM emerge from the various couplings of the weak gauge fields with the Higgs field. Moreover, gauge invariant couplings with the quark and lepton fields generate mass terms for these particles as well, without breaking the overall gauge invariance of the theory. We begin by writing the *most general* parameterization for the model. The mass terms for the gauge bosons arise from the following term in the Lagrangian,

$$\frac{1}{4}\Phi^\dagger \left(g_2\sigma_{ij}^i W_\mu^i(x) + g_1\delta_{ij} B_\mu^a(x) \right) \left(g_2\sigma_{jk}^i W_\mu^i(x) + g_1\delta_{jk} B_\mu^a(x) \right) \Phi. \quad (1.26)$$

If we redefine the fields as

$$W_\mu^\pm = \frac{W_\mu^1 \pm iW_\mu^2}{\sqrt{2}}, \quad (1.27)$$

$$g_0 Z_\mu = g_2 W_\mu^3 - g_1 B_\mu, \quad (1.28)$$

$$g_0 A_\mu = g_1 W_\mu^3 + g_2 B_\mu, \quad (1.29)$$

where $g_0 = \sqrt{g_1^2 + g_2^2}$, we find that the following mass term arises:

$$M_W^2 (W_\mu^+ W_\mu^-) + \frac{1}{2} M_Z^2 |Z_\mu|^2. \quad (1.30)$$

whereas the field A_μ is massless. This expression now contains explicit formulas for the gauge boson masses

$$M_W^2 = g_2^2 \left(\frac{v^2}{4}\right), \quad (1.31)$$

$$M_Z^2 = g_0^2 \left(\frac{v^2}{4}\right) = (g_1^2 + g_2^2) \left(\frac{v^2}{4}\right), \quad (1.32)$$

Hence, we identify the fields W_μ^\pm and Z_μ as massive phenomenological gauge particles; whereas the field A_μ maintains a local $U(1)$ symmetry and is identified with the photon field. It is straightforward to derive the expression for the electromagnetic charge $e = \frac{g_1 g_2}{g_0}$ by rewriting the covariant derivative in terms of the field A_μ . It is also customary to define the *Weinberg angle*, $\sin \theta_W \equiv g_2/g_0$.

1.3.3 Fermion Masses and the CKM Matrix

One may also postulate interactions between the Higgs field and the fermions of the standard model. We may write this Yukawa interaction with the fermions:

$$\begin{aligned} L_{Yukawa} &= (y_e^{nm} \bar{e}_R^n \Phi^\dagger L_L^m + (C.C.)) \\ &+ (y_u^{nm} \bar{u}_R^n \Phi^\dagger Q_L^m + (C.C.)) \\ &+ (y_d^{nm} \bar{d}_R^n \tilde{\Phi}^\dagger Q_L^m + (C.C.)), \end{aligned} \quad (1.33)$$

where n and m run over the fermion families. The field $\tilde{\Phi}^\dagger$ is related to the complex conjugate of the Higgs field by

$$\tilde{\Phi} = -i\sigma_y\Phi^*. \quad (1.34)$$

This expression is the most general term that we may write. Note that there is no requirement that the Yukawa matrix y_{nm} be diagonal or real. It will, in general, mix electroweak eigenstates of the fermions. This has the implication that CP symmetry is violated in a general theory with a Higgs.

First, let's consider the leptons. Since the neutrinos are considered to be massless, and have only a left hand component, we may freely redefine the fields such that the mass matrix is diagonal. The three diagonal coefficients of the mass matrices are then interpreted as the masses of the leptons. The diagonal Yukawa matrix elements are then the masses of the three leptons with the factor $v/\sqrt{2}$ scaled out; that is, $m_l = y_l v/\sqrt{2}$. Note that this also implies that the Higgs boson couples to leptons with strength $y_l = \sqrt{2}m_l/v$; that is, the coupling is directly proportional to the lepton mass. This is true of the Higgs coupling to all particles, and is of great importance in phenomenology, as we shall see in the next section.

The up and down mass matrices, due to their additional complexity, may not be simultaneously diagonalized. It is conventional to choose a basis in which the up type quarks are diagonal, and the down type quarks are off-diagonal. One then finds that since the W^\pm terms mix quark mass eigenstates, the W Boson violates “quark family number.”

Let's consider this situation in a little more detail. Since in the Standard Model the only coupling which actually mixes isospin-up and isospin-down fermions is the coupling to W^\pm , we find family mixing terms in the couplings between the fermions and the W boson terms. That is, the W couples to “weak eigenstates”

which differ from mass eigenstates by the rotation matrix, V :

$$\begin{pmatrix} d \\ s \\ b \end{pmatrix}_{Weak} = \begin{pmatrix} V_{ud} & V_{us} & V_{ub} \\ V_{cd} & V_{cs} & V_{cb} \\ V_{td} & V_{ts} & V_{tb} \end{pmatrix} \begin{pmatrix} d \\ s \\ b \end{pmatrix}_{Mass}. \quad (1.35)$$

This is the so called Cabibbo-Kobayashi-Maskawa (CKM) matrix [5]. This matrix has the standard parameterization

$$\begin{pmatrix} c_{12}c_{13} & s_{12}c_{13} & s_{13}e_{13} \\ -s_{12}c_{23} - c_{12}c_{23}s_{13}e_{13} & c_{12}c_{23} - s_{12}s_{23}s_{13}e_{13} & s_{23}c_{13} \\ s_{12}s_{23} - c_{12}c_{23}c_{13}e_{13} & -c_{12}s_{23} - s_{12}c_{23}s_{13}e_{13} & c_{23}c_{13} \end{pmatrix}, \quad (1.36)$$

where $c_{ij} = \cos(\theta_{ij})$, $s_{ij} = \sin(\theta_{ij})$, and $e_{ij} = \exp(-i\delta_{ij})$. In the Standard Model, these angles are not constrained by any symmetry, and must be determined experimentally. It may not be possible to make these same arguments in extended models, and one may consider searching for deviations in the CKM matrix as an indication of physics beyond the SM. See [6] for an excellent discussion of these indicators.

If the neutrino sector of the theory contains a Dirac mass term, we must forego the previous analysis, as one cannot simultaneously diagonalize the electron and neutrino mass matrices unless at least one of the two is completely massless. Recent measurements of neutrino oscillations [7] do seem to suggest that the neutrino species have a mass difference (and therefore, masses), which of course must be accounted for theoretically. One may postulate the existence of an additional right-handed component, which will in general have its own coupling to the Higgs. After diagonalizing the charged leptons, the neutrino components are left with off-diagonal terms. These terms, while extremely important to astrophysics, do not contribute much to conventional high energy physics collider experiments, where the approximation that the

neutrino is massless is certainly viable.

Chapter 2

The Higgs Boson:

Phenomenological Overview

The Higgs boson is currently the only missing component of the Standard Model. Precise knowledge of Higgs physics will most likely give the first glimpses of the underlying structure responsible for electroweak symmetry breaking. Since the couplings of the Higgs to the various particles in the Standard Model are already determined, any deviation from the rates computed using these couplings could be an indication of new physics.

However, in order to examine these rates, we must first find a Higgs and measure its mass. The Higgs mass is not fixed by any theoretical argument in the Standard Model. In fact, a tree-level analysis quickly reveals that there are no constraints whatsoever on the Higgs mass.

At the 1-loop and higher orders, however, constraints do arise on the Higgs mass. A renormalization group analysis reveals that the Higgs mass cannot be too large or too small relative to the Weak scale. The former results in *triviality*, while the latter in *vacuum instability*. The Higgs mass also appears in 1-loop corrections

to $e\bar{e} \rightarrow Z \rightarrow f\bar{f}$, and so by precisely measuring the cross section to this process, we may constrain the Higgs mass indirectly, as was done for the top quark before its discovery in 1995 [8, 9].

2.1 Vacuum Stability and Triviality

We begin our analysis of Higgs phenomenology by considering some theoretical issues concerning the mass of the Higgs. As mentioned before, the classical theory of the Higgs and its couplings to the other Standard Model particles does not in any way restrict the Higgs mass. However, radiative corrections cause the VEV and the quartic coupling to run, and can cause problems if the Higgs mass is too far removed from the other electroweak parameters.

One-loop corrections to the Higgs effective potential lead to vacuum stability constraints. These result from the fact that the asymmetric electroweak-violating vacuum could decay into a symmetric one, therefore destroying the universe as we know it. Typically, these analyses put lower bounds on the Higgs mass which are far less than the current mass bound from LEP.

Triviality arises from the fact that the quartic coupling λ in ϕ^4 theory exhibits a Landau pole [10], and therefore the theory becomes strongly coupled at some high energy scale. To see this, consider the expression for λ running from some energy scale μ_0 to μ ,

$$\lambda(\mu) = \lambda_0 \left(1 + \frac{3\lambda_0}{4\pi} \log \left(\frac{\mu_0}{\mu} \right) \right)^{-1}. \quad (2.1)$$

Since λ_0 is related to the Higgs mass through the VEV (i.e. $m_H^2 = \lambda v^2$), the requirement that the coupling remain finite below some relevant scale puts an upper constraint on the Higgs mass. If the theory is to remain perturbative up to the Planck Scale, then the Higgs mass cannot be more than about 1 TeV.

Since this behavior is essentially nonperturbative, such calculations are best done on the lattice.¹ A recent lattice study [11] has placed an upper bound on the Higgs mass of about 460 GeV, if no new physics arises before then².

2.2 Electroweak Precision Data and the Rho Parameter

The masses, decay widths and cross sections for W and Z also receive corrections from virtual Higgs loops. The result is that the ρ parameter,

$$\rho = \frac{m_W^2}{m_Z^2 \cos^2(\theta_W)}, \quad (2.2)$$

which is 1 at tree level, picks up the following corrections from virtual top and Higgs loops:

$$\rho = 1 + \frac{3e^2}{64\pi^2 \sin^2 \theta_W} \frac{m_t^2}{m_W^2} - \frac{3g^2}{32\pi^2} \tan^2(\theta_W) \log\left(\frac{m_H}{m_W}\right) + \dots \quad (2.3)$$

All of the fermion loop corrections to ρ vary quadratically with their masses, so it is easy to see that the top gives the dominant contribution. Therefore, a precise knowledge of θ_W , m_W , m_Z , and m_t can be used to constrain the Higgs mass.

The major problem with indirectly measuring the Higgs mass is that the corrections to the ρ parameter vary only logarithmically with M_H , rather than quadratically, as do the top corrections. It is hence very difficult to have enough statistics and eliminate enough systematic uncertainty to put a precise constraint on the mass.

As of this writing, the upper limit from the electroweak precision data is 224.8

¹Lattice Gauge Theory is an attempt to formulate quantum field theories numerically by placing them on a discrete space-time lattice, and evaluating the path integral numerically.

²Reference [10] is an excellent introduction to these theoretical issues, including the theoretical issues surrounding the Higgs phenomenon in extended models.

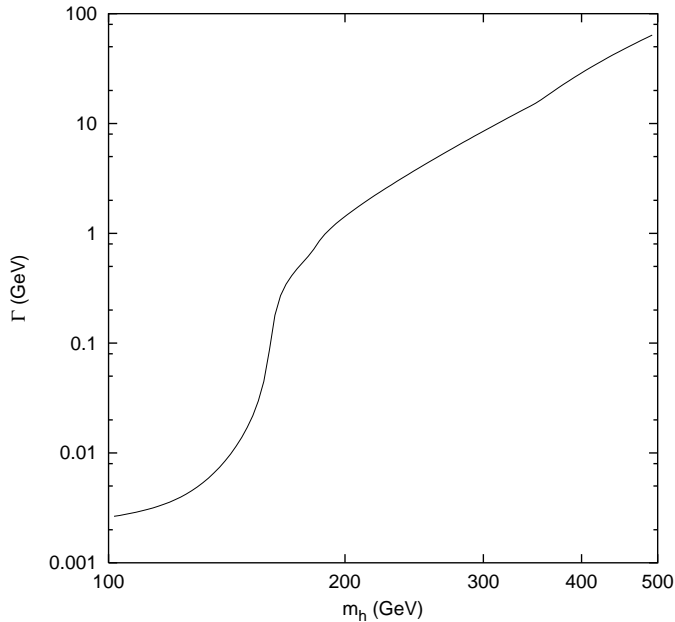


Figure 2.1: Higgs Width vs Mass

GeV. The lower bound on the Higgs mass is most strongly constrained by the direct search at LEP[12]. They find a lower bound of 114.1 GeV at 95% confidence level.

2.3 Phenomenology at Colliders

In order to search for the Higgs in a collider experiment, we must have a precise understanding of how it is produced, and how it decays. This is the main topic of this section.

2.3.1 Width and Branching ratios

A graph of the Higgs width as a function of mass is provided in Figure 2.1³. As can be plainly seen, the width increases dramatically around 160 GeV. This dramatic

³This graph and the branching ratio graph (figure 2.2) were generated using the program HDECAY [13]

increase in the width is due to the fact that the Higgs is now massive enough to decay into weak bosons, with which it has a comparatively strong coupling. Higgs particles that can decay into weak bosons have a collider phenomenology dramatically different than those which cannot decay to weak bosons. The former are referred to in this work as *heavy Higgs*, and the latter *intermediate mass Higgs*.

Looking at the branching ratios for a Higgs in the intermediate mass range (Figure 2.2) , we see why its detection is so problematic. As noted in the last section, the Higgs couples to particles with a coupling strength that is proportional to the particle mass. Therefore, it prefers to decay to the heaviest particles for which it is kinematically allowed. For the intermediate mass Higgs, it decays most of the time into bottom quarks, which are swamped by QCD background events. If one wishes to look for the Higgs through the $b\bar{b}$ channel, one must be able to efficiently tag bottom quarks, via vertex detection. It is not clear that bottom tagging will have the resolution necessary to see Higgs events.

About 18% of the time, the Higgs will decay into taus, charms or gluons. The decay to taus is also a very promising mode, since taus usually decay into electroweak particles. Observations of Higgs decays to charm quarks is basically out of the question, since the ability of detectors to tag charm quarks is extremely unreliable. Gluons are out of the question as well, since they may not be tagged at all.

The mode $H \rightarrow \gamma\gamma$, which arises through loop effects, is quite rare, with a branching ratio of 10^{-3} . This, in particular, is quite unfortunate, since this mode offers the best chance for detection in a hadron-hadron collider [14, 15]. This process has been called the “golden mode”, since the energy resolution of these events in a particle detector is relatively fine and its background is fairly small. One can hope to measure the rate to γ 's and look for the characteristic enhancement in the transverse momentum spectrum, provided that one has a precise prediction of the spectrum of

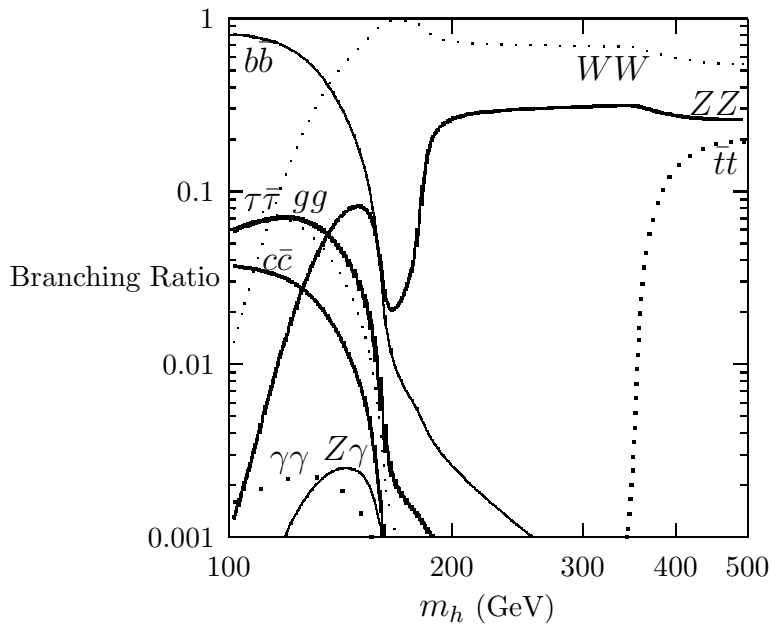


Figure 2.2: Higgs Branching Ratios

background events.

The situation is better for a heavy Higgs, which decays predominately to W 's, Z 's or top quarks. While the production rate for a Higgs in this mass range is just too small to measure at the Tevatron, these rates can presumably be measured at the LHC, provided that the Higgs mass is within this range.

2.3.2 Cross Sections

Overall, the best way to search for a Higgs is with a lepton collider, such as LEP, since one has a precise knowledge of the initial state energies of the interacting particles. At these machines, one begins to expect Higgs particles around an energy of $E_{\text{COM}} = M_Z + M_H$, with the Higgs radiating from the final state Z boson. The decay into jets or leptons is relatively clean, allowing the invariant mass of such events to be reconstructed. If the Higgs mass were within the accessible range of LEP, then it most surely would have been discovered. This allows a lower bound to be placed

on the Higgs mass, which is currently 114.1 GeV. Recently, a recent analysis by the ALEPH collaboration revealed an excess in events at LEP at around 206 GeV [12]. These events, while still preliminary, are very suggestive of a Higgs with $M_H \approx 115$ GeV.

Producing a Higgs boson at a hadron-hadron collider is generally not difficult. In fact, even at the Tevatron (FNAL), there are most likely dozens of Higgs produced each year that the laboratory takes data (depending on the Higgs mass). The real problem is detection; if the mass is less than 135 GeV, the Higgs decays predominately into $b\bar{b}$ pairs. Since these particles generally show up in the detector as jets, this process is swamped by QCD background events. Therefore, for Higgs bosons below 135 GeV, the most likely channel for discovery at the Tevatron is the associated production channels $p\bar{p} \rightarrow HZ$ and $p\bar{p} \rightarrow HW$. For these channels, tagging of b-quarks is crucial. For $m_H > 135$ GeV, the WW^* decay mode (where W^* represents an off-shell W boson) becomes available. The actual reach at the Tevatron at Run II depends on the total integrated luminosity, of course. A recent study [16] found that for 20 fb^{-1} , the Tevatron can exclude a Higgs at 95% confidence level up to 180 GeV, and could discover it at the 3σ level if the mass is below 125 GeV.

If the Higgs boson is not discovered at the Tevatron, then the Large Hadron Collider (LHC) at CERN, which is due to start runs around 2006, will find the Higgs particle. The main advantage of the LHC is that there will simply be more events, due to the extremely large luminosity of this machine, as well as the enhanced cross section. This allows for a much better chance for detection, especially in the $H \rightarrow \gamma\gamma$ mode. We will therefore focus our discussion on this device, where the discovery of the Higgs will most likely happen.

There are a number of ways that a Higgs boson can be produced at a hadron collider. One notable mechanism is the production rate through the gluon fusion

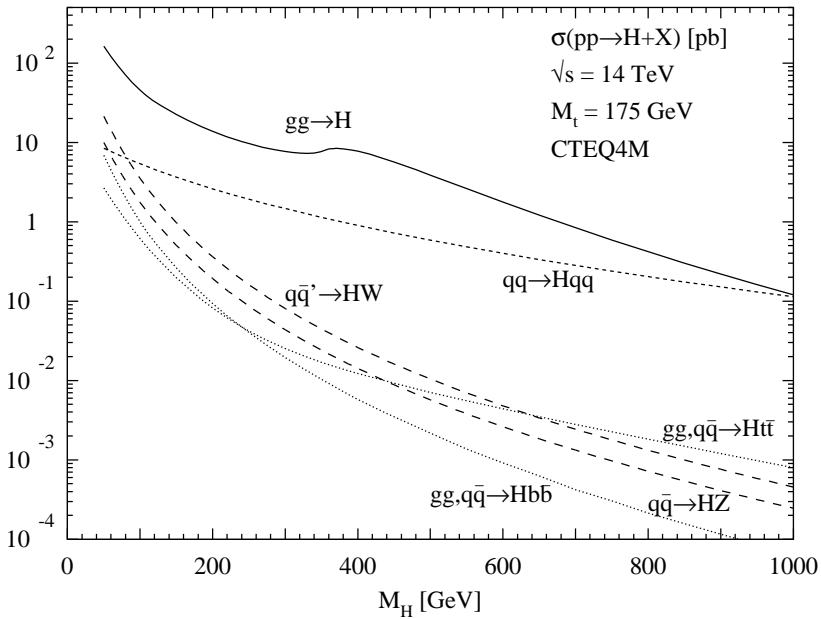


Figure 2.3: Higgs production rates at the LHC

process, $gg \rightarrow H$, which dominates the overall production rate. Other ways to produce a Higgs generally fall into the category of radiation from electroweak bosons, production through electroweak boson fusion, and radiation from heavy quarks. The expected values of these cross sections at the LHC are given in Figure 2.3⁴.

Clearly, the process $gg \rightarrow H$ dominates the total production rate at the LHC. Therefore, we will concentrate our discussion on this particular production mechanism. This mechanism is not only the most dominant production mechanism, but is the least understood in a quantitative sense. In particular, we will show that the QCD corrections to the overall cross section as well as the differential cross section are sizeable.

⁴We thank Michael Spira for the generous use of this plot, as well as the program HDECAY [14, 13].

Chapter 3

Perturbation Theory

If one wishes to search for a Higgs particle in a high energy collision, one needs to have an accurate prediction of its behavior in such an event. For instance, we would like to know in what kinematic regions we should search for decay products. In order to do so, we are going to have to calculate observables using the theoretical apparatus of Quantum Field Theory.

Integrations over momentum in such theories are plagued with divergences of several types. We will therefore have to come up with a consistent way to render these integrals finite, so that the divergences may be dealt with in a rigorous manner.

Once the divergences are regularized, we need a systematic procedure for eliminating them from our predictions. Fortunately, in a well defined theory, these divergences will either cancel amongst themselves or we will be able to factorize them into universal parameters of the theory in a process known as *renormalization*. These procedures, if applied rigorously and correctly, will allow us to compute precise, divergence-free expressions for observables in particle accelerators.

3.1 Divergences and Regularization Schemes

3.1.1 Divergences

When one calculates an amplitude in QCD or any other field theory, one typically gets expressions which are poorly behaved in the large energy region of phase space. These are known as *ultraviolet* (UV) divergences, since they correspond to a divergence in the number of high energy (frequency) fluctuations. An example of an integral which contains these types of divergences is

$$\lim_{\Lambda \rightarrow \infty} \int_0^{\Lambda^2} \frac{d(p^2)}{p^2 - m^2} = \lim_{\Lambda \rightarrow \infty} \log \left(\frac{\Lambda^2 - m^2}{-m^2} \right). \quad (3.1)$$

Clearly this expression diverges in the limit that the regularization parameter Λ goes to infinity.

In addition, if the mass of the particles is small, two additional types of divergences appear, which are collectively called *infrared* (IR) singularities. First, there is a proliferation in the number of particles generated at low energy. This is known as a *soft* singularity, called such since it causes little recoil when emitted from a more energetic particle. In a renormalizable quantum theory such as QCD, these infrared singularities will cancel in the calculation of any properly defined “infrared safe” observable quantity. We will return to the question of what it means to be an “infrared safe” observable later.

The other type of infrared singularity that one may have is called a *collinear* or mass singularity, which occurs, for instance, in QCD. A collinear singularity occurs when the momenta of two massless particles line up. To be more precise, as the invariant mass of the two distinct particles becomes zero, the resultant jets that are produced when the particles hadronize become indistinguishable from one another.

Therefore, one does not really know whether a jet of hadrons came from one particle or two or more that were collinear. We will discuss how to handle such divergences in the section on perturbative QCD.

3.1.2 Historical Regularization Schemes

In this subsection, we shall discuss two regularization schemes that were used historically to quantify the ultraviolet and infrared divergences. We will see that they both lead to consistency problems.

In the fictitious mass scheme, one introduces a fictitious mass term into the integration to regularize the soft and collinear divergences. The problem with this is that since mass terms violate gauge invariance, gauge anomalies will in general arise in calculations, and their removal is quite subtle. For this reason, this fictitious mass scheme is rarely used in modern calculations.

The UV divergences were historically handled using the *Pauli-Villars regularization scheme* (PV). PV regularizes the UV divergences through the introduction of a massive scalar ghost field, which converts the problem terms into logs of the PV mass term Δ_{PV} . The ghost fields must be introduced in a gauge-invariant manner, which can become quite complicated for all but the simplest theories.

3.1.3 Dimensional Regularization

Almost all current calculations use *dimensional regularization* (DR) to regularize the divergences. Using dimensional regularization has a number of advantages. Since no extraneous fields are introduced, unitarity is manifest, and the gauge invariance of the theory is preserved.

Let us explore the basic ideas of dimensional regularization. In a divergent

field theory, we expect to have terms arise in calculating observables that are poorly behaved in the large (UV) or small (IR) energy limit. Equation 3.1 contains examples of both of these types of divergences. First, it diverges as $\Lambda \rightarrow \infty$. This is the aforementioned *ultraviolet divergence*. Second, the integral also contains an infrared divergence, as $m \rightarrow 0$.

The main idea of dimensional regularization is that divergent integrals of this type may be rendered finite by analytically continuing the number of space-time dimensions to $4 - 2\epsilon$ dimensions. The $d(p^2)$ terms which come from the radial piece of the phase space in 4 dimensions, are replaced with the analogous piece in $4 - 2\epsilon$ dimensions:

$$d^4p \equiv \frac{p^2}{2} d(p^2) d\Gamma \rightarrow d^{4-2\epsilon}p \equiv (p^2)^{1-\epsilon} \frac{d(p^2)}{2} d\Gamma^\epsilon. \quad (3.2)$$

Where $d\Gamma^\epsilon$ is the $4 - 2\epsilon$ dimensional angular measure. The net result of our efforts is that the divergent p^2 integral, which arises from evaluating the phase space in 4 dimensions, picks up an additional factor $p^{-2\epsilon}$:

$$\int_0^\infty \frac{d(p^2)}{p^2 - m^2} \left(\frac{p^2}{\mu^2} \right)^{-\epsilon}, \quad (3.3)$$

which is well defined for $\epsilon > 0$. The μ term, for now, maintains the dimensionality of the original expression.

We may also regularize the IR divergence in a similar manner. Eliminating the mass term in equation (3.3), and noting that we must carefully separate the IR divergent and the UV divergent regions of phase space, we obtain

$$\begin{aligned} \int_0^\infty \frac{d(p^2)}{p^2} \left(\frac{p^2}{\Lambda^2} \right)^{-\epsilon} &\rightarrow \int_0^m \frac{d(p^2)}{p^2} \left(\frac{p^2}{\Lambda^2} \right)^{-\epsilon} + \int_m^\infty \frac{d(p^2)}{p^2} \left(\frac{p^2}{\Lambda^2} \right)^{-\epsilon} \\ &= \frac{1}{-\epsilon_{IR}} \left(\frac{m^2}{\Lambda^2} \right)^{-\epsilon_{IR}} - \frac{1}{-\epsilon_{UV}} \left(\frac{m^2}{\Lambda^2} \right)^{-\epsilon_{UV}}, \end{aligned} \quad (3.4)$$

where we have defined $\epsilon_{UV} > 0$ and $\epsilon_{IR} < 0$ to represent the ultraviolet and infrared poles, respectively. In QCD, we also find that poles arise from the angular integration piece, where the internal partons become collinear. These poles in ϵ also contribute infrared poles to the matrix element.

In dimensional regularization, then, we find that we have traded a poorly behaved log for a pole of the form, $-\frac{1}{\epsilon}$. These poles must either cancel amongst themselves (which is the case for the infrared poles), or they must cancel against renormalization counterterms (as is the case for ultraviolet or collinear poles), which we will discuss shortly. If everything works as it should, we should be able to analytically continue the complete expression, including counterterms, from $\epsilon = \pm\infty \rightarrow 0$ *without hitting any poles*. That is, all poles of the form $(-\epsilon - n)^{-1}$, where n is an integer must cancel¹. We may therefore set $\epsilon \rightarrow 0$ with good conscience.

Now that we have examined the basic ideas of dimensional regularization, let us examine the finer details. Immediately, we see an ambiguity in this scheme. It is not immediately obvious how to handle quantities that are only well-defined in integer dimensions, like the number of spins, nor is it obvious what to do with antisymmetric tensors like γ^5 (which depends crucially on the integer nature of N_{dim}). The most common prescription is to continue the number of spins of bosons by setting $N_{spin} = 2(1 - \epsilon)$, and by demanding that:

- γ^5 *anticommutes* with $\gamma^0, \gamma^1, \gamma^2, \gamma^3$, and
- *commutes* with all other γ 's.

This convention was developed by t'Hooft and Veltman [17], and is the standard way of handling this problem. Gauge invariance is manifest in this scheme, and there

¹ $n/2$ is the *degree of divergence* of the theory, that is, a quadratically divergent theory will typically have terms like $(\epsilon - 1)^{-1}$. All of the interactions of the Standard Model save that of the Higgs are logarithmically divergent, so all of these superficially higher order divergences must cancel amongst themselves.

are precisely two chirality states (defined in terms of projection operators) for the fermions. Thus, this scheme avoids any anomalous degrees of freedom which could arise with other “generalizations” of γ^5 . By setting the number of gluon helicities equal to $N_{spin} = 2(1 - \epsilon)$, we avoid having to separate out the $g_{\mu\nu}$ tensors that arise from the internal spin sums. This way of handling the helicities, where the gauge boson spins are manifestly continued to $2 - 2\epsilon$ and the number of fermion helicities is fixed to be 2, is known as *Conventional Dimensional Regularization*.

3.2 Renormalization

Having regularized the divergent pieces, we now seek to eliminate them from our predictions in a manner which is consistent with our theory. We will take advantage of the freedom that our theory provides to absorb these divergent terms into the definitions of the wave function normalization, the definition of the charge, and the definition of the mass. That is, we have the freedom to fix our normalizations to whatever we wish. We may, for example, make the replacements

$$\begin{aligned}
 \phi &\rightarrow \sqrt{Z_\phi}\phi, \\
 e &\rightarrow Z_e e, \\
 m_\phi &\rightarrow Z_m m_\phi.
 \end{aligned}
 \tag{3.5}$$

These reparameterizations will allow us to absorb the ultraviolet divergences into these definitions. Provided that we do this consistently, we arrive at a well-defined, finite prediction for our observable. The gauge invariance of the theory will in general impose relations between these normalization constants, but in general, we still have significant room to absorb the ultraviolet divergences.

3.2.1 Modified Minimal Subtraction

Even with the gauge restrictions, we find that we have significant freedom to reparameterize the theory. We must therefore set down conventions for the inclusion of the UV counterterms. These terms, which arise because of a redefinition of the normalization constants in the field theory, are somewhat ambiguous. This ambiguity arises since renormalization group analysis only defines how one modifies the charge to $O[\epsilon^{-1}]$. We wish to remove the poles in ϵ , but we also have the freedom to add any finite piece to the renormalized charge that we wish. Consider

$$g^{(0)} \rightarrow g^{(1)} = g^{(0)} \left(1 - \frac{\alpha_s}{4\pi} \beta_0 \left(\frac{1}{\epsilon} + O[\epsilon^0] \right) \right), \quad (3.6)$$

where the coefficient β_0 is the first *renormalization group coefficient*. The details of this coefficient depends on the symmetry of the group, and the number of fermions interacting with the gauge bosons. $O[\epsilon^0]$ represents terms that are unspecified by any gauge or other restrictions.

In modified minimal subtraction ($\overline{\text{MS}}$), we keep finite terms which tend to arise from the finite phase space integration in the dimensional regularization procedure outlined above. Instead of subtracting just the ϵ pole, we subtract off the piece

$$g^{(0)} \rightarrow g^{(1)} = g^{(0)} \left(1 - \frac{1}{\epsilon} \frac{(4\pi)^\epsilon}{\Gamma(1-\epsilon)} \frac{\alpha_s}{4\pi} \beta_0 \right) \quad (3.7)$$

in $\overline{\text{MS}}$. Again, this is a just a convention which is used to remove the extraneous universal pieces that tend to complicate calculations in dimensional regularization. There are a number of other ways of expressing the $\overline{\text{MS}}$ counterterm, which are technically different from this one at $O[\epsilon]$. However, since these $O[\epsilon]$ terms will eventually be set to zero in a next-to-leading order calculation, the same result is obtained.

In principle, the subtraction scheme should not matter when one is calculating an observable. In practice, however, different subtraction schemes can cause significant variations in the final result at a fixed order in perturbation theory. One must also consistently use the same subtraction scheme to calculate the parton distribution functions from the raw deep inelastic scattering (DIS) data [18], as well as to calculate the UV counterterm from the charge renormalization. If one wishes to do a calculation in a different scheme, one must either know how to convert the result in that scheme back into $\overline{\text{MS}}$, or one must be able to show that the scheme produces the same results at that order of perturbation theory. Since it is fairly involved to do either of these things, most calculations are done using the modified minimal subtraction scheme.

3.3 Quantum Chromodynamics

Quantum Chromodynamics is the theory of the strong interaction at high energies. This model introduced dynamics to the quarks of the Gell-Mann $\text{SU}(3)_{\text{flavor}}$ model, and proposed a carrier of the strong nuclear force, the gluon. We shall begin by discussing the *Naive Parton Model*, which explains the behavior of the hadrons in a qualitative sense, and then move on to *perturbative QCD*, which allows one to compute much more precise expressions for collider observable quantities.

3.3.1 The Naive Parton Model

We shall begin the discussion of Quantum Chromodynamics (QCD) by introducing the *parton model*, due to Bjorken and Feynman. The parton model was introduced in an effort to explain the deep inelastic scattering data, which seemed to indicate that the proton had a definite substructure. As originally proposed, the parton model

suggested that hadrons consisted of massless point particles which could then interact electroweakly with the scattering electrons to produce *jets* (semi-collinear collections of hadrons). The model originally had no other interactions built in to explain any of the strong coupling effects seen. This model is known as the *naive parton model*, and ignores any perturbative QCD effects. Indeed, this model did seem to describe the data in a qualitative fashion, and it was later deduced from the DIS data that the components of the proton that were interacting with the electron were spin 1/2 objects. This is precisely what one would expect if these “partons” were to be identified with the quarks of the Gell-Mann $SU(3)_{\text{flavor}}$ model.

The naive parton model assumes the high energy limit, in which both quarks and hadrons are massless. To calculate a cross section in DIS, we convolve a partonic cross section with a form factor $f_{H \rightarrow q}(\xi)$. In other words, the hadronic cross section is

$$d\sigma_{eH \rightarrow eX} = \int_0^1 d\xi f_{H \rightarrow q}(\xi) d\hat{\sigma}_q(\xi), \quad (3.8)$$

where we have introduced $f_{H \rightarrow q}(x)$, the process-independent *parton distribution functions* (PDF). These empirically measured functions represent the probability of the interacting parton having a fraction ξ of the parent hadron’s momentum. In the limit that both particles are massless, the hadron momentum is given in terms of the proton momentum as

$$p_p = \xi p_H. \quad (3.9)$$

The hadron-hadron cross section is defined in a similar fashion, where the structure functions are deemed to be *universal*, that is, process independent. We may then measure the parton distribution functions through DIS and apply them to any process we wish. The hadron-hadron cross section is then given by

$$d\sigma_{HH' \rightarrow X} = \int_0^1 d\xi_a f_{H \rightarrow a}(\xi_a) \int_0^1 d\xi_b f_{H \rightarrow b}(\xi_b) d\hat{\sigma}_{ab}(\xi_a, \xi_b). \quad (3.10)$$

In equation (3.8), q may be a quark or an anti-quark, and in equation (3.10), a and b may be any species of parton. These expressions must be summed over the parton species, q , a , and b , since partons may not be directly observed.

3.3.2 Perturbative Quantum Chromodynamics: Improved Parton Dynamics

Ideally, one would like to extend the qualitative successes of the naive parton model with a dynamic theory. Such a theory would have the same qualitative behavior of the naive parton model, but with enough computational power to make precise analytic predictions of observable quantities.

We find that, if we allow the quarks of the Gell-Mann model to interact dynamically via an unbroken $SU(3)$ Yang-Mills theory, we succeed in extending the parton model. This theory contains generalizations of the hadron structure functions mentioned in the previous subsection, and allows improvements of the predictions of that model by the dynamic interaction with the $SU(3)$ gluon field.

This model based on the $SU(3)$ gauge theory is called *Quantum Chromodynamics* (QCD). QCD is an (unbroken) $SU(3)$ gauge theory in which the quarks of Gell-Mann's flavor model interact with spin-1 bosons known as gluons. There are eight of these, interacting with the quarks via a three-dimensional quantum number known as *color*. One may show that such a theory satisfies *asymptotic freedom*, in which the coupling becomes very small at high energy scales.

This theory is also interesting, since it gives an explanation as to why the quarks are never seen in nature. The coupling α_s of the $SU(3)$ gauge theory actually diverges for a small energy scale, indicating that any perturbation theory is poorly defined in this limit. In quantum mechanics, small energies are equivalent to large

distances. This implies that any attempt to pull quarks away from one another results in a steady increase in energy, until the available energy is enough to create a quark anti-quark pair out of the vacuum. In order to examine such behavior, one must be able to calculate exact expressions, without resorting to perturbation theory.

If the interaction is over a very small distance (large energy scale), one may use perturbation theory, since α_s is small over these distances. Such an expansion, and the requisite renormalization of the PDF's and the coupling constant, are known as *perturbative QCD*. For very "hard" scattering processes, where a significant amount of energy is exchanged among the hadrons, we may calculate corrections to the naive parton model. This consists of calculating a parton-level cross section in standard perturbation theory, then inserting the results into the convolution equations above.

QCD, like all gauge theories, is poorly behaved in the ultraviolet region. Wave function renormalization removes the ultraviolet singularities that occur. In addition, two other types of singularities occur, *collinear* (or mass) singularities, and *soft* (or infrared) singularities. The soft singularities must cancel when all of the pieces of the cross section are added together, but the collinear singularities do not cancel against any other pieces of the calculation. However, the collinear poles are universal (process independent), and may be absorbed into the (universal) structure functions. That is,

$$f_{h \rightarrow p}(z) \rightarrow \int_0^1 dx/x f_{h \rightarrow p'}(x/z, \mu_F) K_{p' \rightarrow p}(z), \quad (3.11)$$

where the convolution kernel $K_{p \rightarrow p'}(z)$ is

$$K_{p' \rightarrow p}(z) = \delta(1-z)\delta_{pp'} - \left(\frac{\alpha_s}{2\pi\epsilon}\right) \left(\frac{4\pi\mu_R}{\mu_F}\right)^\epsilon \frac{P_{p \rightarrow p'}(z)}{\Gamma(1-\epsilon)} + \text{finite}. \quad (3.12)$$

The convolution kernel may be thought of as being analogous to the normalization constants Z in the ultraviolet renormalization procedure. The *splitting kernels* $P(z)$

in equation (3.12) are

$$P_{q \rightarrow q}(z) = \frac{4}{3} \left(\frac{1+z^2}{(1-z)_+} \right) + 2\delta(1-z) \quad (3.13)$$

$$P_{q \rightarrow g}(z) = \frac{4}{3} \left(\frac{1+(1-z)^2}{z} \right) \quad (3.14)$$

$$P_{g \rightarrow g}(z) = 6 \left(\frac{1-z}{z} + \frac{z}{(1-z)_+} + z(1-z) \right) + \left(\frac{11}{2} - \frac{n_f}{3} \right) \delta(1-z) \quad (3.15)$$

$$P_{g \rightarrow q}(z) = \frac{1}{2}(z^2 + (1-z)^2). \quad (3.16)$$

In the preceding relations, we have introduced the “+” prescription, which is defined through the relation

$$\int_0^1 dz \frac{1}{(1-z)_+} g(z) = \int_0^1 dz \frac{g(z) - g(1)}{(1-z)} \quad (3.17)$$

for any arbitrary function $g(z)$.

In equation (3.12) we have introduced another dimensional byproduct of the renormalization process, the factorization scale μ_F . We have also made explicit the separate scales introduced in ultraviolet and infrared regularization processes; the ultraviolet renormalization scale will be referred to as μ_R . In practice, one generally takes these scales to be the same, though there is no theoretical argument that they *should* be taken to be the same. When we have set these scales equal to each other, we will refer to the resulting parameter as μ , to emphasize it’s generic nature.

The physical interpretation of the factorization scale is somewhat different than that of the renormalization scale. Indeed, the factorization scale represents the cutoff scale for so-called “hard processes.” In other words, it quantifies exactly how much of the soft QCD radiation is to be included in the partonic matrix element, and how much is to be absorbed into the parton distributions. The renormalization scale represents the cutoff scale at both the large energy end, where we expect new physics

to come into play, and the low end, where we absorb the remaining IR singularity into the quantum mechanical excitations.

Now, in order to cancel the soft poles that occur in the matrix element, we must carefully define our observables. In general, an observable O may be a function of the number of particles, as well as the kinematics of the system. In order for an observable to be *infrared safe*, we guarantee that (for N and $N + 1$ parton systems):

$$O_{N+1}(E_1 \rightarrow 0) = O_N. \quad (3.18)$$

That is, $O(N + 1)$ is infrared safe if, as the energy of one of the partons vanishes, $O(N + 1)$ becomes identical to the analogous function with one less parton, $O(N)$. Similarly, an observable is *collinear safe* if for two particles with momenta p_1, p_2 , we have that

$$O_{N+1}(S_{12} \rightarrow 0) = O_N, \quad (3.19)$$

where $(S_{12} = (p_1 + p_2)^2)$. If O satisfies these two conditions, then the cross-section is guaranteed to be finite to NLO in perturbative QCD.

This process may be generalized. We may calculate cross sections and other observables to any order in perturbation theory that we wish. These calculations tend to be quite complicated, as the additional complexity of the SU(3) gauge group tends to generate large numbers of contributing graphs. This is especially true in processes that involve large numbers of gluons, since gluons can couple not only to fermions, but to other gluons as well.

3.4 Helicity Amplitudes and Color Ordering

In recent years, many techniques have been developed to simplify the computation of multi-parton amplitudes in QCD [19, 20]. By using techniques such as helicity amplitudes and gauge-invariant color orderings, one may simplify a calculation greatly. This technique significantly reduces the number of diagrams that one has to evaluate in computing, for instance, gluon amplitudes.

In order to avoid calculating things redundantly, one may make use of some of the symmetry properties of QCD. In the approximation that all of the partons are massless, the spinor states of the partons become true helicity eigenstates. Since some of these states are related to other states by charge conjugation, Bose symmetry, or parity, one avoids calculating redundant helicity states. Also, each non-cyclic color projection is gauge invariant from other non-cyclic projections, so we may reduce the number of terms by calculating a single cyclically related color projection.

Another simplification lies in the fact that these projections of color and helicity are gauge invariant, so that one may choose a different gauge to evaluate the partonic matrix element for each different helicity state. It is generally convenient to express polarization vectors in terms of massless Weyl spinors [21, 22]. The polarization vectors for a gluon of momentum p may be written

$$\epsilon_\mu(p, q) = \mp \frac{\langle \pm p | \gamma^\mu | q \pm \rangle}{\sqrt{2} \langle \mp q | p \pm \rangle}, \quad (3.20)$$

where

$$|p \pm \rangle = \frac{1 \pm \gamma^5}{2} u(p) \quad (3.21)$$

is a massless spinor, and q is some arbitrary massless reference momentum such that $q \cdot p \neq 0$. Since a change in q is equivalent to adding a piece proportional to p , we

have basically absolute freedom to choose q . The terms proportional to p will then cancel in gauge invariant amplitudes via the Ward identities.

Using these expressions, the number of terms one needs to calculate a QCD observable is reduced considerably. However, ambiguities arise at NLO, where we would like to analytically continue the number of dimensions. The number of spins states in a conventional $\overline{\text{MS}}$ calculation is generally taken to be $2(1 - \epsilon)$ which is quite clearly an abstraction. If we consider actual helicity states, the number of external particles *must be two exactly*. Internal (loop) particles may have either, but are generally taken to have $2(1 - \epsilon)$ helicity states. Therefore, when calculating expressions using helicity states, one must know how to alter the resultant expressions in order to obtain the conventional $\overline{\text{MS}}$ expression. We will encounter this issue later, during our calculation of the Higgs differential cross section at NLO in QCD.

Chapter 4

The Higgs Boson Cross Section and Transverse Momentum Spectrum: Leading Order Calculation

One of the most important quantities that will be measured at the LHC is the production rate of the Higgs [14, 23, 24]. Therefore, a precise theoretical understanding of the rate of Higgs production is critical to any attempts to search for the particle. Since the cross section is dominated by the gluon-fusion process [14], this process must be calculated as precisely as possible, in order to precisely determine how many of these particles will be produced in a year of running.

Aside from having a good idea of the overall production rate of the Higgs, the transverse momentum spectrum and the rapidity spectrum of the Higgs boson is of great interest to the LHC project. Since the detectors themselves must ideally be designed around the kinematic regions where one expects to see the Higgs, having a reliable prediction for these differential cross sections is of particular importance.

Unfortunately, QCD observables are notoriously unreliable at leading order,

and these must generally be calculated to NLO (at least) in order to have a reliable prediction for their behavior. Moreover, leading order QCD calculations tend to exhibit a strong dependence on the factorization/renormalization scale, μ , which reflects this theoretical uncertainty.

The focus of this work is to calculate a reliable numerical estimate of the transverse momentum/rapidity spectrum. In order to improve the existing calculation, we will add to it radiative corrections which will hopefully have less scale dependence, and therefore less theoretical uncertainty. Since the procedure for calculating this differential cross section at NLO includes calculating the LO spectrum, it is instructive to begin with the much simpler LO calculation. We will then show in the next chapter how to modify this expression in order to obtain the differential cross section at NLO.

We will assume in this calculation that the dominant contributions to the transverse momentum spectrum come from the aforementioned gluon-fusion process. We will calculate the LO production rate both for a finite top quark mass, and in the limit that the top mass goes to infinity (the *large m_t limit*). We will then argue that in the Higgs mass range under consideration, the finite mass calculation and the infinite-mass approximation give virtually the same result, whereas the QCD corrections give very large contributions to both the transverse momentum spectrum as well as the overall production rate.

4.1 The Gluon Fusion Cross Section

The gluon fusion process proceeds through a virtual top quark loop as represented by the Feynman diagram in figure 4.1. As this process is well known in the literature

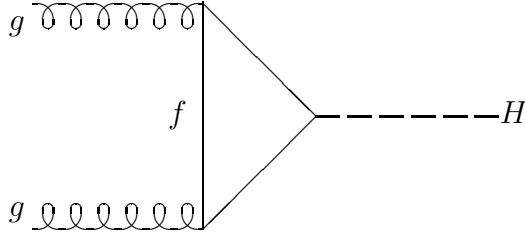


Figure 4.1: Feynman Diagram for Higgs Production through Gluon Fusion

[25], we will just present the result

$$\hat{\sigma} = \frac{\alpha_s^2}{256\pi v^2} |A|^2 \delta \left(1 - \frac{m_H^2}{s} \right). \quad (4.1)$$

The form factor A is

$$A(\tau) = \tau [1 + (1 - \tau) f(\tau)] \quad (4.2)$$

where

$$f(\tau) = \arcsin^2 \left(\sqrt{\frac{1}{\tau}} \right) \quad \text{for } \tau < 1, \quad (4.3)$$

$$f(\tau) = -\frac{1}{4} \left(\log \left(\frac{1 + \sqrt{1 - \tau}}{1 - \sqrt{1 - \tau}} \right) - i\pi \right) \quad \text{for } \tau > 1, \quad (4.4)$$

and $\tau = 4m_{\text{top}}^2/m_H^2$. In the limit of a large quark mass, this form factor converges to a constant

$$A(\tau \rightarrow \infty) = -\frac{2}{3}, \quad (4.5)$$

which results in the cross section in the limit of a large quark mass;

$$\hat{\sigma}(\tau \rightarrow \infty) = \frac{\alpha_s^2}{576\pi v^2} \delta \left(1 - \frac{m_H^2}{s} \right). \quad (4.6)$$

A graph of the exact hadronic cross section is given in Figure 4.2 for a top mass of 174 GeV. In addition, the corresponding infinite mass limit is plotted on the same graph as a reference. Clearly, both graphs are qualitatively the same for an

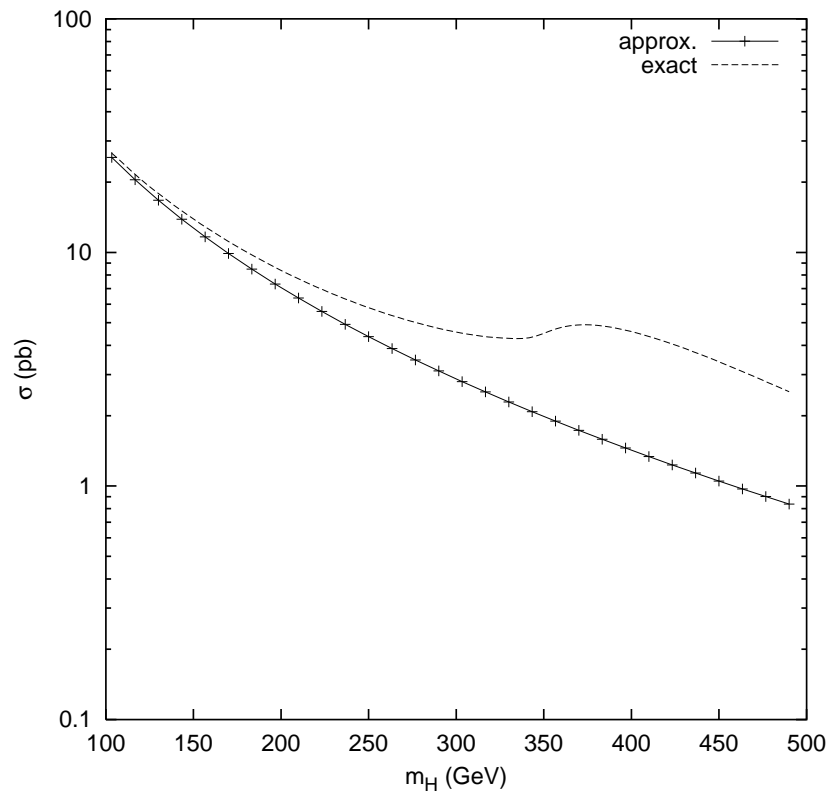


Figure 4.2: Comparison of the infinite quark mass approximation with the $m_{\text{top}} = 174$ GeV calculation.

intermediate mass Higgs ($m_H \approx 100\text{-}200$ GeV), which is the region that we will be considering. If we assume that the LHC will run at a luminosity of approximately $\approx 300 \text{ fb}^{-1} \text{ yr}^{-1}$ [1], then we may compute the expected number of Higgs produced in one year of continuous running by multiplying this figure by the cross section. Looking at the data on this graph, we see that the LHC will produce approximately $0.4 - 4 \times 10^6$ Higgs bosons in a year of running, depending on the Higgs mass. We can conclude that Higgs production will be quite prolific at this machine.

The close correspondence of the finite calculation with the infinite mass limit calculation seems to suggest that in the infinite quark mass limit, the dynamics of the loop freezes out, allowing us to replace the loop with an effective coupling. As long as the relevant energy scales in the problem do not become too large, we can be confident that the results of this calculation give a fairly good approximation to the true cross section.

Even in the region where the energy scale is approximately the top quark mass, the infinite mass approximation is quite good. The $O[m_{\text{top}}^{-2}]$ give additive corrections [26] which behave as

$$\sigma(m_{\text{top}}) \approx \sigma(m_{\text{top}} = \infty) \left(1 + \frac{7}{15} \left(\frac{m_H}{2m_{\text{top}}} \right)^2 \right) \quad (4.7)$$

so that for a Higgs mass with a mass as large as 200 GeV, the exact leading-order expression differs from the large m_{top} approximation by $\approx 15\%$. Since every experimental indicator tells us that the Higgs is very likely below this limit, we can with good faith apply this effective theory to the inclusive cross section.

We may also note that the cross section calculated in the large m_{top} limit *underestimates* the Higgs mass over the entire range of plotted masses. As we argued earlier, it is highly improbable that the Higgs mass is outside of this range. We

therefore expect that the infinite mass effective theory will be quite good over the entire range of applicable masses. Moreover, recent work [27, 28] seems to suggest that the ratio of the next-to-leading order calculation to the leading order calculation is more or less independent of the top quark mass. Therefore, one may compute the next-to-leading order corrections using the infinite top mass limit, divide that value by the leading order, infinite mass limit result, and apply the resulting enhancement to the leading order expression with confidence.

4.2 Low Energy Effective Lagrangian

Since the large m_{top} approximation is quite valid in our leading order calculation of the cross section, a systematic way to calculate the various Higgs observables using this approximation is desirable. We may therefore propose a low energy effective theory to do gluon fusion calculations ¹.

This idea of freezing the top quark inside the loop, and replacing it with an effective coupling leads to the following effective Lagrangian,

$$\mathcal{L} = -\frac{1}{4} \left(\frac{\alpha_s}{3\pi v} \right) (1 + \Delta) H G^{\mu\nu} G_{\mu\nu}, \quad (4.8)$$

where the top-loop dynamics have been replaced by an effective coupling ², $\frac{\alpha_s}{3\pi v}$. In order to be valid, the relevant energy scales of the process must be less than the top mass, and even outside that neighborhood this approximation generally underestimates the cross section, so that one errs on the conservative side. We may derive the

¹Aside from the original leading order calculation [29], The radiative corrections using this infinite m_{top} limit have also been computed [26, 30]. Moreover, progress has recently been made on the NNLO calculation [31, 32].

²The effective coupling $\alpha_s/3\pi v$ receives a finite renormalization at each order in perturbation theory. We represent this with a constant Δ , which is zero at leading order. there is a contribution from Δ at NLO which one must take care to include.

following Feynman rules from this effective low energy Lagrangian:

The Higgs-gluon-gluon coupling is

$$H_{ab}^{\mu\nu}(p_1, p_2) = -iA\delta_{ab}(p_1 p_2 g^{\mu\nu} - p_1^\nu p_2^\mu), \quad (4.9)$$

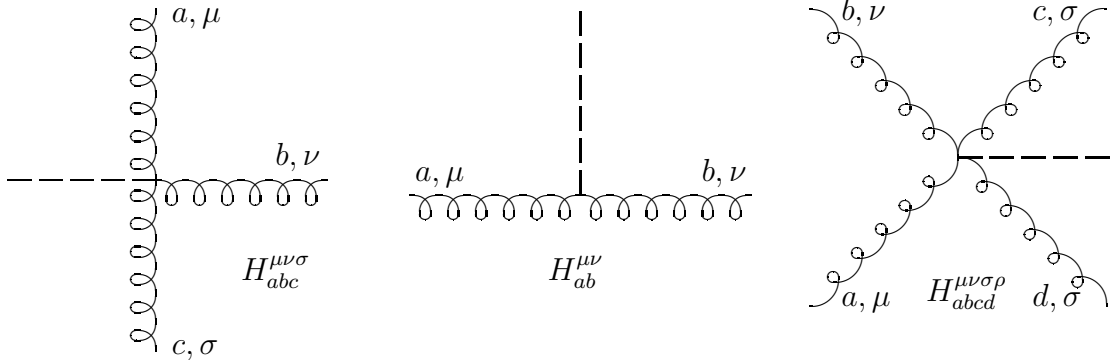
the Higgs-three gluon coupling is

$$H_{abc}^{\mu\nu\sigma}(p_1, p_2, p_3) = gA f_{abc}((p_1 - p_2)^\sigma g^{\mu\nu} + (p_2 - p_3)^\mu g^{\nu\sigma} + (p_3 - p_1)^\nu g^{\mu\sigma}), \quad (4.10)$$

and the Higgs-four gluon coupling is

$$\begin{aligned} H_{abcd}^{\mu\nu\sigma\rho}(p_1, p_2, p_3, p_4) = ig^2 A [& f_{abe} f_{cde} (g^{\mu\rho} g^{\nu\sigma} - g^{\mu\sigma} g^{\nu\rho}) \\ & f_{ace} f_{bde} (g^{\mu\nu} g^{\rho\sigma} - g^{\mu\sigma} g^{\nu\rho}) \\ & f_{ade} f_{bce} (g^{\mu\nu} g^{\rho\sigma} - g^{\mu\rho} g^{\nu\sigma})], \end{aligned} \quad (4.11)$$

where $A = \left(\frac{\alpha_s}{3\pi v}\right)(1 + \Delta)$ is the effective coupling and f_{abc} are the $SU(3)$ group coefficients in the adjoint representation. These are represented graphically as:



In the preceding expressions and diagrams, the gluon a has color a , momentum p_1 ,

and helicity index μ , with analogous relations for the remaining particles. Note that these rules become those for QCD if one simply takes the limit $p_H \rightarrow 0$ and replaces the coupling A with 1.

4.3 The Leading Order p_\perp spectrum in the large

m_{top} limit

By far, the most significant contribution to Higgs production is through the gluonic coupling via a virtual top quark loop. Not only is the rate enhanced by the large top Yukawa coupling, it is also enhanced considerably by the large number of gluons (in comparison to quarks) inside the proton. Therefore, in computing the transverse momentum spectrum, we shall restrict our calculation to radiative corrections of the $gg \rightarrow H$ cross section. In particular, those that produce a nontrivial transverse momentum will be considered. When we refer to the *Leading Order* or *Tree Level* contribution, we mean the lowest order in perturbation theory which produces this nontrivial contribution.

At a proton-proton collider such as the LHC, by far the most dominant contribution is the process $gg \rightarrow Hg$. This is simply because the gluon distributions are much larger than the quark distributions at these energies. The quark anti-quark mechanism is also small, since the antiquark distributions are also very small.

We would like to use our effective theory to calculate this process, but we have provided no arguments that the effective theory will be any good whatsoever in this markedly different calculation. Therefore, we will compare it to the finite top mass calculation done in reference [33]. Indeed, we will present the argument that the effective theory does quite nicely as long as the mass scales in the problem (in this case, m_H and p_\perp) are fairly low in comparison to the top quark mass.

4.3.1 Kinematics and Notation

We begin by defining our kinematics, and establishing our notation for the calculation. As is the convention of parton model, we relate the hadron momenta, P_a, P_b to the parton momenta p_a, p_b via momentum fractions, ξ_a, ξ_b ;

$$p_a = \xi_a P_a, \quad p_b = \xi_b P_b. \quad (4.12)$$

We will sometimes use the convenient shorthand $a = p_a, b = p_b$ for the parton level momenta. It is important to note that the final state parton momentum will be called Q in this work. This differs from many similar calculations in which the momentum of the final-state massive particle is referred to as Q . We therefore have the following momentum conservation relation;

$$p_a + p_b = p_H + Q. \quad (4.13)$$

We shall define the parton Mandelstam invariants in the usual fashion:

$$\begin{aligned} s &= (p_a + p_b)^2, \\ t &= (p_a - p_H)^2, & u &= (p_b - p_H)^2. \end{aligned} \quad (4.14)$$

If we define the hadronic Mandelstam variables analogously

$$S = (P_a + P_b)^2, \quad T = (P_a - p_H)^2, \quad U = (P_b - p_H)^2, \quad (4.15)$$

these are related to the partonic variables via

$$\begin{aligned} s &= \xi_a \xi_b S, \\ t &= m_H^2(1 - \xi_a) + \xi_b T, & u &= m_H^2(1 - \xi_a) + \xi_b U. \end{aligned} \quad (4.16)$$

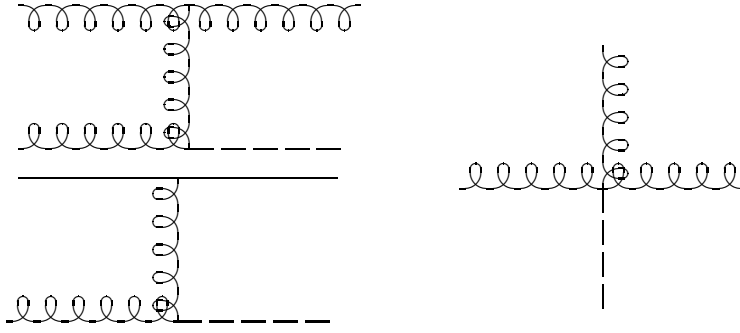


Figure 4.3: Feynman diagrams for Higgs production in the large m_\perp limit.

If we choose to evaluate the Higgs momentum in the hadron-hadron center of momentum (COM) frame, as is usually the convention, we may re-express the hadronic variables as;

$$\begin{aligned}
 S &= E_{COM}^2, \\
 T &= m_H^2 - m_\perp E_{COM} \exp(-y_H), & U &= m_H^2 - m_\perp E_{COM} \exp(y_H).
 \end{aligned}
 \tag{4.17}$$

Here, the rapidity of the Higgs in the COM frame is denoted y_H , and m_\perp denotes the transverse mass ($= \sqrt{m_H^2 + p_\perp^2}$). Therefore the partonic momenta can be expressed in terms of the traditional external variables and the momentum fractions;

$$\begin{aligned}
 s &= \xi_a \xi_b E_{COM}^2, \\
 t &= m_H^2 - \xi_a m_\perp E_{COM} \exp(-y_H), & u &= m_H^2 - \xi_b m_\perp E_{COM} \exp(y_H).
 \end{aligned}
 \tag{4.18}$$

4.3.2 Analytic Procedure

The Higgs p_\perp spectrum has three contributing partonic processes at leading order, $gg \rightarrow Hg$, $q\bar{q} \rightarrow Hg$, and $gq \rightarrow Hq$. These may be derived from the graphs in Figure

4.3 using the Feynman rules outlined above. We find the following expressions for the (helicity-averaged) matrix elements in $d = 4 - 2\epsilon$ dimensions

$$|\overline{M}_{gg \rightarrow gH}|^2 = \frac{24}{256(1-\epsilon)^2} \frac{4\alpha_s^3}{9\pi v^2} \left\{ (1-\epsilon) \frac{s^4 + t^4 + u^4 + m_H^8}{stu} - 4\epsilon m_H^2 \right\}, \quad (4.19)$$

$$|\overline{M}_{q\bar{q} \rightarrow gH}|^2 = \frac{16}{9(36)} \frac{\alpha_s^3}{\pi v^2} \left\{ \frac{t^2 + u^2}{s} (1-\epsilon) - 2\epsilon \frac{tu}{s} \right\}, \quad (4.20)$$

and

$$|\overline{M}_{gq \rightarrow qH}|^2 = \frac{16}{9(96)(1-\epsilon)} \frac{\alpha_s^3}{\pi v^2} \left\{ \frac{s^2 + u^2}{-t} (1-\epsilon) - 2\epsilon \frac{su}{-t} \right\}. \quad (4.21)$$

Because of CP invariance, the process $gq \rightarrow qH$ is identical to the expression for $g\bar{q} \rightarrow \bar{q}H$, and the matrix element for $q\bar{q} \rightarrow gH$ may be derived from the latter expression using crossing symmetry. The appropriate spin and color averaging factors must, of course, be substituted. These have been included in the preceding expression.

The general expression for a 2 to 2 partonic differential cross section is given by

$$\frac{d\hat{\sigma}}{dp_{\perp}^2 dy} = \frac{\delta(Q^2)}{16\pi s} |\overline{M}|^2. \quad (4.22)$$

The hadronic cross section is related to the partonic cross section via the double convolution, as outlined in Chapter 3;

$$d\sigma_{AB} = \sum_i \sum_j \int_0^1 d\xi_a f_{A \rightarrow i}(\xi_a, \mu_F) \int_0^1 d\xi_b f_{B \rightarrow j}(\xi_b, \mu_F) d\hat{\sigma}_{ij}(\xi_a, \xi_b). \quad (4.23)$$

Using the expression for cross section found in the appendix D and the expression for the partonic cross section, Eq. (4.22), we may derive the following expression for the differential cross section:

$$\frac{d\sigma_{pp \rightarrow HX}}{dp_{\perp}^2 dy_H} = \sum_i \sum_j \int_0^1 d\xi_a f_{A \rightarrow i}(\xi_a, \mu_F) \int_0^1 d\xi_b f_{B \rightarrow j}(\xi_b, \mu_F) \delta(Q^2) \frac{1}{16\pi s} |\overline{M}_{ij}|^2. \quad (4.24)$$

Noting that the double convolution of the delta function may be written (also Appendix D)

$$\int_0^1 d\xi_a \int_0^1 d\xi_b \delta(Q^2) \rightarrow \int_{x_+}^1 \frac{d\xi_a}{\xi_a S + T - M_H^2} + \int_{x_-}^1 \frac{d\xi_b}{\xi_b S + U - M_H^2}, \quad (4.25)$$

where

$$x_{\pm} = \frac{m_{\perp} + p_{\perp}}{\sqrt{S}} \exp(\pm y_H), \quad (4.26)$$

we arrive at our final expression for the differential cross section,

$$\begin{aligned} \frac{d\sigma_{pp \rightarrow HX}}{dp_{\perp}^2 dy_H} &= \sum_i \sum_j \left(\int_{x_+}^1 \frac{d\xi_a}{\xi_a S + T - M_H^2} + \int_{x_-}^1 \frac{d\xi_b}{\xi_b S + U - M_H^2} \right) \\ &\quad \times f_{A \rightarrow i}(\xi_a, \mu_F) f_{B \rightarrow j}(\xi_b, \mu_F) \frac{1}{16\pi S} |\overline{M}_{ij}|^2. \end{aligned} \quad (4.27)$$

Note that there is only one degree of freedom in the integration, as the momentum fractions are fixed by the on-shell condition in each term.

4.3.3 Numerical Procedure and Results

The convolution (4.27) must be evaluated numerically since the parton distribution functions are empirically determined. We shall use the CTEQ5L parton distributions [34], and we shall choose our scale to be the transverse energy, m_{\perp} . The number of (light) quarks n_f is 5 throughout the calculation.

The finite-mass calculation proceeds identically to the one outlined above. One simply replaces the effective theory expression for the matrix element with the exact result [33]. Because the mass of the top quark is so large, we expect the large m_{top} limit to be quite good out to very large transverse momentum.

Figure 4.4 displays a graph of the transverse momentum spectrum at zero rapidity for a Higgs of mass $m_h = 115$ GeV calculated using the full m_{top} dependence

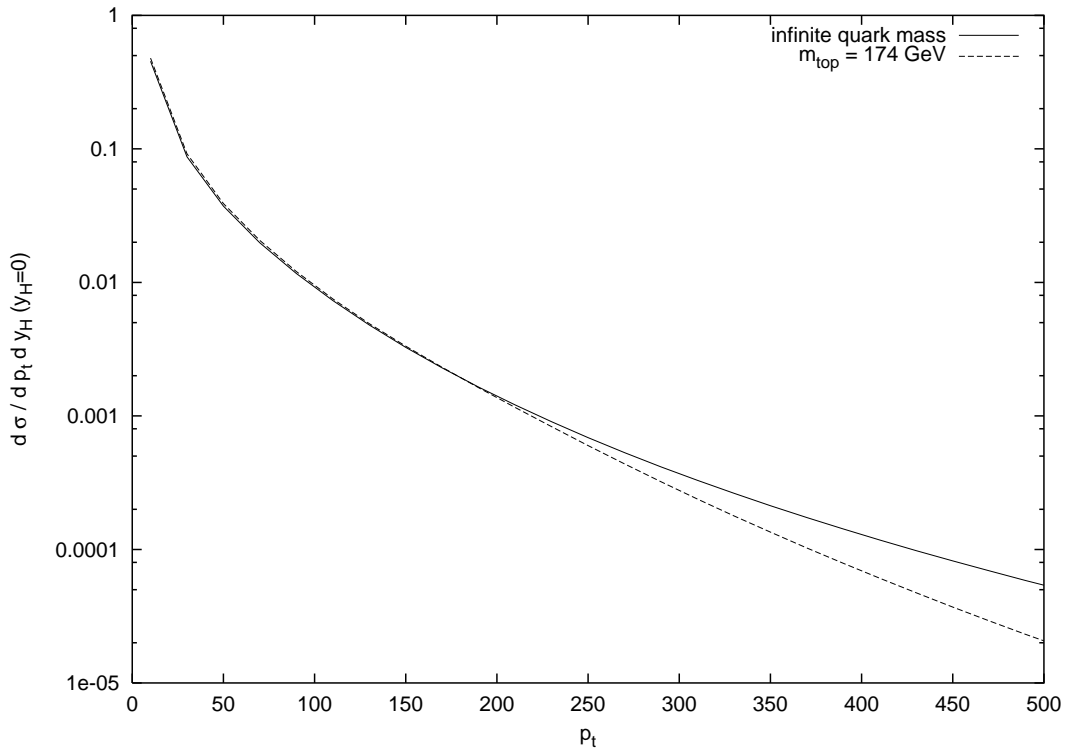


Figure 4.4: Comparison of the exact leading-order p_{\perp} spectrum with the effective theory calculation.

(dotted line). Superimposed over this graph is the identical calculation performed with the simplification that the fermion mass is taken to be infinite. It is plain to see that the agreement is quite good out to the very large p_{\perp} region, which is roughly about 300 GeV. There is really no reason to suspect that the behavior of any of the higher-order corrections will behave any differently than this.

It is advantageous to break the infinite-mass limit calculation up into the various contributions from its partonic constituents, so that we may see which partonic graphs contribute the most to the cross section. A plot of the various contributions to the p_{\perp} spectrum at leading order for a Higgs with a mass of 115 GeV is given in Figure 4.5. All of the terms exhibit the expected divergent behavior as p_{\perp} goes to zero, with the exception of the s-channel piece, $q\bar{q} \rightarrow Hg$.

As can be plainly seen in the graph, the dominant contribution to the total

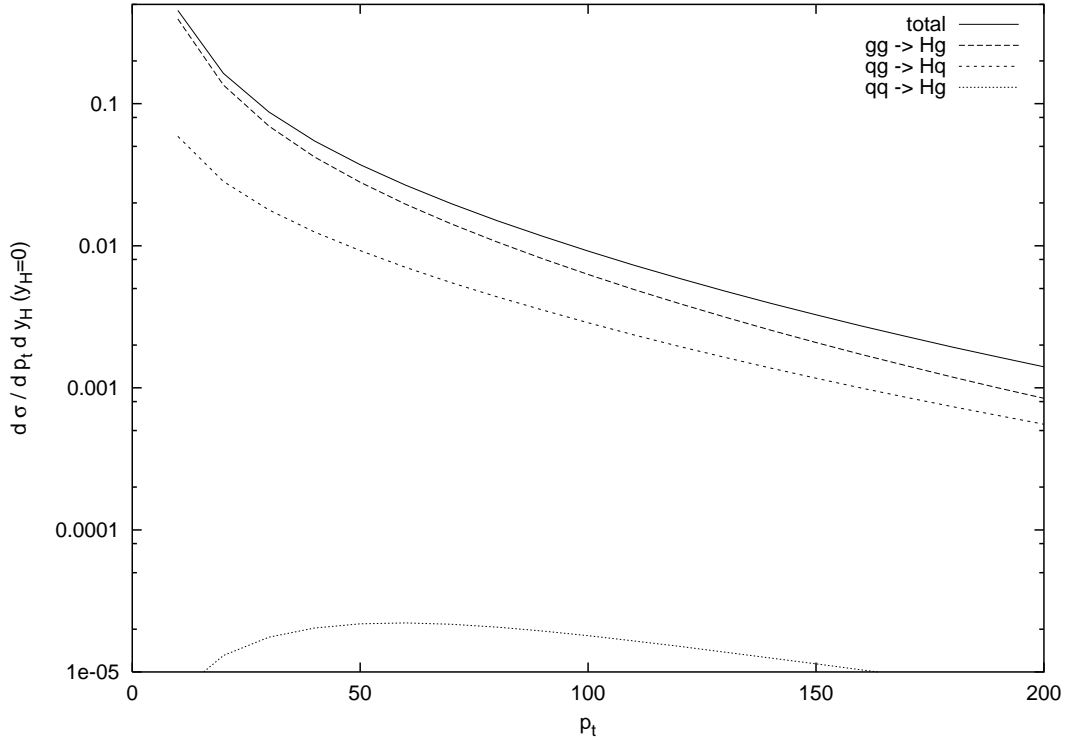


Figure 4.5: The Higgs p_{\perp} spectrum at leading order

cross section (solid black line) comes from the gluon initiated process, $gg \rightarrow Hg$ (long dashes). This contribution is roughly an order of magnitude larger than the next largest contribution, $qg \rightarrow Hg$ (dashed line), in the small transverse momentum region. Even in the large p_{\perp} region, the gluon initiated process is twice as large as the gluon-quark initiated one. The process $q\bar{q} \rightarrow Hg$ is completely negligible compared to these other two processes.

To summarize, the gluon fusion process dominates at the LHC, and working with an effective field theory in which the heavy top loop is replaced with an effective vertex is a quite good approximation. Even for the inclusive cross section, the NLO pieces are found to produce enhancements which are much larger than the difference between the finite m_{top} calculation and this infinite limit, at least for Higgs masses in the expected mass range, 100-200 GeV. Since the differential cross sections at leading-order tend to be even more unreliable than the leading-order cross sections,

it is imperative that we include some of these next-to-leading order terms in order to improve our estimate for the differential cross section.

Chapter 5

The Higgs Boson Transverse Momentum Spectrum: Gluonic Radiative Corrections

In the previous chapter, we found that the dominant production mechanism for producing a Higgs boson at the LHC was that of gluon fusion, and that this process is well represented by an effective theory in which the massive quark in the loop is replaced by an effective coupling between the Higgs boson and two or more gluons.

Moreover, the dominant partonic process is the gluon initiated $gg \rightarrow Hg$ process, which is responsible for about 90% of the total cross section. This is primarily due to the large number of gluons in the protons compared to the quarks.

As we have mentioned previously, leading-order calculations in QCD are at best an order of magnitude approximation to the actual process. This is reflected in a large scale dependence in the leading order cross section. If one wishes to have a more precise prediction for the cross section, one needs to carry out the calculation of the differential cross section to next-to-leading order in perturbative QCD. It is

hoped that the resulting calculation will have less scale dependence, and therefore, less theoretical uncertainty.

There are several different methods for doing this. One notable method is using a Monte-Carlo event generator to do the entire integration [35]. Since the matrix element contains soft and collinear divergences, one must take care to extract the divergent pieces and integrate them in $4 - 2\epsilon$ dimensions in order to cancel the divergences in the virtual pieces. A calculation of this sort has been done [36].

Nonetheless, it is advantageous to do the entire calculation analytically for several reasons. First, one would like to calculate the process using conventional $\overline{\text{MS}}$, and show that it agrees with the Monte Carlo calculation. Second, one needs an analytic formula in order to expand the matrix element around small transverse momentum. This is necessary to calculate the $B^{(2)}$ coefficient in Collins-Soper-Sterman resummation scheme, and compare it to the result calculated in a different manner in reference [37]. To have a complete next to leading order calculation, good for all transverse momentum, the intermediate p_\perp calculation included herein should be combined with a resummed curve good in the small p_\perp limit [38, 39, 40, 41].

In this chapter, we will be computing the dominant piece of the NLO corrections, the partonic process represented by gluonic radiation from the leading order process, $gg \rightarrow Hg$. This, we will argue, dominates the NLO cross section in the intermediate p_\perp region with which we are concerned.

To do this analytically, we will use the procedure outlined in Chapter 3. Since, in these corrections, we will be required to renormalize ultraviolet divergences and factorize collinear divergences, we will have to carefully compute the matrix elements in $d = 4 - 2\epsilon$ dimensions. The parton distributions that we will be using are calculated from deep inelastic scattering data using the $\overline{\text{MS}}$ factorization/renormalization scheme, so we must use the same scheme in order to obtain a meaningful result. Once

we have a finite expression, the convolutions with the structure functions may be evaluated numerically to obtain the cross section as a function of the various kinematic parameters.

5.1 Notational Conventions

The notations that we will be using are in complete analogy to those of the previous section. The 4-momenta of the hadrons shall be taken to be P_a and P_b , and the 4-momenta of the partons shall be denoted $p_a, p_b (= \xi_{a,b} P_{a,b})$. The Higgs boson momentum shall be denoted H and the mass m_H , the transverse momentum p_\perp , and the rapidity y_H . Therefore, the hadronic (S, T, U) and partonic (s, t, u) Mandelstam variables have precisely the same form as the previous chapter.

It is also convenient to define crossed momenta, $p_{1,2} = -p_{a,b}$, and to label the final state partons p_3, p_4 . This allows us to express the invariants of the $2 \rightarrow 3$ process in terms of generalized Mandelstam variables,

$$S_{ij} = (p_i + p_j)^2, \quad S_{ijk} = (p_i + p_j + p_k)^2. \quad (5.1)$$

The invariant mass Q^2 of the final state gluons and the Higgs invariants $t = (a - H)^2$, $u = (b - H)^2$ are related to these via

$$Q^2 = S_{34} = (p_3 + p_4)^2, \quad t = S_{234} = (p_2 + p_3 + p_4)^2, \quad (5.2)$$

and

$$u = S_{134} = (p_1 + p_3 + p_4)^2. \quad (5.3)$$

One may then show that the Higgs mass M is related to the remaining variables by

$$M^2 = s + t + u - Q^2, \quad (5.4)$$

and that the transverse momentum p_\perp of the Higgs may be expressed as

$$p_\perp^2 = \frac{(t - Q^2)(u - Q^2)}{s} - Q^2, \quad (5.5)$$

$$= \frac{tu - Q^2 M^2}{s}. \quad (5.6)$$

We will find it convenient to define the parameters Q_\perp, ν as follows:

$$Q_\perp = \sqrt{Q^2 + p_\perp^2},$$

$$\nu = Q^2/Q_\perp^2. \quad (5.7)$$

The physical interpretation of Q_\perp is that it is the transverse mass of the gluon pair.

Finally, we will also use S_t and S_u , which are defined as

$$S_u = S_{13} + S_{14} = u - Q^2, \quad (5.8)$$

$$S_t = S_{23} + S_{24} = t - Q^2, \quad (5.9)$$

and we will occasionally use the parameter S_H ,

$$S_H = S_{123} + S_{124} = M^2 + Q^2 - s. \quad (5.10)$$

5.2 Cross Section at NLO

To next-to-leading order, the two-to-two ($2 \rightarrow 2$) differential cross section is:

$$d\sigma_{NLO} = d\sigma_{2 \rightarrow 2}^{(0)} + d\sigma_{2 \rightarrow 2}^{(1)} + d\sigma_{2 \rightarrow 3}^{(0)}. \quad (5.11)$$

Here, $d\sigma_{2 \rightarrow 2}^{(0)}$ is the tree-level contribution, $d\sigma_{2 \rightarrow 2}^{(1)}$ is the expression for the 1-loop virtual corrections, and $d\sigma_{2 \rightarrow 3}^{(0)}$ is radiative corrections to the leading order process. If we include a collinear counterterm $d\sigma_{2 \rightarrow 2}^{AP}$ and a UV counterterm $d\sigma_{2 \rightarrow 2}^{UV}$, then the cross section may be written as

$$\begin{aligned} \frac{d\sigma}{dp_{\perp}^2 dy_H} &= \int \int d\xi_a f(\xi_a, \mu_F) d\xi_b f(\xi_b, \mu_F) s \times \\ &\left\{ \delta(Q^2) \left(\frac{d\sigma_{2 \rightarrow 2}^{(0)}}{dt} + \frac{d\sigma_{2 \rightarrow 2}^{(1)}}{dt} + \frac{d\sigma_{2 \rightarrow 2}^{UV}}{dt} \right) + \frac{d\sigma_{2 \rightarrow 3}^{(0)}}{dt du} + \frac{d\sigma_{2 \rightarrow 3}^{AP}}{dt du} \right\}. \end{aligned} \quad (5.12)$$

Since these are to be computed using the conventional dimensional regularization, we must be careful to include all ϵ dependence in the latter two terms. Note that the expression for the $2 \rightarrow 2$ differential cross section becomes

$$\frac{d\sigma_{2 \rightarrow 2}}{dt} = \left(\frac{4\pi\mu^2}{p_{\perp}^2} \right)^{\epsilon} \frac{|\overline{M}|^2}{16\pi s^2 \Gamma(1-\epsilon)}. \quad (5.13)$$

The expressions from the other two $2 \rightarrow 2$ terms (the virtual corrections and UV counterterm) are identical to this one with the exception that one must substitute the requisite matrix elements.

The contribution coming from the radiative corrections (those involving 5 particles) may be written

$$\frac{d\sigma_{2 \rightarrow 3}^{(0)}}{dt du} = \left(\frac{4\pi\mu^2}{p_{\perp}^2} \right)^{\epsilon} \left(\frac{4\pi\mu^2}{Q^2} \right)^{\epsilon} \frac{1}{\Gamma(1-2\epsilon)} \frac{1}{(2\pi)(4\pi)^2}$$

$$\times 2 \int_0^\pi d\theta (\sin(\theta))^{1-2\epsilon} \int_0^\pi d\phi (\sin(\phi))^{-2\epsilon} \frac{|\overline{M}|^2}{16\pi s^2}. \quad (5.14)$$

The contribution from the Altarelli-Parisi term is

$$\begin{aligned} \frac{d\sigma_{2\rightarrow 3}^{AP}}{dt du} &= \left(\frac{4\pi\mu}{p_\perp^2} \right)^\epsilon \frac{\alpha_s}{2\pi} \frac{(4\pi)^\epsilon}{\epsilon \Gamma(1-\epsilon)^2} \frac{1}{16\pi s^2} \times \\ &\int_0^1 \frac{dz_a}{z_a} P(z_a) \delta(z_a(s+t-M^2)+u) |\overline{M}(\xi_a z_a, \xi_b)|^2 + (t \leftrightarrow u). \end{aligned} \quad (5.15)$$

In the preceding expressions, we must note that we have suppressed the sum over parton species for clarity.

The angles θ, ϕ in the expression for the $2 \rightarrow 3$ cross section will be the polar angles of the final state partons in the Q^2 rest frame. The z axis in this frame will be defined by either initial state parton or the Higgs boson, whichever is convenient. See Appendix B for a further discussion on the explicit evaluation of these angular integrals. Once these integrations are calculated, we need only concern ourselves with the end result.

5.3 Angular Integration of Real Emission Piece

To calculate the real contribution, we must integrate the two angular degrees of freedom occurring in the matrix element. While there are a large number of terms to integrate, the calculation lends itself to an algorithm very nicely. The basic procedure for the angular integration is the following:

1. Partial fraction the amplitudes using the relationship amongst the various Mandelstam invariants. This will reduce all of the integrals to the form $(\text{const}) \times S_{ijk}^a S_{mn}^b$ or $(\text{const}) \times S_{ij}^a S_{mn}^b$, for which standard formulae exist. Here, const is some collection of kinematic invariants that does not depend on the angular

variables θ and ϕ .

2. Extract the terms proportional to $1/(1+\epsilon)$ and verify that they cancel amongst themselves. This verifies that there are no quadratically divergent pieces in the amplitude (which is true in general for QCD).
3. Extract the universal $-1/\epsilon$ piece and verify that it cancels algebraically against the collinear counterterm.
4. Regularize the soft divergences ($Q^2 \rightarrow 0$), and extract the universal soft pole. This will cancel against the soft pole in the virtual piece.

Once this is done, the real matrix element is integrable over the convolution space outlined in Appendix D. The final integral must, of course, be done numerically.

As discussed in chapter 3, the helicity amplitudes obtained in the literature are computed using gluons with two polarizations. To use $\overline{\text{MS}}$, we must have expressions for the matrix elements with $2 - 2\epsilon$ gluon polarizations. Therefore, in order to use $\overline{\text{MS}}$, we will need to calculate the $O[\epsilon]$ corrections to these expressions due to higher dimensional gluon spin effects. This calculation is much simpler than the original matrix element calculation, since we need only to calculate the matrix element in the collinear limit. We will explain this shortly.

5.3.1 $gg \rightarrow Hgg$

We now restrict ourselves to the process $gg \rightarrow Hgg$. To begin, we first break the cross section into two sections, a piece which represents the sum over the $(+++)$ and $(--++)$ helicity configurations, and a piece which represents a sum over the

odd-helicity components, $(-+++)$. Let

$$\frac{d\hat{\sigma}_{gg \rightarrow Hgg}^{(0)}}{dtdu} = \left(\frac{d\hat{\sigma}_{gg \rightarrow Hgg}}{dtdu} \right)_1 + \left(\frac{d\hat{\sigma}_{gg \rightarrow Hgg}}{dtdu} \right)_2, \quad (5.16)$$

with

$$\begin{aligned} \left(\frac{d\hat{\sigma}_{gg \rightarrow Hgg}}{dtdu} \right)_1 &= \Gamma(1 - \epsilon) \left(\frac{p_\perp^2}{4\pi \mu^2} \right)^{-\epsilon} \int \frac{d\Phi}{16\pi^2 s^2} \times \\ &2 \left(|M(1^+2^+3^+4^+)|^2 + |M(1^-2^+3^+4^-)|^2 + \right. \\ &\left. |M(1^+2^-3^+4^-)|^2 + |M(1^+2^+3^-4^-)|^2 \right), \end{aligned} \quad (5.17)$$

and

$$\begin{aligned} \left(\frac{d\hat{\sigma}_{gg \rightarrow Hgg}}{dtdu} \right)_2 &= \Gamma(1 - \epsilon) \left(\frac{p_\perp^2}{4\pi \mu^2} \right)^{-\epsilon} \int \frac{d\Phi}{16\pi^2 s^2} \times \\ &2 \left(|M(1^-2^+3^+4^+)|^2 + 3 \text{ cyclic spin perms} \right). \end{aligned} \quad (5.18)$$

In these expressions, the remaining parts of the $2 \rightarrow 3$ phase space $d\Phi$ may be succinctly written

$$d\Phi = \frac{1}{8\pi^2} \frac{\Gamma(1 - \epsilon)}{\Gamma(1 - 2\epsilon)} \left(\frac{4\pi\mu^2}{Q^2} \right)^\epsilon d\Omega^{(\epsilon)}, \quad (5.19)$$

where $d\Omega^{(\epsilon)}$ is the $4 - 2\epsilon$ angular integration measure,

$$d\Omega^{(\epsilon)} = \frac{1}{2\pi} \int_0^\pi d\theta (\sin(\theta))^{1-2\epsilon} \int_0^\pi d\phi (\sin(\phi))^{-2\epsilon}, \quad (5.20)$$

which is defined in Appendix B.

First, we define

$$\sigma_\epsilon = \frac{\alpha_s^2}{256\pi s^2} \frac{N_c^2}{N_c^2 - 1} \left(\frac{\alpha_s}{3\pi v_e^2} \right)^2 \left(\frac{4\pi\mu}{Q^2} \right)^\epsilon \left(\frac{4\pi\mu}{p_\perp^2} \right)^\epsilon \frac{1}{\Gamma(1 - 2\epsilon)}. \quad (5.21)$$

Then, the angular integral of the first contribution in (5.16) yields

$$\begin{aligned}
\left(\frac{d\hat{\sigma}_{gg \rightarrow Hgg}}{dtdu}\right)_1 &= 4\sigma_\epsilon \times \left\{ -\left(\frac{1}{\epsilon}\right) \frac{M^8 + \hat{s}^4 + S_u^4 + S_t^4 + Q^8}{\hat{s}^2 Q^2 p_\perp^2} \times \right. \\
&\quad \left[(1+\nu)(1-\nu)^{-\epsilon} + (1-\nu)\nu^{-\epsilon} \left(1 + \frac{\epsilon^2 \pi^2}{6}\right) \right] + \\
&\quad \frac{S_u^4 + S_t^4}{\hat{s}^2 Q^2 p_\perp^2} \left(-\frac{67\epsilon}{18} + \frac{1-\nu}{6} (40\nu^3 - 42\nu^2 + 30\nu - 11) \right. \\
&\quad \left. - \frac{(\nu^4 + (1-\nu)^4 - 1)}{\epsilon} \right) \\
&\quad \left. + 4 \left(-\frac{2\nu}{1-\nu} + \ln(1-\nu) \right) + \frac{\epsilon}{3\nu} + \frac{17}{3} \right\}. \tag{5.22}
\end{aligned}$$

Noteworthy are the terms that behave like $\frac{\ln(1-\nu)}{1-\nu}$ and $\frac{1}{p_\perp^2}$, which diverge as $p_\perp \rightarrow 0$, as well as the universal $\frac{1}{\epsilon}$ pole.

For the $(-, +, +, +)$ terms, we write the results as a sum of the universal divergent pieces and an analytic piece which is finite as Q and p_\perp go to zero. We find from the symmetries of the matrix element that there are in actuality only 4 independent terms, and that the sum over the odd-helicity components may written

$$\begin{aligned}
\sum_{\text{colors}, (-, +, +, +)} |M|^2 &\rightarrow 4 \left\{ \left(m(1-, 2+, 3+, 4+) + \frac{1}{2} m(1-, 4+, 2+, 3+) + (u \leftrightarrow t) \right) \right. \\
&\quad \left. + 2 m(3-, 4+, 1+, 2+) + m(3-, 2+, 4+, 1+) \right\}. \tag{5.23}
\end{aligned}$$

Using this relationship, we may write

$$\begin{aligned}
\left(\frac{d\hat{\sigma}_{gg \rightarrow Hgg}}{dtdu}\right)_2 &= 2\sigma_\epsilon \{ [2\Omega(1, 2, 3, 4) + 2\Omega(3, 4, 1, 2) + \Omega(1, 4, 2, 3) + \Omega(3, 2, 4, 1)] \\
&\quad + (u \leftrightarrow t) \}, \tag{5.24}
\end{aligned}$$

where the Ω 's are defined as the angular integrations of the helicity subamplitudes, e.g.

$$\Omega(1, 2, 3, 4) = \int \frac{d\Omega}{2\pi} |m(1^+, 2^-, 3^-, 4^-)|^2, \tag{5.25}$$

with similar relationships for the other subamplitudes.

The angular integration over the (1-, 2+, 3+ 4+) helicity configuration may be written as a sum over two terms, a term that is finite as $Q, \epsilon \rightarrow 0$ which we shall call $\Omega_0(1, 2, 3, 4)$, and a term which contains the pole structure, which we shall call $\Omega_{div.}(1, 2, 3, 4)$; i.e.,

$$\Omega(1, 2, 3, 4) = \Omega_0(1, 2, 3, 4) + \Omega_{div.}(1, 2, 3, 4). \quad (5.26)$$

The second term in this equation is

$$\begin{aligned} \Omega_{div.}(1, 2, 3, 4) = & -\frac{1}{\epsilon} \frac{1}{Q^2 s^2 p_{\perp}^2} \left[\left(\frac{M^2 Q^2}{u} \right)^4 + \left(\frac{s p_{\perp}^2}{u} \right)^4 + t^4 - 2 \frac{M^4 t^3 s Q^2}{u(M^2 - u)(M^2 - t)} \right] \\ & - \frac{1}{\epsilon} \frac{2M^4 t^3}{s Q_{\perp}^2 u(M^2 - t)(M^2 - u)} (1 - \nu)^{-1-\epsilon}, \end{aligned} \quad (5.27)$$

and the term $\Omega_0(1, 2, 3, 4)$ may be found in Appendix C. The matrix element with the same color ordering, but with the final-state gluons having the opposing helicities, integrates to

$$\begin{aligned} \Omega_{div.}(3, 4, 1, 2) = & \left\{ -\frac{1}{\epsilon} \frac{1}{Q^2 s^2 p_{\perp}^2} \left[\left(\frac{su}{u - Q^2} \right)^4 + \left(\frac{M^2(Q^2 - t)}{t} \right)^4 + \left(\frac{sQ^2 p_{\perp}^2}{(t - Q^2)t} \right)^4 \right. \right. \\ & \left. \left. - \frac{2Q^2 s M^4 (M^2 - u)^3}{(M^2 - t)tu} \right] - \frac{1}{\epsilon} \frac{2M^4 (M^2 - u)^3}{(M^2 - t)stu Q_{\perp}^2} (1 - \nu)^{-1-\epsilon} \right. \\ & \left. + \left(-\frac{11}{6} - \frac{67\epsilon}{18} \right) \frac{M^8 + s^4}{Q^2 s^2 Q_{\perp}^2} - \frac{\epsilon}{3} \frac{M^4}{Q^2 Q_{\perp}^2} \right\}. \end{aligned} \quad (5.28)$$

The term with the complicated pole structure (1324) yields

$$\begin{aligned} \Omega_{div.}(1, 3, 2, 4) = & \left\{ -\frac{2}{\epsilon} \frac{1}{Q^2 s^2 p_{\perp}^2} \left[\left(\frac{M^2 Q^2}{u} \right)^4 + \left(\frac{s p_{\perp}^2}{u} \right)^4 + t^4 \left(1 - 2 \frac{s p_{\perp}^2}{tu} \right) \right. \right. \\ & \left. \left. - 2 \frac{M^4 t^3 s Q^2}{u(M^2 - u)(M^2 - t)} \right] - \frac{2}{\epsilon} \frac{2(1 - \nu)^{-1-\epsilon} M^4 t^3}{s Q_{\perp}^2 u(M^2 - t)(M^2 - u)} \right\} \end{aligned}$$

$$-\frac{2}{\epsilon} \frac{2t^3}{usQ_{\perp}^2} \nu^{-1-\epsilon} \left(1 + \epsilon^2 \frac{\pi^2}{6}\right) \} \quad (5.29)$$

for the term where the initial state particles have the opposing helicities, and

$$\begin{aligned} \Omega_{div.}(3, 2, 4, 1) = & \left\{ -\frac{1}{\epsilon} \frac{1}{Q^2 s^2 p_{\perp}^2} \left[\left(\frac{su}{u-Q^2} \right)^4 + \left(\frac{M^2(Q^2-t)}{t} \right)^4 + \left(\frac{sQ^2 p_{\perp}^2}{(t-Q^2)t} \right)^4 \right. \right. \\ & \left. \left. - \frac{2Q^2 s M^4 (M^2-u)^3}{(M^2-t)tu} - \frac{s p_{\perp}^2}{tu} (M^8 + Q^8 + s^4) \right] \right. \\ & \left. - \frac{1}{\epsilon} \frac{2M^4 (M^2-u)^3}{(M^2-t)stuQ_{\perp}^2} (1-\nu)^{-1-\epsilon} - \frac{1}{\epsilon} \frac{M^8 + Q^8 + s^4}{sQ_{\perp}^2 tu} \nu^{-1-\epsilon} \left(1 + \epsilon^2 \frac{\pi^2}{6}\right) \right. \\ & \left. + (u \leftrightarrow t) \right\} \quad (5.30) \end{aligned}$$

for the terms that have the final-state gluons with opposing helicities. Again, the expressions for the Ω_0 's may be found in Appendix C.

In using the helicity amplitudes to calculate the amplitude squared, we have neglected terms of $O[\epsilon]$ which appear naturally from the sum over spins. If these $O[\epsilon]$ spin pieces are proportional to a collinear singularity, they will contribute to the finite pieces left over from the collinear cancellation, and hence, the cross section. Therefore, it is necessary to calculate these terms in order to complete the next-to-leading order calculation.

While it may seem formidable to calculate these terms, one realizes that one only needs the terms proportional to collinear poles in the matrix element, since the remaining terms vanish when the limit $\epsilon \rightarrow 0$ is taken. The correction term may be calculated in this manner. For the (1234) color ordering, we find the correction term to be

$$|\overline{M}_{cor.}|^2 = -2\epsilon (A)^2 g^2 \frac{N^2}{(N^2-1)} \left(\frac{S_{14}S_{23} - S_{13}S_{24}}{S_{34}} \right)^2 \left(\left(\frac{M^2}{S_{134}S_{234}} \right)^2 + \frac{1}{S_{12}^2} \right). \quad (5.31)$$

In this expression, everything save the $(S_{14}S_{23} - S_{13}S_{24})^2 / S_{34}^2$ is evaluated in the limit

$S_{34} \rightarrow 0$. The remaining divergent pieces (as $S_{23} \rightarrow 0$ and $S_{14} \rightarrow 0$) may be obtained from this one by cyclically permuting the momenta in the above expression for the amplitude, and taking the subsequent limit. Upon integrating this term, we find the following correction to the (1234) piece,

$$\sum_{poles} \int \left(\frac{d\Omega}{2\pi} \right) \frac{1}{2} |\overline{M_{cor.}}|_{1234}^2 = \left(-2\epsilon (A)^2 g^2 \frac{N^2}{(N^2 - 1)} \right) (T_1 + T_2 + T_3), \quad (5.32)$$

where

$$T_1 = \frac{1}{3} \frac{p_{\perp}^4}{sQ^2} \left(1 + \frac{M^4}{p_{\perp}^4} \right), \quad (5.33)$$

$$T_2 = \frac{-2}{\epsilon} \left(\frac{Q^2}{p_{\perp}^2} \right) \left(1 + \frac{M^4 p_{\perp}^4}{u^4} \right), \quad (5.34)$$

and

$$T_3 = T_2(u \leftrightarrow t). \quad (5.35)$$

The integral over the (1342) ordering yields precisely the same result. The (1423) piece simply gives

$$\sum_{poles} \int \left(\frac{d\Omega}{2\pi} \right) \frac{1}{2} |\overline{M_{cor.}}|_{1423}^2 = \left(-2\epsilon (A)^2 g^2 \frac{N^2}{(N^2 - 1)} \right) (2T_2 + 2T_3). \quad (5.36)$$

Note that, when added to the previous expression, all of the extraneous pole behavior of the form ϵ/Q^2 is eliminated.

5.4 Extraction of Soft Divergences and Collinear Renormalization

The expression for the real piece contains collinear singularities, which must be absorbed into the PDF's. The expression for the splitting function is

$$\begin{aligned} s \frac{d\sigma}{dt}_{\text{AP}} &= \frac{1}{16\pi s} \int_0^1 \frac{dz}{z} \frac{1}{\epsilon} \frac{\alpha_s P_{b' \rightarrow b}(z)}{2\pi \Gamma[1-2\epsilon]} |M_{a,b}^{(0)}|^2(\xi_a, z\xi_{b'}) (4\pi)^{-\epsilon} \delta(z(t-Q^2)-t) \\ &+ \frac{1}{16\pi s} \int_0^1 \frac{dz}{z} \frac{1}{\epsilon} \frac{\alpha_s P_{a' \rightarrow a}(z)}{2\pi \Gamma[1-2\epsilon]} |M_{a,b}^{(0)}|^2(z\xi_{a'}, \xi_b) (4\pi)^{-\epsilon} \delta(z(u-Q^2)-u). \end{aligned} \quad (5.37)$$

Using the δ function to evaluate the z integrals gives the following:

$$\begin{aligned} s \frac{d\sigma}{dt}_{\text{AP}} &= \frac{(4\pi)^{-\epsilon}}{16\pi s} \frac{1}{\epsilon} \frac{\alpha_s P_{b' \rightarrow b}(z_t)}{2\pi \Gamma[1-2\epsilon]} \frac{|M_{a,b}^{(0)}|^2(\xi_a, z_t \xi_{b'})}{-t} \\ &+ \frac{(4\pi)^{-\epsilon}}{16\pi s} \frac{1}{\epsilon} \frac{\alpha_s P_{a' \rightarrow a}(z_u)}{2\pi \Gamma[1-2\epsilon]} \frac{|M_{a,b}^{(0)}|^2(\xi_u z_{a'}, \xi_b)}{-u}, \end{aligned} \quad (5.38)$$

where the parton momentum fractions are defined via the delta functions to be

$$z_{t,u} = \frac{t, u}{t, u - Q^2}. \quad (5.39)$$

For the process in question, the matrix elements above become

$$|M_{gg \rightarrow gH}^{(0)}|^2(\xi_a, z_t \xi_{b'}) = \frac{g^2 A^2 N_c (N_c^2 - 1)}{4(N_c^2 - 1)^2} \frac{M^8 + (z_t s)^4 + t^4 + \left(\frac{z_t s p_\perp^2}{t}\right)^4}{z_t^2 s^2 p_\perp^2}, \quad (5.40)$$

while the splitting kernel $P_{g \rightarrow g}(z_t)$ is

$$P_{g \rightarrow g}(z_t) = \frac{(1 + (1 - z_t)^4 + z_t^4)}{z_t (1 - z_t)_+} + \beta_0 \delta(1 - z_t). \quad (5.41)$$

The second term in (5.38) is related to this one by $u \leftrightarrow t$.

The entire pole behavior of the matrix element may be expressed as

$$\begin{aligned}
s \frac{d\sigma}{dt du} &= \sigma_\epsilon \left\{ -\frac{1}{N_c \epsilon} \frac{P_{g \rightarrow g}^\epsilon(z_t)}{-t} \frac{M^8 + (z_t s)^4 + t^4 + (z_t s p_\perp^2/t)^4}{z_t^2 s^2 p_\perp^2} \right. \\
&\quad - \frac{1}{\epsilon} \left(\nu^{-\epsilon} \left(1 + \frac{\pi^2 \epsilon^2}{6} \right) - 1 \right) \frac{M^8 + (z_t s)^4 + t^4 + (z_t s p_\perp^2/t)^4}{z_t^2 s^2 p_\perp^2 Q^2} \\
&\quad \left. - \frac{1}{2} \left(\frac{11}{6} + \frac{67\epsilon}{18} \right) \frac{M^8 + (z_t s)^4 + t^4 + (z_t s p_\perp^2/t)^4}{z_t^2 s^2 p_\perp^2 Q^2} + (t \rightarrow u) \right\} \\
&\quad + \text{Reg.}, \tag{5.42}
\end{aligned}$$

where ‘‘Reg.’’ represents all of the remaining nonsingular (as $Q^2 \rightarrow 0$) pieces of the cross section. The functions $P_{g \rightarrow g}^\epsilon$ are defined to be

$$P_{g \rightarrow g}^\epsilon(z) = N_c \frac{(1 + z^4 + (1 - z)^4)}{z(1 - z)}. \tag{5.43}$$

This term, when multiplied by the $Q^{-2\epsilon}$ implicit in σ_ϵ , contains both soft and collinear poles. We must take care to extract the poles from this term, and cancel them accordingly. In addition, the term in the second line is also poorly behaved as $Q^2 \rightarrow 0$, although it is free of any collinear divergences.

In order to extract the infrared pole from the expression (5.42), so that we may cancel the remaining (collinear) pole against the Altarelli-Parisi expression (5.38), we make use of the identity

$$\left(\frac{1}{Q^2} \right)^{1+n\epsilon} = -\frac{1}{n\epsilon} (-\hat{t})^{-n\epsilon} \delta(Q^2) + \left(\frac{z_t}{-t} \right)^{1+n\epsilon} \left\{ \left(\frac{1}{1 - z_t} \right)_+ - n\epsilon \left(\frac{\ln(1 - z_t)}{1 - z_t} \right)_+ \right\}.$$

This allows us to write the pole term as

$$\begin{aligned}
s \frac{d\sigma}{dt du} &= \sigma_\epsilon \left\{ \left(\frac{\pi^2}{12} + \frac{1}{\epsilon^2} \left[1 + \frac{1}{2} \left(\frac{p_\perp^2}{-t} \right)^\epsilon \right] + \frac{\beta_0}{\epsilon N_c} + \frac{1}{2\epsilon} \frac{11}{6} \right) \times \right. \\
&\quad \left. \left(\frac{-t}{\mu^2} \right)^{-\epsilon} \delta(Q^2) \frac{M^8 + s^4 + t^4 + u^4}{s^2 p_\perp^2} \right\}
\end{aligned}$$

$$\begin{aligned}
& -\frac{1}{N_c \epsilon} \frac{P_{g \rightarrow g}(z_t)}{-t} \frac{M^8 + (z_t s)^4 + t^4 + (z_t s p_\perp^2 / t)^4}{z_t^2 s^2 p_\perp^2} \\
& + \frac{z_t}{-t} \left[\left(\frac{\log(1 - z_t)}{1 - z_t} \right)_+ - \log \left(-\frac{z_t \mu^2}{t} \right) \left(\frac{1}{1 - z_t} \right)_+ \right] \times \\
& \quad \frac{1}{N_c \epsilon} \frac{P_{g \rightarrow g}^{(0)}(z_t)}{-t} \frac{M^8 + (z_t s)^4 + t^4 + (z_t s p_\perp^2 / t)^4}{z_t^3 s^2 p_\perp^2} \\
& + \frac{z_t}{-t} \left[\left(\frac{\log(1 - z_t)}{1 - z_t} \right)_+ - \log \left(-\frac{z_t Q_\perp^4}{\mu^2 t} \right) \left(\frac{1}{1 - z_t} \right)_+ \right] \times \\
& \quad \frac{M^8 + (z_t s)^4 + t^4 + (z_t s p_\perp^2 / t)^4}{z_t^2 s^2 p_\perp^2} \\
& - \frac{1}{2} \frac{11}{6} \left(\frac{1}{1 - z_t} \right)_+ \frac{M^8 + (z_t s)^4 + t^4 + (z_t s p_\perp^2 / t)^4}{z_t s^2 p_\perp^2 (-t)} + (t \rightarrow u) \Big\} \\
& + \text{Reg.}, \tag{5.44}
\end{aligned}$$

where $P_{g \rightarrow g}(z)$ is the gluon splitting kernel, and

$$P_{g \rightarrow g}^{(0)}(z) = N_c \frac{1 + z^4 + (1 - z)^4}{z}. \tag{5.45}$$

The second line now cancels identically against the gluonic contribution to the Altarelli-Parisi counterterm; equation (5.38). The remainder is finite with the exception of the infrared pole proportional to the delta function. It should be noted that while this expression is now well behaved for any invariant mass Q^2 , it is poorly behaved as $p_\perp \rightarrow 0$.

5.5 Virtual Contribution

The second term that contributes to the NLO cross section is the one-loop virtual correction [42]. This expression contains both ultraviolet and soft divergences. The ultraviolet divergence cancels against the charge renormalization counterterm, whereas the soft divergence cancels against the soft divergence in the real contribution.

The complete 1-loop correction, including the ultraviolet renormalization piece, may be written as follows:

$$s \frac{d\sigma}{dt du} = 4\sigma_\epsilon \left(1 + \frac{\pi^2}{3}\right) U_\epsilon \frac{M^8 + s^4 + t^4 + u^4}{stu} + \frac{4}{3} \left(1 - \frac{n_f}{N_c}\right) \sigma_\epsilon \frac{s^2 p_\perp^2 M^2 + M^4 s (M^2 - s + p_\perp^2)}{s^2 p_\perp^2}. \quad (5.46)$$

In this expression, U_ϵ is the universal singular piece, which has been renormalized as described in Chapter 3 and Appendix B. Explicitly, it is

$$\begin{aligned} U_\epsilon = & -\frac{1}{\epsilon^2} \left[\left(\frac{\mu^2}{-t}\right)^\epsilon + \left(\frac{\mu^2}{-u}\right)^\epsilon + \left(\frac{\mu^2}{s}\right)^\epsilon \right] + \frac{\pi^2}{6} + \frac{11}{N_c} + \frac{3\beta_0}{\epsilon N_c} \\ & + \log\left(\frac{m_H^2}{s}\right)^2 + \log\left(\frac{m_H^2}{m_H^2 - t}\right)^2 + \log\left(\frac{m_H^2}{m_H^2 - u}\right)^2 \\ & - \log\left(\frac{s}{m_H^2}\right) \log\left(\frac{-t}{m_H^2}\right) - \log\left(\frac{s}{m_H^2}\right) \log\left(\frac{-u}{m_H^2}\right) - \log\left(\frac{-u}{m_H^2}\right) \log\left(\frac{-t}{m_H^2}\right) \\ & + 2\text{Li}_2\left(1 - \frac{m_H^2}{s}\right) + 2\text{Li}_2\left(\frac{m_H^2}{m_H^2 - t}\right) + 2\text{Li}_2\left(\frac{m_H^2}{m_H^2 - u}\right). \end{aligned} \quad (5.47)$$

In this expression, we have rewritten the dilogarithm functions Li_2 using several transformation formulae. The above expression is completely real over the physical range of the parameters.

5.6 Cancellation of Soft Singularities and Renormalization of Ultraviolet Singularities

When the contribution from the virtual matrix element (5.47) is combined with the term proportional to $\delta(Q^2)$ from (5.42), we find that all of the singular terms cancel, up to terms of order n_f , which we are neglecting. Therefore the finite remainder of

the cancellation of the soft singularities U_{reg} is

$$\begin{aligned}
U_{\text{reg}} = & +\frac{\pi^2}{3} + \frac{67}{18} + \frac{11}{N_c} + \frac{1}{2} \log\left(\frac{u}{t}\right)^2 + \frac{11}{12} \log\left(\frac{\mu^4}{sp_{\perp}^2}\right) \\
& + \log\left(\frac{m_H^2}{s}\right)^2 + \log\left(\frac{m_H^2}{m_H^2 - t}\right)^2 + \log\left(\frac{m_H^2}{m_H^2 - u}\right)^2 \\
& - \log\left(\frac{s}{m_H^2}\right) \log\left(\frac{-t}{m_H^2}\right) - \log\left(\frac{s}{m_H^2}\right) \log\left(\frac{-u}{m_H^2}\right) - \log\left(\frac{-u}{m_H^2}\right) \log\left(\frac{-t}{m_H^2}\right) \\
& + 2\text{Li}_2\left(1 - \frac{m_H^2}{s}\right) + 2\text{Li}_2\left(\frac{m_H^2}{m_H^2 - t}\right) + 2\text{Li}_2\left(\frac{m_H^2}{m_H^2 - u}\right) \\
& + O[n_f],
\end{aligned} \tag{5.48}$$

where we have set n_f equal to zero. To complete the cancellation of the soft poles, the soft singularities resulting from the process $gg \rightarrow Hq\bar{q}$ must be also included. This piece contributes the remaining $n_f/6$ piece required to cancel the (complete) β_0 pole.

For the present calculation, we will assume that these fermionic pieces do cancel, and that the finite remainder contributes very little to the overall cross section. With this simplification, we take $\beta_0 \rightarrow N_c 11/6$, and the pole cancellation is complete. While this will probably give us a very good approximation to the cross section, the gluon initiated process $gg \rightarrow Hq\bar{q}$ is probably of the same order of magnitude as the pure gluonic process [43], and must eventually be included in a complete analysis.

5.7 Numerical Procedure and Results

In order to generate a transverse-momentum spectrum that may be observed in nature, we must numerically evaluate the convolutions of the preceding quantities with the parton distribution functions. We choose to use the CTEQ5 structure functions [34]. The convolutions of the matrix elements with these structure functions must be evaluated numerically. We use a simple Gaussian integration routine, as found in

Numerical Recipes for C [44].

With this code, we may generate the differential cross section for any transverse momentum or rapidity (assuming of course that these are kinematically allowed). The process is to be plotted as observed at the LHC, a proton-proton collider running at a COM energy of $\sqrt{S} = 14$ TeV. Unless otherwise stated, we shall use a Higgs mass of 115 GeV in our evaluations.

The leading order cross section, when shown, was computed using the CTEQ5L distributions, together with the leading order definition of α_s . The next-to-leading order cross section will always be computed using the NLO definitions of the CTEQ PDF's, namely the CTEQ5M1 distributions. In particular, we have taken care to define the K factor as it is traditionally defined, as the ratio of the NLO cross section (with NLO PDF's and α_s) to the LO cross section (with LO PDF's and α_s). Also, all contributions involving quarks have been ignored in this calculation ¹. We do however, keep $n_f = 5$ in the parton distributions and the strong coupling α_s .

We shall begin with a discussion of the transverse momentum spectrum, focusing on how it differs from the leading order behavior. Then, the scale dependence is addressed. We close by looking at the dependence on rapidity and the behavior of the cross section at small transverse momentum.

5.7.1 p_\perp Spectrum and the K Factor

Theoretically, the dramatic scale dependence of the cross section at LO should be reduced significantly at NLO. Figure 5.1 shows the cross section at NLO superimposed over the cross section at leading order over a wide range of rapidity. We have chosen to plot bands in this case in which the scale has been varied from $.5m_\perp \rightarrow 2m_\perp$. The leading order graph (light grey) clearly varies more over the chosen scale range

¹For the sake of consistency, we use only the gluon-initiated graphs in the LO piece.

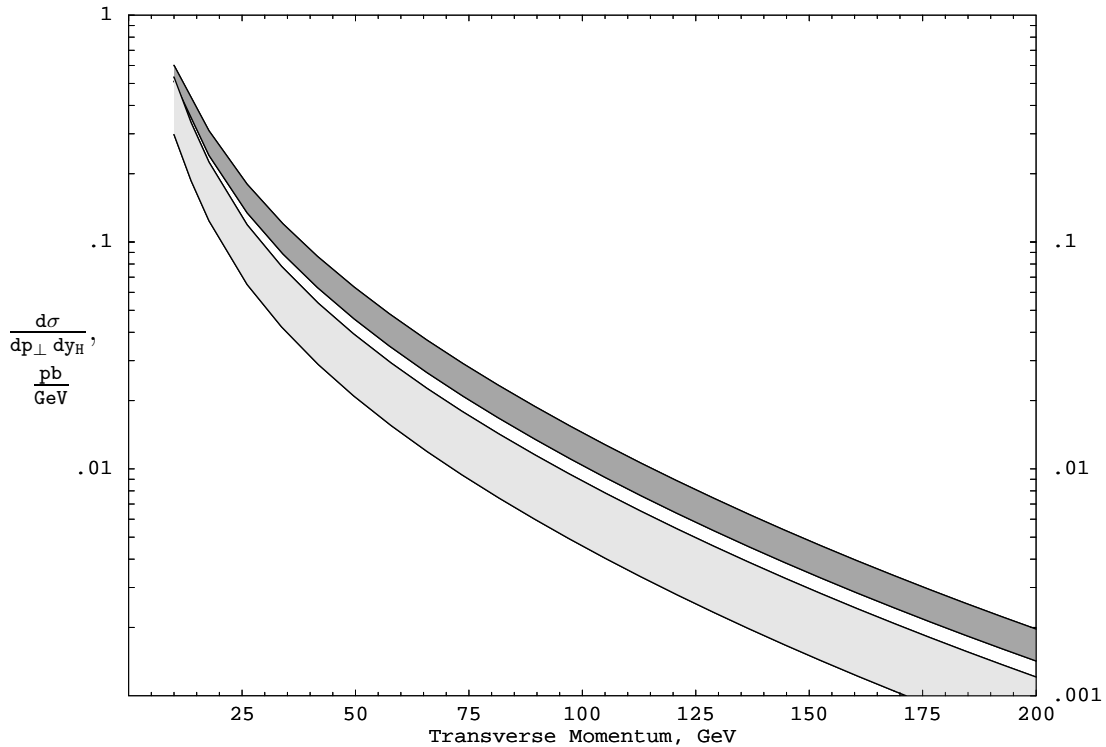


Figure 5.1: Variation of the p_{\perp} spectrum with scale

than the next-to-leading order graph. Again, this improvement is exactly what one expects for an NLO calculation, as the scale dependence represents the theoretical uncertainty in the calculation. As we improve our calculation order-by-order in QCD, our dependence on this artificial parameter should decrease.

The graph of Figure 5.2 displays the dependence of the next-to-leading-order cross section on scale (dashed line) compared with the scale dependence of the leading-order calculation (solid line). We display the ratio of the cross section at a scale $\mu = \lambda m_{\perp}$, normalized to the cross section for $\lambda = 1$. The quantity plotted, then, is basically the fractional uncertainty in each distribution which is purely due to theory.

As can be plainly seen in the graph, the leading order cross section increases monotonically as $\lambda \rightarrow 0$, whereas the NLO cross section appears to be approaching a peak around $d\sigma/d\sigma_0 = 1.4$. Eventually, the NLO graph will turn over and begin

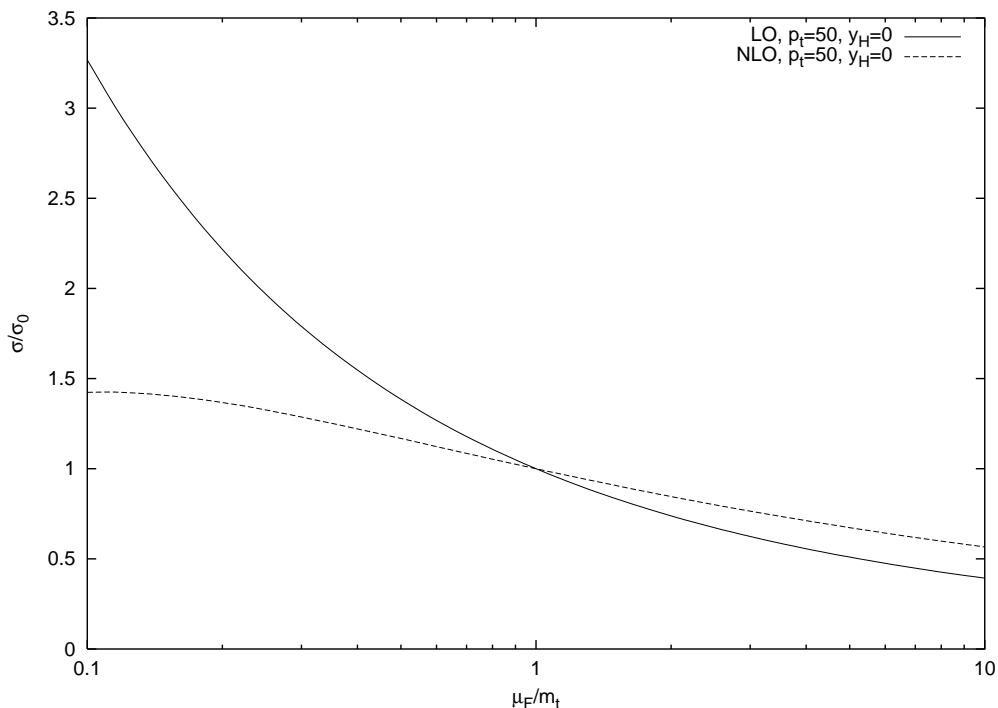


Figure 5.2: Scale dependence at $p_{\perp} = 50\text{GeV}$

to drop to zero as the scale approaches Λ_{QCD} . However, it is very clear the NLO calculation represents a dramatic improvement in the theoretical uncertainty due to scale dependence. For instance, for a typical range $.5 < \lambda < 2, 0$, the leading order cross section varies from 75% to 140% of the $\lambda = 1$ value, whereas the NLO cross section only varies from 85% to 115%.

In looking at Figure 5.1, it is clear that the enhancement over the leading order approximation is very significant. The graph of the NLO cross section divided by the LO cross section (called the *K Factor*) is, perhaps more interesting, since it entails explicitly the magnitude of these corrections relative to the LO approximation. This is displayed in Figure 5.3.

The *K Factor* as a function of p_{\perp} is fairly flat down to about 25 GeV, where it begins a dramatic decline. This is to be expected, since for small p_{\perp} , the NLO p_{\perp} spectrum behaves roughly like $\log^3(p_{\perp}/m_H)/p_{\perp}^2$, which diverges to negative infinity, while the leading order expression goes to positive infinity for small p_{\perp} .

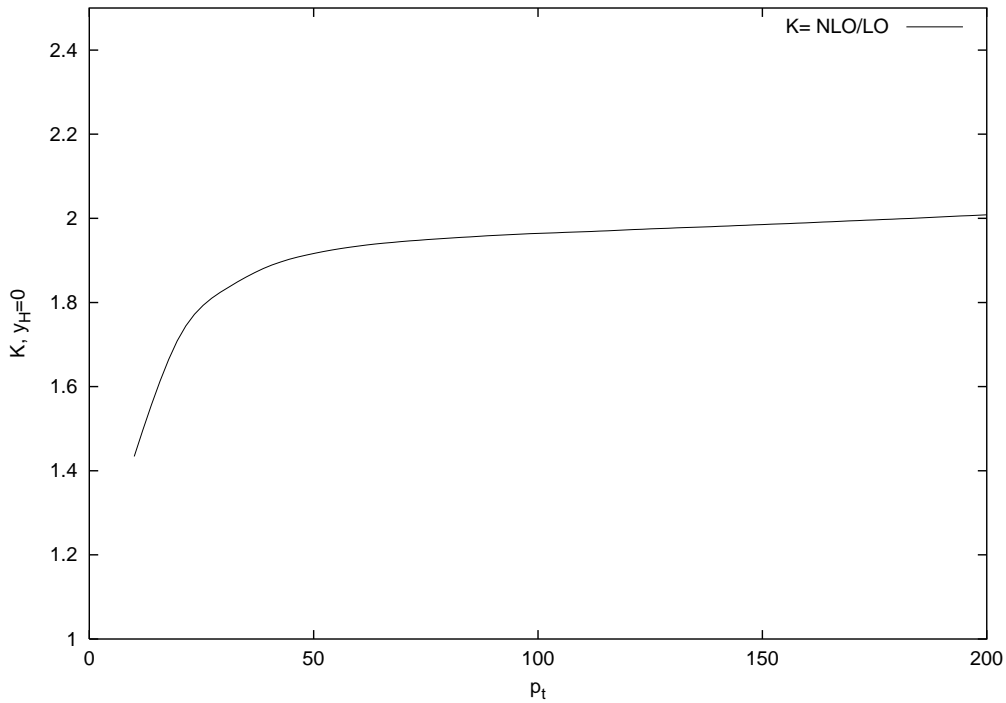


Figure 5.3: K factor at the LHC ($\sqrt{S} = 14 \text{ TeV}$)

We should note that our expression disagrees substantially with the previous Monte Carlo calculation [36]. Whereas their K factor is about 1.5, ours is roughly 1.9. The most likely reason for this discrepancy is that we have not included the quark graphs in our calculation, whereas the Monte Carlo calculation has these pieces included. It should be noted that our K factor is computed at $y_H = 0$, whereas the Monte Carlo calculation integrates over y_H . As we shall soon see, the K factor appears to exhibit a minimum at $y_H = 0$, and therefore the integral over rapidity is unlikely to be the source of the disagreement. Were we to compute the integrated K factor, it would most likely disagree by an even wider margin. However, before claiming a discrepancy with the calculation in reference [36], we must include the quark pieces in our calculation, or at least establish that their contribution is non-negative.

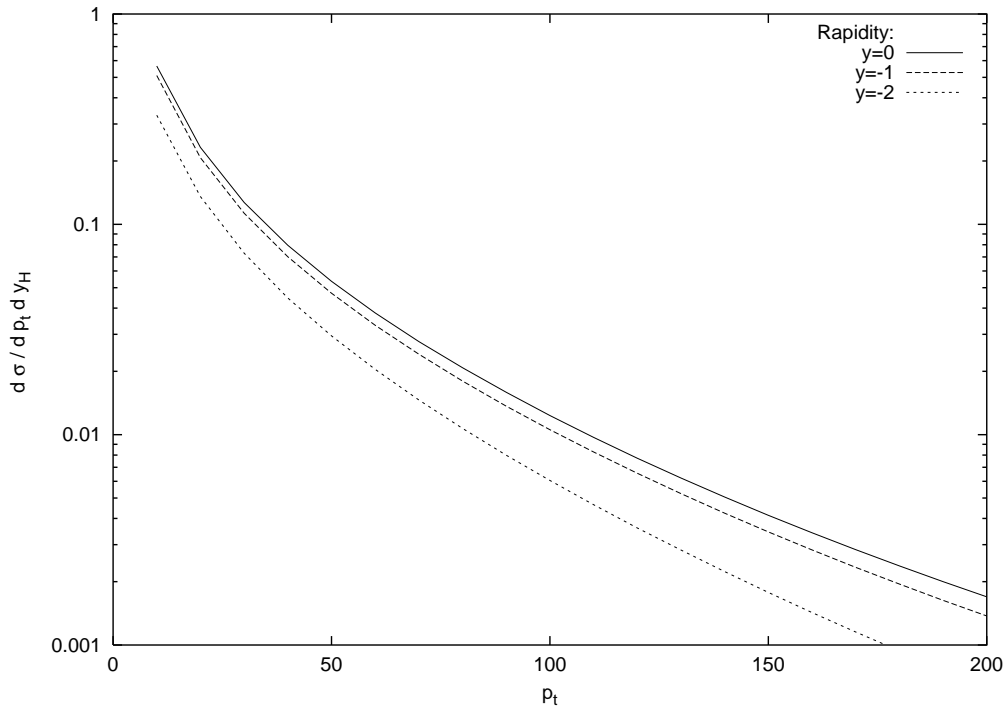


Figure 5.4: NLO Higgs p_{\perp} spectrum at the LHC ($\sqrt{S} = 14$ TeV) for various values of the Higgs rapidity, y_H

5.7.2 Rapidity Spectrum

Kinematically, it is simply less probable to produce a massive particle at large rapidity unless the transverse momentum is small. Therefore, the cross section should fall off rapidly for large rapidity. Figure 5.4 is a graph of the complete p_{\perp} spectrum at next-to-leading order for various rapidities, $y_H = 0, 1, 2$, which are the solid, dashed, and dotted lines respectively. The graphs indeed decrease rapidly as the absolute value of the rapidity is increased.

Figure 5.5 is a plot of the complete next-to-leading order rapidity spectrum at the LHC for p_{\perp} values of 50 GeV and 100 GeV. This graph displays the classic peak at $y_H = 0$, and rapidly drops to zero as the edges of accessible phase space is approached. That is, the maximum rapidity of a Higgs Boson is governed by

$$(p_{\perp} + m_{\perp}) \exp |y_H| < \sqrt{S} \quad (5.49)$$

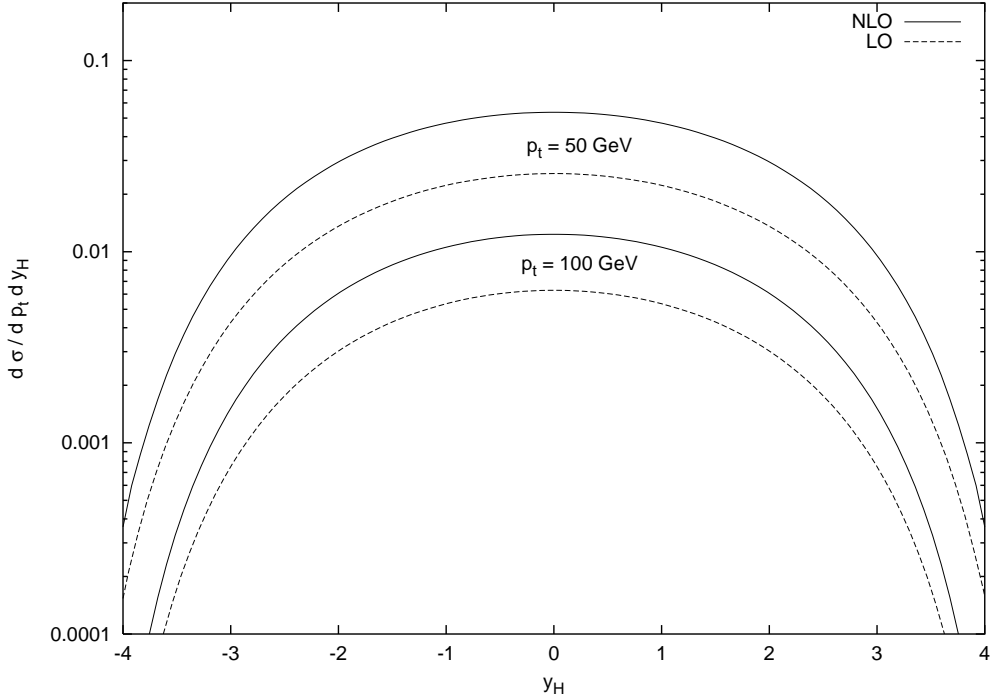


Figure 5.5: Rapidity Spectrum at the LHC ($\sqrt{S} = 14$ TeV). The dotted lines are the leading order calc, and the solid lines are the NLO calc.

beyond which it is kinematically forbidden to produce a Higgs.

The rapidity dependence of the K factor is plotted in Figure 5.6. The first thing to note is that the graph is very flat as a function of rapidity, indicating that the phase space limitations more or less govern the shape of this graph. Also, note the minimum that we mentioned earlier at $y_H = 0$, indicating that an integral over the rapidity will further enhance our expression for the K factor. Were we to integrate over y_H , this would most likely increase our K factor slightly. Again, this is interesting due to our disagreement with [36].

5.7.3 Small p_{\perp} Behavior

The transverse momentum spectrum calculation at any fixed order in perturbation theory is poorly behaved for very small p_{\perp} , as it is dominated by logarithms of the

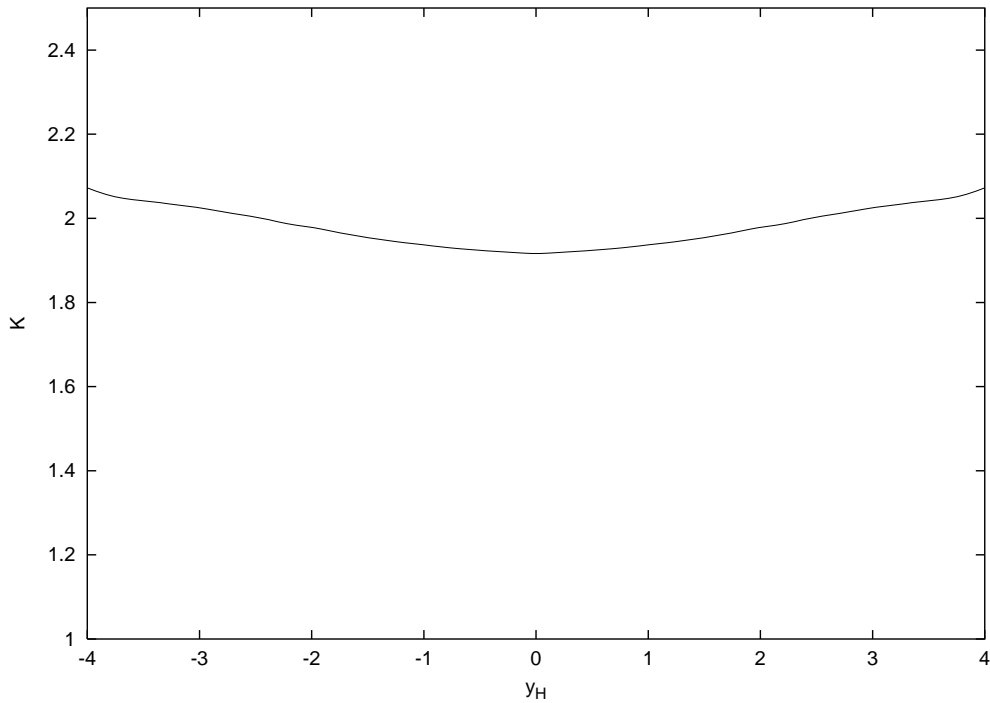


Figure 5.6: Rapidity dependence of the K factor ($\sqrt{S} = 14 \text{ TeV}$)

transverse momentum divided by the Higgs mass in this limit. At each order in perturbation theory, the coefficient of the leading divergence changes sign, therefore rendering the predictive power of traditional perturbation theory useless in this limit.

For our calculation, we expect to see exactly this. The cross section should display a peak in the small p_\perp region, after which the cross section starts to diverge to negative infinity. We expect that our calculation will be a fairly good approximation beyond this peak.

Our plot, Figure 5.7, of the small p_\perp region displays just this behavior (dotted line). Again we have superimposed the leading order calculation (solid line) as a reference. Our calculation displays a prominent peak around 2.1 GeV for our standard choice of the Higgs mass, 115 GeV.

If one wishes to have a good prediction of the cross section in the small p_\perp region, one may resum the large logarithmic behavior via the techniques developed

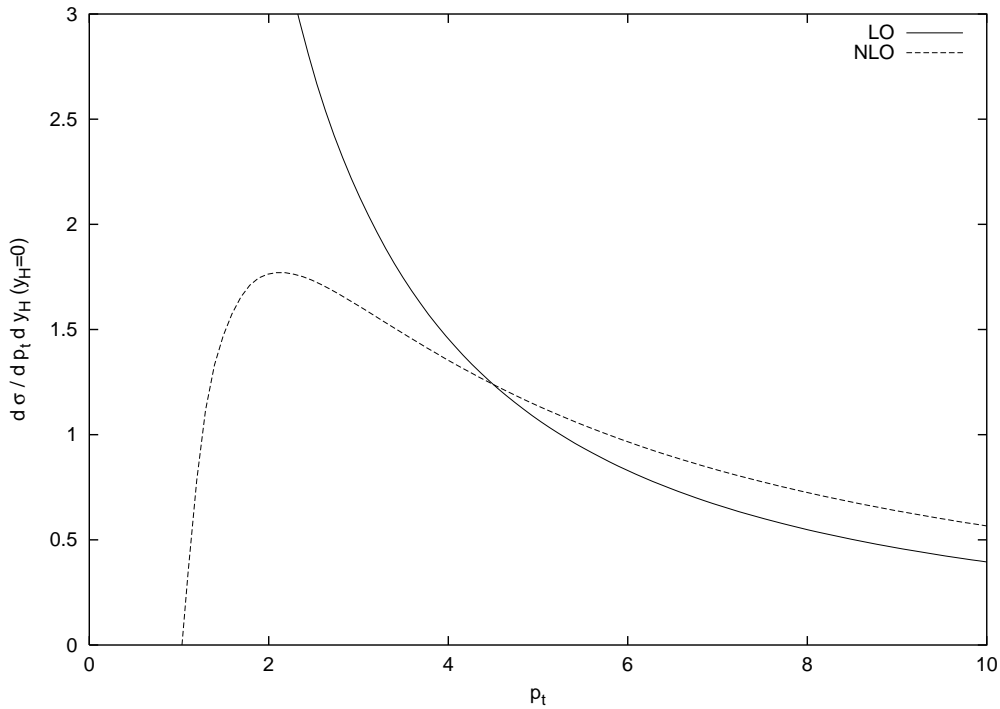


Figure 5.7: Small p_{\perp} dependence of the cross section, $y_H = 0$.

by Collins, and Soper [45], and Sterman [46]. The first order of business for a calculation of this nature would be to expand our analytic result, and extract the $B^{(2)}$ resummation coefficient. This could then be used to verify the result of reference [37]. In order to have a complete small transverse momentum calculation, one needs to analytically calculate the contributions from the process $gg \rightarrow q\bar{q}H$ in the small p_{\perp} limit.

This work is a major part of a larger calculation. Whereas we have the dominant part of the cross section, the gluonic piece, completed, we need the quark contributions to have a complete and reliable prediction. One also wishes to have a reliable calculation at small transverse momentum, which involves calculating the resummation coefficient mentioned above. Including the quarks is work in progress, as is the computation of the resummation coefficient from the asymptotic expansion of our analytic results.

Chapter 6

Conclusions

In this work we have seen how the Standard Model of particle physics, while close to being complete from a phenomenological standpoint, still lacks a crucial piece, the Higgs Boson. The advent of the LHC, which in effect will be a “Higgs factory”, will allow us to study this component of the SM in considerable detail. If we are to understand the mechanism behind electroweak symmetry breaking, we must understand the behavior of a pure Standard Model Higgs as much as possible.

One of the most important properties to understand is the transverse momentum spectrum of the Higgs at the LHC. Primarily, one needs to know what to expect in a detector as far as the decay product energies, among other things. Since higher order corrections to p_{\perp} spectra from QCD radiation tend to be quite significant, one may not consider the LO process to be reliable.

As we have seen, the results herein have verified that perturbative corrections to the Higgs boson transverse momentum spectrum are very significant. The terms that we have calculated enhance the cross section by a factor of approximately 2 in the large transverse momentum region. In addition, we find that the theoretical uncertainty due to varying the renormalization scale is far less than the leading order

result, indicating, that our calculation is more reliable. This result also agrees with the expected asymptotic behavior in the small p_{\perp} region, and agrees qualitatively with the Monte Carlo calculation by DeFlorian et.al. [36]. In order to precisely compare their the results with this calculation, the NLO quark terms, which have been neglected, must be included.

In the next ten to twenty years, much will change as to our understanding of the fundamental building blocks of nature. In particular, many clues to the fundamental phenomenon behind electroweak symmetry breaking lie in wait to be uncovered. The discovery of the phenomenon behind the electroweak symmetry breaking mechanism will probably be the first significant increase in our understanding of particle physics since the development of the Standard Model in the 1970's. Discovering the Higgs, and understanding its properties, is the first crucial step.

Appendix A

Matrix Elements

In this appendix, we include the expressions for the (unintegrated) matrix elements for the $2 \rightarrow 2$ and $2 \rightarrow 3$ gluonic parton processes, computed in the large quark mass limit. Moreover, we include the expressions for the $2 \rightarrow 2$ process $H \rightarrow gq\bar{q}$, so that the complete leading-order transverse momentum spectrum may be computed in the large m_{top} limit. $H \rightarrow ggg$ and $H \rightarrow gq\bar{q}$ amplitudes have been known in the literature for a while [33, 26], as have the expressions entailing the process $H \rightarrow gggg$ [47]. Moreover, the amplitudes for the virtual corrections to the $2 \rightarrow 2$ partonic processes $H \rightarrow ggg$ and $H \rightarrow gq\bar{q}$ may be found in reference [42]. For simplicity, we give the matrix elements for all particles, except the Higgs, in the final state. The matrix elements relevant to our calculation can be obtained from these by crossing symmetry.

Since we will be using color-ordered helicity amplitudes in our calculation we will begin by reviewing the standard notation and identities associated with the decomposition of QCD amplitudes into color-ordered, gauge-invariant subamplitudes. We will then present the matrix elements relevant to this calculation in their entirety.

A.1 Helicity Amplitudes

We begin by presenting the standard notation used in calculations of amplitudes, and list a series of identities useful in simplifying these same amplitudes ¹. We introduce the following notation for (massless) Dirac spinors,

$$u_{\pm}(p) = |p_{\pm}\rangle. \quad (\text{A.1})$$

In addition, we shall use the following notation for spinor products,

$$\bar{u}_-(p)u_+(q) = \langle p - |q+\rangle = \langle pq\rangle, \quad (\text{A.2})$$

$$\bar{u}_+(p)u_-(q) = \langle p + |q-\rangle = [pq]. \quad (\text{A.3})$$

The momenta p, q are assumed to be massless, and therefore these may also be identified with relativistically invariant chirality states.

The polarization vectors of the gluons are parameterized in a dual basis [21, 22]

$$\epsilon(p, k)_{\pm}^{\mu} = \frac{1}{\sqrt{2}} \frac{\langle k \pm | \gamma^{\mu} | p_{\pm} \rangle}{\langle p \mp | k_{\pm} \rangle}, \quad (\text{A.4})$$

where p is the momentum of the gluon, and k is some arbitrary massless reference vector.

Products of these spinors are found to satisfy the following identities (for massless p, q):

$$\langle pq\rangle [qp] = 2p \cdot q \quad (\text{A.5})$$

$$\langle pq\rangle^* = \text{sgn}(p \cdot q) [qp] \quad (\text{A.6})$$

¹Those who are new to helicity spinor techniques will find references [19] useful.

$$\frac{(1 \pm \gamma_5)}{2} \not{p} = |p_{\pm}\rangle \langle p_{\pm}|. \quad (\text{A.7})$$

From this last relation, we see that we may derive the following identity,

$$\langle +p_1 | -p_2 \rangle \langle -p_2 | +p_3 \rangle \langle +p_3 | -p_4 \rangle \dots \langle -p_n | +p_1 \rangle = \frac{1}{2} \text{Tr} \{ (1 + \gamma_5) \not{p}_1 \not{p}_2 \not{p}_3 \not{p}_4 \dots \not{p}_n \}. \quad (\text{A.8})$$

This last relation is particularly useful in computing absolute squares of matrix elements, and converting them into traces over products of gamma matrices.

A.2 Real Contributions

In order to calculate the p_{\perp} spectrum to next-to-leading order, we need to write down all the separate partonic contributions to this process. They can be broken up into three separate terms; the *leading order* or tree-level process which consists of Higgs to 3-partons, the *virtual* or 1-loop correction to this process, and the 4-parton process, which we refer to as the *real corrections*. The (unintegrated) expressions for these have been computed in works outlined below.

One may compute the *spin- and color-averaged* matrix element squared by simply summing over colors, adding up the 2^N spin terms, then dividing by the number of spins and colors of the particles in the initial state. That is, if $N_{a,b}$ are the number of spins and $C_{a,b}$ are the number of colors of the initial-state partons a and b , then

$$\overline{|M(a, b; 1, 2, \dots, n)|^2} = \frac{1}{C_a C_b N_a N_b} \sum |M(a^{\lambda_a}, b^{\lambda_b}; 1^{\lambda_1}, 2^{\lambda_2}, \dots, n^{\lambda_n})|^2, \quad (\text{A.9})$$

where the λ_i represent the helicity of particle i , and the sum is implicitly over the spins and colors, unless noted otherwise. Generally, the amplitudes for the process

involving initial state partons may be computed using crossing symmetry, and being careful to note that certain terms can pick up a sign via equation (A.6).

A.2.1 $H \rightarrow ggg$

We shall begin by writing down our expressions for the Higgs production matrix elements. The matrix element with the full ϵ -dependence was first computed by S. Dawson [26]. It is fairly straightforward to compute from the conventional Feynman rules (together with the non-conventional ones from our low energy Higgs model).

There are 2 independent subprocesses that contribute to the leading-order expression. The $H \rightarrow ggg$ piece is given by

$$M(1^+, 2^+, 3^+) = \frac{gA f_{abc} M_H^4}{\sqrt{2} \langle 12 \rangle \langle 23 \rangle \langle 31 \rangle}, \quad (\text{A.10})$$

$$M(1^-, 2^+, 3^+) = \frac{gA f_{abc} [23]^3}{\sqrt{2} [12] [13]}. \quad (\text{A.11})$$

The remaining contributions may be obtained through parity and charge conjugation operations. If we sum this over spins and colors, we find

$$\sum |M(H \rightarrow ggg)|^2 = \frac{g^2 A^2 N_c (N_c^2 - 1)}{S_{12} S_{13} S_{23}} (S_{12}^4 + S_{13}^4 + S_{23}^4 + M_H^8). \quad (\text{A.12})$$

The remaining subprocess that we will consider for the leading-order transverse momentum spectrum is $H \rightarrow q\bar{q}g$. The matrix element for this subprocess is given by

$$M(1^+, 2^-, 3^+) = -\frac{igT_{ij}^a A [13]^2}{\sqrt{2} [12]}. \quad (\text{A.13})$$

This may be also be easily summed over spins and colors

$$\sum |M(H \rightarrow gq\bar{q})|^2 = \frac{g^2 A^2 (N_C^2 - 1) u^2 + t^2}{4 s}. \quad (\text{A.14})$$

It should be noted that each of these amplitudes were computed using the conventional normalization for the SU(3) generators, $\text{Tr}[T_a T_b] = \frac{1}{2} \delta_{ab}$.

A.2.2 $H \rightarrow gggg$

In order to facilitate the calculation, it is beneficial to break up the subamplitude into color-ordered *helicity subamplitudes*

$$M(1^{\lambda_1}, 2^{\lambda_2}, 3^{\lambda_3}, 4^{\lambda_4}) = 2A g^2 \sum_{\text{colors}} \text{Tr}[T^a T^b T^c T^d] m(1^{\lambda_1}, 2^{\lambda_2}, 3^{\lambda_3}, 4^{\lambda_4}). \quad (\text{A.15})$$

These amplitudes are cyclically symmetric in the colors, they are invariant under reversal of the color indices, and they satisfy the dual Ward Identities [19]. There are three independent helicity subamplitudes for this process:

$$m(1^+, 2^+, 3^+, 4^+) = \frac{M_{\text{H}}^4}{\langle 12 \rangle \langle 23 \rangle \langle 34 \rangle \langle 41 \rangle}, \quad (\text{A.16})$$

$$m(1^-, 2^+, 3^+, 4^+) = -\frac{\langle 1 - \not{p}_{\text{H}} | 3^- \rangle^2 [24]^2}{S_{124} S_{12} S_{14}} - \frac{\langle 1 - \not{p}_{\text{H}} | 4^- \rangle^2 [23]^2}{S_{123} S_{12} S_{23}} - \frac{\langle 1 - \not{p}_{\text{H}} | 2^- \rangle^2 [34]^2}{S_{134} S_{14} S_{34}} + \frac{[24]}{[12] \langle 23 \rangle \langle 34 \rangle [41]} \left\{ S_{23} \frac{\langle 1 - \not{p}_{\text{H}} | 2^- \rangle}{\langle 41 \rangle} + S_{34} \frac{\langle 1 - \not{p}_{\text{H}} | 4^- \rangle}{\langle 12 \rangle} - [24] S_{234} \right\}, \quad (\text{A.17})$$

$$(\text{A.18})$$

and

$$m(1^-, 2^-, 3^+, 4^+) = -\frac{\langle 12 \rangle^4}{\langle 12 \rangle \langle 23 \rangle \langle 34 \rangle \langle 41 \rangle} - \frac{[34]^4}{[12][23][34][41]}. \quad (\text{A.19})$$

The remaining terms can be related to these by using the charge conjugation and time reversal transformations, and the dual Ward identities.

A.3 Virtual

The expression for the virtual $H \rightarrow ggg$ amplitude was calculated in reference [42]. We define the amplitudes in precisely the same way that we defined the leading-order pieces, in terms of helicity amplitudes. The resulting expressions are then related to the leading-order amplitudes via a coefficient. These are outlined in the following subsections. To construct the contribution to the amplitude squared, use the formula

$$|M^{(0)} + M^{(1)}|^2 = \sum_{\text{spins}} |M^{(0)}|^2 + 2 \sum_{\text{spins}} \text{Re}[M^{(0)} (M^{(1)})^*] + \dots \quad (\text{A.20})$$

In this expression, $M^{(0)}$ and $M^{(1)}$ represent generic LO and 1-loop amplitudes. For clarity, the spin dependence has been suppressed in this equation.

A.3.1 $H \rightarrow ggg$

The expressions for the virtual $H \rightarrow ggg$ subamplitudes are

$$\begin{aligned} M^{(1)}(1^+, 2^+, 3^+) &= M^{(0)}(1^+, 2^+, 3^+) \frac{\alpha_s}{4\pi} r_\Gamma \left(\frac{4\pi\mu^2}{-M_H^2} \right)^\epsilon \left[N_c U \right. \\ &\quad \left. + \frac{1}{3}(N_c - n_f) \frac{S_{31}S_{23} + S_{31}S_{12} + S_{12}S_{23}}{M_H^4} \right] \\ M^{(1)}(1^-, 2^+, 3^+) &= M^{(0)}(1^-, 2^+, 3^+) \frac{\alpha_s}{4\pi} r_\Gamma \left(\frac{4\pi\mu^2}{-M_H^2} \right)^\epsilon \left[N_c U \right. \\ &\quad \left. + \frac{1}{3}(N_c - n_f) \frac{S_{31}S_{12}}{S_{23}^2} \right], \end{aligned} \quad (\text{A.21})$$

where the prefactor is

$$r_\Gamma = \frac{\Gamma(1+\epsilon)\Gamma^2(1-\epsilon)}{\Gamma(1-2\epsilon)} = \frac{\Gamma(1-\epsilon)}{\Gamma(1-2\epsilon)} \left(1 + \epsilon^2 \frac{\pi^2}{3} \right), \quad (\text{A.22})$$

and

$$\begin{aligned}
U = & \frac{1}{\epsilon^2} \left[- \left(\frac{-M_H^2}{-S_{12}} \right)^\epsilon - \left(\frac{-M_H^2}{-S_{23}} \right)^\epsilon - \left(\frac{-M_H^2}{-S_{31}} \right)^\epsilon \right] + \frac{\pi^2}{2} \\
& - \ln \left(\frac{-S_{12}}{-M_H^2} \right) \ln \left(\frac{-S_{23}}{-M_H^2} \right) - \ln \left(\frac{-S_{12}}{-M_H^2} \right) \ln \left(\frac{-S_{31}}{-M_H^2} \right) - \ln \left(\frac{-S_{23}}{-M_H^2} \right) \ln \left(\frac{-S_{31}}{-M_H^2} \right) \\
& - 2 \operatorname{Li}_2 \left(1 - \frac{S_{12}}{M_H^2} \right) - 2 \operatorname{Li}_2 \left(1 - \frac{S_{23}}{M_H^2} \right) - 2 \operatorname{Li}_2 \left(1 - \frac{S_{31}}{M_H^2} \right). \tag{A.23}
\end{aligned}$$

It should be noted that all of the singular behavior (including as $p_\perp \rightarrow 0$) is contained within terms proportional to U .

Since we are working with an effective theory, we obtain a finite renormalization at each order of perturbation theory,

$$M^{(1)} \rightarrow M^{(1)} + (\Delta + 3\delta_g) M^{(0)}, \tag{A.24}$$

where Δ is the finite renormalization of the effective Hgg operator, at this order in perturbation theory, and δ_g is the gauge-coupling counterterm. Using the $\overline{\text{MS}}$ subtraction scheme, the counterterm is

$$\delta_g = -\frac{1}{\epsilon} \frac{\alpha_s}{4\pi} \Gamma(1 + \epsilon) (4\pi)^\epsilon \left[\frac{11N_c}{6} - \frac{n_f}{3} \right], \tag{A.25}$$

and the finite renormalization coefficient is

$$\Delta = 11 \left(\frac{\alpha_s}{2\pi} \right). \tag{A.26}$$

Appendix B

Formulas for Angular Integration

In this appendix, we give detailed formulas for the angular integration of all the terms appearing in the partial-fractioned matrix element. There are two different cases:

- when the two invariants involve massless particles, and
- when one of the invariants contains a mass term.

Momentum conservation may be used to reduce all of the matrix elements into sums of terms of this form, multiplied by a coefficient which has no angular dependence.

B.1 General Expression for terms of the form $\frac{1}{S_{13}^m S_{23}^n}$

We begin by evaluating integrals involving two massless invariants. There are two forms that occur, and these are related by a $\nu \rightarrow (1 - \nu)$ symmetry:

$$\Omega^{(m,n)}(\nu) = S_u^m S_t^n \int d\Omega^{(\epsilon)} \frac{1}{S_{13}^m S_{24}^n}, \quad (\text{B.1})$$

$$\Omega^{(m,n)}(1 - \nu) = S_u^m S_t^n \int d\Omega^{(\epsilon)} \frac{1}{S_{13}^m S_{23}^n}. \quad (\text{B.2})$$

We recall the explicit definition of ν ,

$$\begin{aligned}\nu &= \frac{1}{2}(1 - \cos(\theta_0)) \\ &= \frac{Q^2}{Q_\perp^2}.\end{aligned}\tag{B.3}$$

Those that involve the other combinations of the invariants are related to these via the freedom to relabel the final state parton indices, that is exchange $3 \leftrightarrow 4$.

First, we evaluate the phase space in the Q^2 rest frame. Then without losing any generality, we perform this integration assuming that the invariant S_{13} is independent of the azimuthal angle ϕ . The following definitions are useful:

$$\omega_{13} = S_{13}/(S_{13} + S_{14}),\tag{B.4}$$

$$= S_{13}/S_u,\tag{B.5}$$

$$\omega_{14} = S_{14}/(S_{13} + S_{14}),\tag{B.6}$$

$$= S_{14}/S_u,\tag{B.7}$$

$$\omega_{23} = S_{23}/(S_{23} + S_{24}),\tag{B.8}$$

$$= S_{23}/S_t,\tag{B.9}$$

$$\omega_{24} = S_{24}/(S_{23} + S_{24}),\tag{B.10}$$

$$= S_{24}/S_t.\tag{B.11}$$

Taking the gluon a to lie along the z axis, we find

$$\omega_{13} = \frac{1}{2}(1 - \cos(\theta_{13})),\tag{B.12}$$

and

$$\omega_{23} = \frac{1}{2}(1 - \cos(\theta_0) \cos(\theta) - \sin(\theta_0) \sin(\theta) \cos(\phi)).\tag{B.13}$$

The integrals (B.2) become

$$\Omega^{(m,n)}(\nu) = \int d\Omega^{(-\epsilon)} \omega_{13}^{-m} \omega_{24}^{-n} \quad (\text{B.14})$$

$$\Omega^{(m,n)}(1-\nu) = \int d\Omega^{(-\epsilon)} \omega_{13}^{-m} \omega_{23}^{-n}. \quad (\text{B.15})$$

These may be evaluated in general in terms of hypergeometric functions [48]. The explicit expression (for arbitrary ϵ) is

$$\Omega^{(m,n)}(\nu) = \frac{\Gamma^2(1-\epsilon)}{\Gamma(1-2\epsilon)} \frac{\Gamma(1-n-\epsilon)\Gamma(1-m-\epsilon)}{\Gamma(2-n-m-2\epsilon)} F_{1,2}(m, n, 1-\epsilon, 1-\nu). \quad (\text{B.16})$$

One may easily prove that the relations for $3 \leftrightarrow 4$ yield precisely the same result.

B.2 Expressions for terms of the form $\frac{1}{S_{13}^n S_{123}^m}$

For these expressions, a considerable simplification is attained if one rotates the preceding frame so that the Higgs momentum lies in the direction of the z axis. In the Q^2 rest frame, this is equivalent to a frame where $\mathbf{a} + \mathbf{b} = \hat{z} |\mathbf{a} + \mathbf{b}|$. The rotation angle is then given by

$$\cos(\chi) = \frac{-B}{\sqrt{B^2 + C^2}}, \quad (\text{B.17})$$

and therefore the invariant $S_{123(4)}$ is given by

$$S_{123(4)} = A \mp \sqrt{B^2 + C^2} \cos \theta_H, \quad (\text{B.18})$$

where we have defined

$$A = \frac{1}{2}(2s + S_u + S_t), \quad (\text{B.19})$$

$$B = \frac{1}{2}(S_u + S_t \cos \theta_0), \quad (\text{B.20})$$

$$C = \frac{1}{2}(S_u + S_t \cos \theta_0). \quad (\text{B.21})$$

The kinematic invariants S_{13} , etc. take on the requisite form

$$S_{13} = \frac{S_u}{2} (1 - \cos \chi \cos \theta_H - \sin \chi \sin \theta_H \cos \phi), \quad (\text{B.22})$$

$$S_{23} = \frac{S_t}{2} (1 - \cos \chi \cos \theta_H - \sin \chi \sin \theta_H \cos \phi). \quad (\text{B.23})$$

$$(\text{B.24})$$

where the other terms are related by $B \rightarrow -B$.

We therefore seek to evaluate expressions of the form

$$\Omega_H^{n,m} = \int d\Omega S_{13}^{-n} S_{123}^{-m}. \quad (\text{B.25})$$

All of the other angular form factors may be obtained from these by either exchanging $B \leftrightarrow -B$ or $u \leftrightarrow t$. Their explicit expressions are (to $O[\epsilon^0]$)

$$\Omega_H^{1,1} = \frac{1}{A + B' \cos \chi} \Omega_\epsilon^{0,1}(\nu) + \left(\frac{1}{2a}\right) \frac{1}{A + B' \cos \chi} \log \frac{(A + B' \cos \chi)^2}{A^2 - B'^2} \quad (\text{B.26})$$

$$\Omega_H^{2,1} = \frac{1}{(A + B' \cos \chi)^2} \Omega_\epsilon^{0,1}(\nu) + \left(\frac{1}{2a}\right) \frac{1}{(A + B' \cos \chi)^2} \times \left[\log \frac{(A + B' \cos \chi)^2}{A^2 - B'^2} + \frac{2B'^2 + 2AB' \cos \chi}{A^2 - B'^2} \right] \quad (\text{B.27})$$

$$\Omega_H^{1,2} = \frac{1}{A + B' \cos \chi} \left[\Omega_\epsilon^{0,2}(\nu) + \left(\frac{AB' \cos \chi + B'^2}{(A + B' \cos \chi)^2}\right) \frac{\Omega_\epsilon^{0,1}(\nu)}{a} \right] \quad (\text{B.28})$$

$$+ \frac{1}{2a^2} \left[\frac{AB' \cos \chi + B'^2}{(A + B' \cos \chi)^3} \log \frac{(A + B' \cos \chi)^2}{A^2 - B'^2} - \frac{2(B' \sin \chi)^2}{(A + B' \cos \chi)^3} \right] \quad (\text{B.29})$$

$$\Omega_H^{2,2} = \frac{\Omega_\epsilon^{0,2}(\nu)}{(A + B' \cos \chi)^2} + \left(\frac{3(B' \cos \chi)^2 + 2B' \cos \chi (A + B' \cos \chi)}{(A + B' \cos \chi)^4} \right) \times \left(\frac{\Omega_\epsilon^{0,1}(\nu)}{2a} + \frac{\log \frac{(A+B' \cos \chi)^2}{A^2 - B'^2}}{a^2} \right) - \frac{4(B' \sin \chi)^2}{a^2 (A + B' \cos \chi)^4} + \frac{B'^2}{a^2 (A^2 - B'^2) (A + B' \cos \chi)^2} \quad (\text{B.30})$$

$$\Omega_H^{1,0} = \frac{1}{2B'} \log \frac{A+B'}{A-B'} \quad (\text{B.31})$$

$$\Omega_H^{2,0} = \frac{1}{A^2 - B'^2} \quad (\text{B.32})$$

$$\Omega_H^{1,-1} = \frac{a}{B'} \left[(B' + A \cos \chi) \Omega_H^{1,0} - \cos \chi \right] \quad (\text{B.33})$$

$$\Omega_H^{2,-1} = \frac{a}{B'} \left[(B' + A \cos \chi) \Omega_H^{2,0} - \cos \chi \Omega_H^{1,0} \right] \quad (\text{B.34})$$

$$\Omega_H^{1,-2} = \frac{a}{B'} \left[(B' + A \cos \chi) \Omega_H^{1,-1} - \cos \chi \Omega_H^{0,-1} \right] \quad (\text{B.35})$$

$$+ \frac{(a \sin \chi)^2}{2B'^2} \left[(B'^2 - A^2) \Omega_H^{1,0} + A \right] \quad (\text{B.36})$$

$$\Omega_H^{2,-2} = \frac{a}{B'} \left[(B' + A \cos \chi) \Omega_H^{2,-1} - \cos \chi \Omega_H^{1,-1} \right] \quad (\text{B.37})$$

$$+ \frac{(a \sin \chi)^2}{2B'^2} \left[(B'^2 - A^2) \Omega_H^{2,0} - 1 + 2A \Omega_H^{1,0} \right] \quad (\text{B.38})$$

$$\Omega_H^{1,-3} = \frac{a}{B'} \left[(B' + A \cos \chi) \Omega_H^{1,-2} - \cos \chi \Omega_H^{0,-2} \right] \quad (\text{B.39})$$

$$+ \frac{3(a \sin \chi)^2}{2B'^2} \left[(B'^2 - A^2) \Omega_H^{1,-1} + A \Omega_H^{0,-1} + B' \left(\frac{a}{3} \right) \cos \chi \right] \quad (\text{B.40})$$

$$\Omega_H^{2,-3} = \frac{a}{B'} \left[(B' + A \cos \chi) \Omega_H^{2,-2} - \cos \chi \Omega_H^{1,-2} \right] \quad (\text{B.41})$$

$$+ \frac{3(a \sin \chi)^2}{2B'^2} \left[(B'^2 - A^2) \Omega_H^{2,-1} + A \Omega_H^{1,-1} + B' \left(\frac{a}{3} \right) \cos \chi \Omega_H^{1,0} \right], \quad (\text{B.42})$$

where $B' = \mp \sqrt{B^2 + C^2}$.

Appendix C

Results of Angular Integration

C.1 Expression for Regular Pieces of $H \rightarrow gggg$ Matrix element

In this section, we give the detailed results for the non-singular parts of complicated $(+ - - -)$ helicity configurations. Recall that the sum over spins of the $H \rightarrow gggg$ amplitude may be written

$$|\overline{M}|^2 = (4\pi \alpha_s)^2 \left(\frac{\alpha_s}{3\pi v} \right)^2 \frac{N^2 (N^2 - 1)}{16 (N^2 - 1)^2} \sum_{\text{hel.}} \left\{ |m(1^{\lambda_1}, 2^{\lambda_2}, 3^{\lambda_3}, 4^{\lambda_4})|^2 + |m(1^{\lambda_1}, 3^{\lambda_2}, 4^{\lambda_3}, 2^{\lambda_4})|^2 + |m(1^{\lambda_1}, 4^{\lambda_2}, 2^{\lambda_3}, 3^{\lambda_4})|^2 \right\}. \quad (\text{C.1})$$

We write the expression as

$$|\overline{M}|^2 = (4\pi \alpha_s)^2 \left(\frac{\alpha_s}{3\pi v} \right)^2 \frac{N^2 (N^2 - 1)}{8 (N^2 - 1)^2} \{m_{++++} + m_{++--} + m_{+---}\}, \quad (\text{C.2})$$

where

$$m_{++++} = |m(1^+, 2^+, 3^+, 4^+)|^2 + |m(1^+, 3^+, 4^+, 2^+)|^2 + |m(1^+, 4^+, 2^+, 3^+)|^2, \quad (\text{C.3})$$

where

$$\begin{aligned}
m_{+++-} = & |m(1^+, 2^+, 3^-, 4^-)|^2 + |m(1^+, 3^+, 4^-, 2^-)|^2 + |m(1^+, 4^+, 2^-, 3^-)|^2 + \\
& |m(1^+, 2^-, 3^+, 4^-)|^2 + |m(1^+, 3^-, 4^+, 2^-)|^2 + |m(1^+, 4^-, 2^+, 3^-)|^2 + \\
& |m(1^+, 2^-, 3^-, 4^+)|^2 + |m(1^+, 3^-, 4^-, 2^+)|^2 + |m(1^+, 4^-, 2^-, 3^+)|^2. \quad (\text{C.4})
\end{aligned}$$

The angular integrals of the preceding expressions are presented in their entirety in chapter 4. The remaining pieces, which we shall refer to as the *odd helicity pieces*, are

$$\begin{aligned}
m_{++++} = & |m(1^+, 2^+, 3^+, 4^-)|^2 + |m(1^+, 3^+, 4^+, 2^-)|^2 + |m(1^+, 4^+, 2^+, 3^-)|^2 + \\
& |m(1^+, 2^+, 3^-, 4^+)|^2 + |m(1^+, 3^+, 4^-, 2^+)|^2 + |m(1^+, 4^+, 2^-, 3^+)|^2 + \\
& |m(1^+, 2^-, 3^+, 4^+)|^2 + |m(1^+, 3^-, 4^+, 2^+)|^2 + |m(1^+, 4^-, 2^+, 3^+)|^2 + \\
& |m(1^+, 2^-, 3^-, 4^-)|^2 + |m(1^+, 3^-, 4^-, 2^-)|^2 + |m(1^+, 4^-, 2^-, 3^-)|^2. \quad (\text{C.5})
\end{aligned}$$

We define the normalized angular integrals of these expressions by

$$\Omega_{++++} = 2 \int d\Omega^{(\epsilon)} m_{++++}. \quad (\text{C.6})$$

$d\Omega^\epsilon$ is the angular measure in $4 - 2\epsilon$ dimensions from appendix B,

$$\int d\Omega^{(\epsilon)} = \frac{1}{2\pi} \int_0^\pi d\theta (\sin(\theta))^{(1-2\epsilon)} \int_0^\pi d\phi (\sin(\phi))^{(-2\epsilon)}. \quad (\text{C.7})$$

Using the various symmetries, as well as the fact that we may freely exchange the partons 3 and 4 (since this does not affect the outcome of the angular integration), we may rewrite this as

$$\Omega_{++++} = 2\Omega(1, 2, 3, 4) + 2\Omega(3, 4, 1, 2) + \Omega(1, 3, 2, 4) + \Omega(3, 2, 4, 1) + (t \leftrightarrow u), \quad (\text{C.8})$$

where

$$\Omega(i, j, k, l) = \int d\Omega^\epsilon, |m(i^-, j^+, k^+, l^+)|^2. \quad (\text{C.9})$$

Finally, we break these into a fairly simple singular term $\Omega_\epsilon(i, j, k, l)$ (given in chapter 4), and a nonsingular piece $\Omega_0(i, j, k, l)$, which contains no ϵ or Q^2 singularities. We have chosen to include a number of (universal) nonsingular factors in the expressions for $\Omega_\epsilon(i, j, k, l)$.

C.1.1 $m(1^-, 2^+, 3^+, 4^+)$

First, let us define

$$\eta = \sqrt{1 - \frac{4 s M^2}{S_H^2}}. \quad (\text{C.10})$$

Then we may write the integral over the angular phase space as

$$\Omega_0(1, 2, 3, 4) = F^{(0)}(s, t, u) + F^{(1)}(s, t, u), \quad (\text{C.11})$$

where

$$\begin{aligned} F^{(0)}(s, t, u) = & -\frac{8 M^4 Q^2 p_\perp^2}{u^4} - \frac{8 M^4 S_u}{s u^2} + \frac{4 M^2 S_H}{s u} + \frac{M^2 (-4 M^2 s + S_H^2)}{s u^2} + \\ & \frac{\log\left(\frac{(Q^2 s + (Q^2 - M^2) S_u)^2}{M^2 s S_u^2}\right) (M^8 + (s + S_u)^4)}{s u (s + S_u) S_H} + \\ & \frac{t^3 \log\left(\frac{(Q^2 s + (Q^2 - M^2) S_t)^2}{M^2 s S_t^2}\right)}{s (s + S_t) S_H} + \frac{t^3 \log\left(\frac{s t^2}{M^2 S_t^2}\right) (Q^2 u + s S_H + u S_H)}{Q^2 s u (s + S_u) S_H} + \\ & \log\left(\frac{s u^2}{M^2 S_u^2}\right) \left(\frac{M^8 Q^8 + t^4 u^4 + s^4 p_\perp^8}{Q^2 s^2 u^4 p_\perp^2} - \frac{2 M^4 t^3}{s u p_\perp^2 (s + S_u) (s + S_t)} \right. \\ & \quad \left. - \frac{M^8 + (s + S_u)^4}{s u (s + S_u) S_H} - \frac{t^3}{s (s + S_t) S_H} \right. \\ & \quad \left. - \frac{t^3 (Q^2 u + s S_H + u S_H)}{Q^2 s u (s + S_u) S_H} \right), \quad (\text{C.12}) \end{aligned}$$

and

$$\begin{aligned}
F^{(1)}(s, t, u) = & \frac{M^2 \left(7s + M^2 \left(-1 + \frac{2s}{S_H} \right) \right)}{s^2} + \frac{\log\left(\frac{1+\eta}{1-\eta}\right) C_\eta}{\eta} + \frac{2M^4 \Gamma_{(-2,2)}(u, t)}{s^2} \\
& - \frac{2M^4 (s + S_u) \left(\Gamma_{(-1,1)}(u, t) - \Gamma_{(-1,1)}(t, u) \right)}{s^2 S_H} \\
& + \frac{2M^4 \left(\Gamma_{(-2,1)}(u, t) + \Gamma_{(-2,1)}(t, u) \right)}{s^2 S_H} + \frac{6M^4 \Gamma_{(-1,2)}(u, t)}{s}. \quad (\text{C.13})
\end{aligned}$$

The angular form factors in $F^{(1)}(s, t, u)$ are

$$\begin{aligned}
\Gamma_{(-2,2)}(u, t) = & \frac{\log\left(\frac{1+\eta}{1-\eta}\right)}{2S_H \eta} \times \left(\frac{4s (S_u^2 + s p_t^2 - s Q^2) (2M^2 Q^2 - u(t+u))}{(S_H^2 - 4s M^2)^2} \right. \\
& \left. + \frac{4S_H s^2 Q^2 p_t^2}{(S_H^2 - 4s M^2)^2} \right) + \frac{(S_u^2 + s p_t^2 - s Q^2)^2 - 4s^2 Q^2 p_t^2}{(S_H^2 - 4s M^2)^2} + \\
& \frac{s (2M^2 Q^2 - u(t+u))^2}{(S_H^2 - 4s M^2)^2 M^2} \quad (\text{C.14})
\end{aligned}$$

$$\Gamma_{(-1,2)}(u, t) = \frac{(2M^2 Q^2 - u(t+u))}{(S_H^2 - 4s M^2) M^2} + \left(\frac{S_u^2 + s p_t^2 - s Q^2}{S_H^2 - 4s M^2} \right) \frac{\log\left(\frac{1+\eta}{1-\eta}\right)}{S_H \eta} \quad (\text{C.15})$$

$$\begin{aligned}
\Gamma_{(-2,1)}(u, t) = & \frac{\log\left(\frac{1+\eta}{1-\eta}\right)}{S_H \eta} \times \left(\frac{s^2 (2M^2 Q^2 - u(t+u))^2}{(S_H^2 - 4s M^2)^2} - \frac{2s^3 p_t^2 Q^2 M^2}{(-4M^2 s + S_H^2)^2} \right) \\
& + \frac{S_u^2 S_H - 2s u S_u}{(-4M^2 s + S_H^2)} + S_H \frac{2s^2 Q^2 p_t^2 - (S_u S_H - 2s u)^2}{2 (S_H^2 - 4s M^2)^2}, \quad (\text{C.16})
\end{aligned}$$

and

$$\Gamma_{(-1,1)}(u, t) = \frac{s (2M^2 Q^2 - u(t+u)) \log\left(\frac{1+\eta}{1-\eta}\right)}{S_H (-4M^2 s + S_H^2) \eta} + \frac{-2s u + S_u S_H}{-4M^2 s + S_H^2}. \quad (\text{C.17})$$

Finally, the coefficient C_η is in this case

$$C_\eta = \frac{-2t^3(t+u)^2}{Q^2 s u S_H^2} - \frac{2}{Q^2 s u S_H^2} \left[-2M^2 t^3 (2Q^2 + t + u) + M^6 (-4Q^4 + 6Q^2 u) + 2M^4 Q^2 (4t^2 - 2tu - u^2 + Q^2(t+u)) \right]. \quad (\text{C.18})$$

Note the existence of a “naive” Q^2 pole $\Omega_0(1, 2, 3, 4)$. It is superficial, since the limit as $Q^2 \rightarrow 0$ yields a finite result.

C.1.2 $m(3^-, 4^+, 1^+, 2^+)$

Again, we write the integral over the angular phase space as a sum of logs,

$$\Omega_0(3, 4, 1, 2) = C_0 + C_1 \log \frac{st^2}{M^2 S_t^2} + C_\eta \frac{\log[\frac{1+\eta}{1-\eta}]}{\eta} + \frac{(M^2 - Q^2 + s)^3}{s(M^2 - t)u} \log \frac{(Q^2 s + (-M^2 + Q^2) S_u)^2}{M^2 s S_u^2}. \quad (\text{C.19})$$

The coefficients C_i in this expression are

$$\begin{aligned} C_0 = & \frac{63 Q^2 + 170 s}{3 s} + \frac{8 Q^4 s^2}{t^4} + \frac{16 Q^4 s}{t^3} + \frac{27 Q^4 - 12 Q^2 s + 13 s^2}{3 t^2} + \\ & \frac{3 Q^6 - 18 Q^4 s + 52 s^3}{3 Q^2 s t} + \frac{s^2}{3 u^2} + \frac{4 s^2}{3 Q^2 u} - \frac{11 (Q^6 - 3 Q^4 s + 3 Q^2 s^2 - s^3)}{3 Q^2 t u} + \\ & \frac{11 Q^4 s^2}{3 S_t^4} - \frac{38 Q^2 s^2}{3 S_t^3} - \frac{2 Q^2 s^3}{3 u S_t^3} + \frac{-9 Q^2 s + 74 s^2}{3 S_t^2} + \frac{-9 Q^2 s^2 + 5 s^3}{3 u S_t^2} + \\ & \frac{22 Q^6 + 66 Q^4 s + 129 Q^2 s^2 - 52 s^3}{3 Q^2 s S_t} + \frac{-18 Q^4 s + 27 Q^2 s^2 - 11 s^3}{3 Q^2 u S_t} + \\ & \frac{23 S_t}{s} + \frac{2 s S_t}{3 u^2} + \frac{2 s S_t}{Q^2 u} + \frac{S_t^2}{3 u^2} + \frac{2 S_t^2}{3 Q^2 u} + \frac{11 Q^4 s^2}{3 S_u^4} + \frac{34 Q^2 s^2}{3 S_u^3} - \frac{2 Q^2 s^3}{3 t S_u^3} + \\ & \frac{2 Q^2 s S_t}{S_u^3} + \frac{s (3 Q^2 + 26 s)}{3 S_u^2} + \frac{3 Q^2 s^2 - 7 s^3}{3 t S_u^2} + \frac{3 s S_t}{S_u^2} + \frac{S_t^2}{2 S_u^2} + \\ & \frac{22 Q^6 + 66 Q^4 s + 93 Q^2 s^2 - 4 s^3}{3 Q^2 s S_u} + \frac{-6 Q^4 s + 15 Q^2 s^2 - 11 s^3}{3 Q^2 t S_u} + \\ & \frac{11 (Q^8 + 4 Q^6 s + 6 Q^4 s^2 + 4 Q^2 s^3 + 2 s^4)}{6 Q^2 s S_t S_u} + \frac{(11 Q^4 + 26 Q^2 s - 2 s^2) S_t}{Q^2 s S_u} + \end{aligned}$$

$$\begin{aligned}
& \frac{2(11Q^2 - s)S_t^2}{3Q^2 s S_u} + \frac{25S_u}{s} + \frac{24Q^4 s S_u}{t^4} - \frac{10Q^2 s S_u}{S_t^3} + \frac{31 s S_u}{S_t^2} + \frac{24Q^4 S_u^2}{t^4} + \\
& \frac{17S_u^2}{2S_t^2} + \frac{8Q^4 S_u^3}{s t^4} - \frac{8Q^2 S_u^3}{s t^3} + \frac{S_u^3}{s t^2} + \frac{8(4Q^4 S_u - Q^2 s S_u)}{t^3} + \\
& \frac{11Q^4 S_u + 34Q^2 s S_u - 26s^2 S_u}{Q^2 s S_t} - \frac{2(6Q^4 S_u - Q^2 s S_u - 13s^2 S_u)}{Q^2 s t} + \\
& \frac{27Q^4 S_u - 66Q^2 s S_u + 26s^2 S_u}{3s t^2} + \frac{2(11Q^2 S_u^2 - 13s S_u^2)}{3Q^2 s S_t} \\
& - \frac{2(27Q^2 S_u^2 - 8s S_u^2)}{3s t^2} + \frac{9Q^2 S_u^2 + 26s S_u^2}{3Q^2 s t} + \frac{16(Q^4 S_u^2 - Q^2 s S_u^2)}{s t^3},
\end{aligned} \tag{C.20}$$

and

$$C_1 = \frac{N_1}{Q^2 s t^4 u (M^2 - t)}, \tag{C.21}$$

where the numerator N_1 is

$$\begin{aligned}
N_1 = & \left((M^2 - Q^2)^4 + s^4 \right) S_t^3 (s + S_u) - Q^{10} \left(6s^3 - S_t (-2s^2 + 2s S_t + S_t^2) \right. \\
& \left. + (4s + S_t)^2 S_u + 3(4s + S_t) S_u^2 + 3S_u^3 \right) \\
& + Q^2 S_t^2 \left(6s^5 + 2s^4 (7S_t + 3S_u) \right. \\
& \left. + s^3 (34S_t^2 + 34S_t S_u - 6S_u^2) \right. \\
& \left. + s (S_t + S_u)^2 (11S_t^2 + 22S_t S_u - 5S_u^2) \right. \\
& \left. + 10s^2 (S_t + S_u) (3S_t^2 + 4S_t S_u - S_u^2) \right. \\
& \left. + (S_t + S_u)^3 (S_t^2 + 5S_t S_u - S_u^2) \right) \\
& + Q^6 \left(2s^5 + 6S_t^5 + S_t^4 (31s + 13S_u) \right. \\
& \left. + S_t^3 (40s^2 + 20s S_u - 2S_u^2) \right. \\
& \left. - S_u (2s + S_u) (4s^3 + 14s^2 S_u + 11s S_u^2 + 3S_u^3) \right. \\
& \left. - 2S_t (s + S_u) (7s^3 + 27s^2 S_u + 23s S_u^2 + 6S_u^3) \right. \\
& \left. + S_t^2 (16s^3 - 2S_u (11s^2 + 25s S_u + 9S_u^2)) \right)
\end{aligned}$$

$$\begin{aligned}
& +Q^4 S_t \left(4 S_t^5 + S_t^4 (29 s + 17 S_u) + 2 S_t^2 (2 s + S_u) \left(12 s^2 + 9 s S_u - S_u^2 \right) \right. \\
& \quad + 2 S_t^3 \left(29 s^2 + 32 s S_u + 9 S_u^2 \right) \\
& \quad + 2 S_t (s + S_u) \left(3 s^3 - 5 S_u (s + S_u) (2 s + S_u) \right) + \\
& \quad \left. (s + S_u) \left(6 s^4 - S_u \left(12 s^3 + 28 s^2 S_u + 16 s S_u^2 + 3 S_u^3 \right) \right) \right) \\
& - 2 Q^8 \left(-2 S_t^4 - S_t^3 (7 s + S_u) + S_t^2 \left(-3 s^2 + 8 s S_u + 5 S_u^2 \right) + \right. \\
& \quad S_t (5 s + 3 S_u) \left(s^2 + 2 S_u (2 s + S_u) \right) \\
& \quad \left. + (s + S_u) \left(6 s^3 + S_u \left(16 s^2 + 3 S_u (4 s + S_u) \right) \right) \right). \tag{C.22}
\end{aligned}$$

Finally, The coefficient C_η in equation (C.19) is

$$\begin{aligned}
C_\eta = & \frac{10 (Q^2 - 2 s) s}{t u} + \frac{\left((M^2 - Q^2)^4 + s^4 \right) \left(1 - \frac{2s}{S_h} \right)}{Q^2 s t u} + \\
& \frac{4 s (Q^4 - 3 Q^2 s + 3 s^2)}{t u S_h} + \frac{2 S_h \left(-4 (Q^2 - 3 s) s - 6 s S_h + S_h^2 \right)}{s t u}. \tag{C.23}
\end{aligned}$$

C.1.3 $m(1^-, 3^+, 2^+, 4^+)$

Recalling $S_H = M^2 + s - Q^2$, we write the result of the integration over the angular phase space as

$$\begin{aligned}
\Omega_0(1, 3, 2, 4) = & \frac{2 M^2 t^2}{s u^2} - \frac{16 M^4 Q^2 p_t^2}{u^4} + \frac{4 M^4 \log \left(\frac{1+\eta}{1-\eta} \right)}{S_H^2 \eta} \\
& + \log \left(\frac{s u^2}{M^2 S_u^2} \right) C_1 + \log \left(\frac{s t^2}{M^2 S_t^2} \right) C_2 \\
& + \frac{2 t^3}{(Q^2 - t) (M^2 - u) S_H} \log \left(\frac{(s Q^2 - (M^2 - Q^2) S_t)^2}{S_t^2 M^2 s} \right) \\
& + \frac{2 (M^8 + (M^2 - t)^4)}{(M^2 - t) (Q^2 - u) u S_H} \log \left(\frac{(s Q^2 - (M^2 - Q^2) S_u)^2}{S_u^2 M^2 s} \right). \tag{C.24}
\end{aligned}$$

The coefficients are

$$\begin{aligned}
C_1 = & \frac{1}{S_H s (M^2 - u) u^4 S_u} \times \left[-2 (M^2 - s) t^3 u^4 + 2 M^2 t^3 u^3 (2 Q^2 + t + 2 u) \right. \\
& + 4 M^{10} (2 Q^6 - 2 Q^4 u + 2 Q^2 u^2 - u^3) \\
& - 4 M^8 (Q^4 (t - 5 u) u + Q^6 (t + 3 u) \\
& \quad \left. - u^3 (t + 3 u) + Q^2 u^2 (t + 6 u)) \right. \\
& - 4 M^4 u^2 (Q^4 (t^2 - u^2) + \\
& \quad \left. Q^2 (t + 2 u) (2 t^2 + u^2) - u^2 (2 t^2 + t u + u^2)) \right. \\
& + 4 M^6 u (Q^6 (t + u) + Q^4 (t^2 + t u - 4 u^2) \\
& \quad \left. + 2 Q^2 u (2 t^2 + t u + 3 u^2) - u^2 (2 t^2 + 2 t u + 3 u^2)) \right] \quad (C.25)
\end{aligned}$$

and

$$C_2 = \frac{2 t^3 (M^2 (2 Q^2 - 2 t - u) + t (-Q^2 + t + u))}{s (M^2 - t) (Q^2 - t) (2 M^2 - t - u) u}. \quad (C.26)$$

C.1.4 $m(3^-, 2^+, 4^+, 1^+)$

The last independent helicity amplitude is $m(3^-, 2^+, 4^+, 1^+)$. We write the finite remainder of the the azimuthal integration as

$$\begin{aligned}
\Omega_0(3, 2, 4, 1) = & \frac{1}{2} C_0 + C_1 \log \frac{s u^2}{M^2 S_u^2} \\
& + C_2 \log \left(\frac{(Q^2 s - (M^2 - Q^2) S_u)^2}{M^2 s S_u^2} \right) + (u \leftrightarrow t), \quad (C.27)
\end{aligned}$$

where

$$C_1 = - \left(\frac{(M^2 - t)^3}{s t (-M^2 + u)} \right) - \frac{(2 t + u) (t^2 + t u + u^2)}{s t u} - \frac{2 M^6 (Q^4 t + (7 t - u) u^2)}{s t u^4}$$

$$\begin{aligned}
& + \frac{M^2 (-4t^3 + 3tu^2 + 3u^3)}{stu^2} + \frac{M^4 (2Q^2t(t+u) + u(14t^2 + 4tu - 3u^2))}{stu^3} \\
& - \frac{(-2M^2 + t + u)^3}{suS_u}, \tag{C.28}
\end{aligned}$$

$$C_2 = - \left(\frac{S_H^3}{(M^2 - t)uS_u} \right), \tag{C.29}$$

and finally, the coefficient C_0 , which is symmetric under the interchange $u \leftrightarrow t$:

$$\begin{aligned}
C_0 = & 5 + \frac{8M^4 - 4M^2t}{t^2} - \frac{2M^2Q^2(4M^4 - M^2t - 3t^2)}{st^3} - \frac{8M^4Q^2t}{su^3} - \frac{7M^4Q^2}{su^2} \\
& + \frac{M^2(M^4(t-u)^2 + t^2(t+u)(t+3u) + M^2t(-t^2 + tu + 4u^2))}{st^2u^2} \\
& + \frac{M^2Q^4(-8M^2tu^4 + t^2u^3(-4t+u) + 8M^4(t^4 + u^4))}{st^4u^4} + \frac{6M^4t^2}{S_t^4} \\
& - \frac{2(3M^4Q^2 - 2M^2Q^2t)}{stu} - \frac{M^2Q^8u}{t^2S_t^4} + \frac{2M^2Q^6u}{tS_t^4} \\
& + \frac{-10M^2Q^4u - 3M^2t^2u + Q^4u^2 + 4Q^2tu^2 + t^2u^2}{S_t^4} \\
& - \frac{6M^2t(2M^2 + t)}{S_t^3} + \frac{2t(Q^2 + 2t)u}{S_t^3} + \frac{10M^4 + 4M^2t + t^2}{S_t^2} \\
& + \frac{2M^4t(M^2 - u)}{suS_t^2} - \frac{4M^2(M^2 + t)}{tS_t} - \frac{2M^4t}{suS_t} + \frac{M^2(-8M^2 + t)S_t}{t^3} \\
& + \frac{6Q^4(M^2 - t)^2}{S_u^4} - \frac{6Q^2(M^2 - t)(Q^2 + t)}{S_u^3} + \frac{4M^4 - 8M^2Q^2 + Q^4}{S_u^2} \\
& + \frac{2M^4Q^2}{tS_u^2} - \frac{2(2M^2 - 5Q^2)t}{S_u^2} + \frac{t^2}{S_u^2} \\
& + \frac{2(M^2t(t-3u) + t(Q^2 + 2t)u + M^4(-2t + u))}{tuS_u}. \tag{C.30}
\end{aligned}$$

Appendix D

Formulas for Cross Sections

Here we provide standard formulas for the evaluation of $2 \rightarrow 2$ and $2 \rightarrow 3$ processes for 2 partons in the initial state, 1 massive particle in the final state, and 1 or 2 massless particles in the final state. We also list convenient variable transformations for the convolutions, which will allow us to directly evaluate the “+” functions.

D.1 Expression for a $2 \rightarrow 2$ Cross Section

The $2 \rightarrow 2$ contribution to the p_\perp may be written

$$\frac{d\sigma_{LO}}{dp_\perp dy_H} = \frac{1}{S} \int_0^1 d\xi_a f(\xi_a) \int_0^1 d\xi_b f(\xi_b) s \frac{d\sigma}{dt} \delta(Q^2), \quad (\text{D.1})$$

where

$$Q^2 = s + t + u - M^2 \quad (\text{D.2})$$

and

$$\frac{d\sigma}{dt} = \frac{1}{4\pi s^2} |\bar{M}|^2, \quad (\text{D.3})$$

where we have suppressed the parton indices for clarity.

The expression for the NLO cross section may be defined likewise:

$$\frac{d\sigma_{\text{NLO}}}{dp_{\perp} dy_H} = \frac{1}{S} \int_0^1 d\xi_a \int_0^1 d\xi_b s \frac{d\sigma_{\Omega}}{dt du} \theta(Q^2), \quad (\text{D.4})$$

where

$$\frac{d\sigma_{\Omega}}{dt du} = \frac{1}{4\pi s^2} \int \frac{d\Omega}{2\pi} |\bar{M}|^2. \quad (\text{D.5})$$

D.2 Evaluating the Convolutions

First, we must evaluate the expression

$$\int_0^1 d\xi_a \int_0^1 d\xi_b \theta(Q^2) = \int_0^1 d\xi_a \int_0^1 d\xi_b \theta(\xi_a \xi_b - x_T \xi_a - x_U \xi_b + \tau), \quad (\text{D.6})$$

where, as before, $x_T = \frac{m_H^2 - T}{S}$, $x_U = \frac{m_H^2 - U}{S}$, and $\tau = \frac{m_H^2}{S}$. Evaluating these in the hadron-hadron COM frame, we find that these expressions become

$$\begin{aligned} x_T &= \sqrt{\frac{m_{\perp}^2}{S}} e^{-y_H}, \\ x_U &= \sqrt{\frac{m_{\perp}^2}{S}} e^{+y_H}. \end{aligned} \quad (\text{D.7})$$

Substituting expressions (D.7) for Q^2 , we find

$$\xi_a \xi_b - x_T \xi_a - x_U \xi_b + \tau = \left(\xi_a e^{-y_H} - \frac{m_{\perp}}{\sqrt{S}}\right) \left(\xi_b e^{+y_H} - \frac{m_{\perp}}{\sqrt{S}}\right) - \frac{p_{\perp}^2}{S}, \quad (\text{D.8})$$

which has the implication that

$$\left(\xi_a e^{+y_H} - \frac{m_{\perp}}{\sqrt{S}}\right) \left(\xi_b e^{-y_H} - \frac{m_{\perp}}{\sqrt{S}}\right) > \frac{p_{\perp}^2}{S}. \quad (\text{D.9})$$

We may break this up into four different phase space regions, each defined by $(\xi_{a,b}e^{\pm y_H} - m_{\perp}/\sqrt{S})$ greater than or less than p_{\perp}/\sqrt{S} . One case of the four is automatically forbidden because it implies $p_{\perp} < 0$. After evaluating the θ -function for each term, we may recombine two of the regions into one region, leaving us with

$$\int_0^1 d\xi_a \int_0^1 d\xi_b \theta(Q^2) = \int_{x_+}^1 d\xi_a \int_{\xi_b(\xi_a)}^1 d\xi_b + \int_{x_-}^1 d\xi_b \int_{\xi_a(\xi_b)}^{x_+} d\xi_a. \quad (\text{D.10})$$

The lower limits of the internal integrals in this expression are solutions to the equation $Q^2 = 0$ for each of the variables. Explicitly, these are

$$\begin{aligned} \xi_b(\xi_a) &= \frac{(x_T - \tau)\xi_a - \tau(1 - \xi_a)}{x_U - \xi_a}, \\ \xi_a(\xi_b) &= \frac{(x_U - \tau)\xi_b - \tau(1 - \xi_b)}{x_T - \xi_b}, \end{aligned} \quad (\text{D.11})$$

whereas the outer limits x_{\pm} are

$$x_{\pm} = \exp(\pm y_H) \left(\frac{m_{\perp} + p_{\perp}}{\sqrt{S}} \right). \quad (\text{D.12})$$

It is quite trivial to convert these terms back into the Q^2 variable. If this is done, the expression for the phase space in reference [49, 50] is recovered identically:

$$\int_0^1 d\xi_a \int_0^1 d\xi_b \theta(Q^2) \rightarrow \int_{x_+}^1 \frac{d\xi_a}{\xi_a - x_U} \int_0^{A_1} d\left(\frac{Q^2}{S}\right) + \int_{x_-}^1 \frac{d\xi_b}{\xi_b - x_T} \int_0^{A_2} d\left(\frac{Q^2}{S}\right). \quad (\text{D.13})$$

In this formula, the limits of integration A_i are

$$A_1 = \xi_a(1 - x_T) - x_U + \tau, \quad (\text{D.14})$$

$$A_2 = x_+ (\xi_b - x_T) - x_U \xi_b + \tau. \quad (\text{D.15})$$

Note that it is quite trivial to evaluate the $\delta(Q^2)$ of the $2 \rightarrow 2$ phase space using this

form of the convolution.

D.2.1 Evaluating Terms With “+” Functions

In the regularization of the soft singularities, terms of the form $f(z_{t,u})_+$ arise, and it is beneficial to change variables from $d(Q^2)$ to $dz_{t,u}$ in order to easily evaluate these “+” functions. Recall the definition of $z_{t,u}$:

$$z_{t,u} = \frac{-t, u}{-t, u + Q^2}. \quad (\text{D.16})$$

Now, consider z_t (a completely analogous analysis will follow for z_u). It is beneficial to first convert to the phase space (D.13) as an intermediate step. We wish to evaluate the Jacobian for the change of variables. This is summarily expressed as

$$\int_0^A d(Q^2) \rightarrow \int_{z_t(A)}^1 \frac{dz_t (-t)^2}{z_t^2 - t_0} \rightarrow \int_{z_u(A)}^1 \frac{dz_u (-u)^2}{z_u^2 - u_0}, \quad (\text{D.17})$$

where $t_0 = t|_{Q^2=0}$ and $u_0 = u|_{Q^2=0}$. Thus

$$\begin{aligned} & \int_0^1 d\xi_a \int_0^1 d\xi_b \theta(Q^2) \rightarrow \\ & \frac{1}{S} \int_{x_+}^1 \frac{d\xi_a}{\xi_a - x_U} \int_{z_t(A_1)}^1 \frac{dz_t (-t)^2}{z_t^2 - t_0} + \frac{1}{S} \int_{x_-}^1 \frac{d\xi_b}{\xi_b - x_T} \int_{z_t(A_2)}^1 \frac{dz_t (-t)^2}{z_t^2 - t_0} \end{aligned} \quad (\text{D.18})$$

The evaluation of “+” functions in this basis is quite straightforward. Converting the phase space into z_u proceeds along similar lines.

References

- [1] P. D. Group, “Review of Particle Physics,” *The European Physical Journal C* **3** (1998).
- [2] C. N. Yang and R. L. Mills, “Conservation of isotopic spin and isotopic gauge invariance,” *Phys. Rev.* **96** (1954) 191.
- [3] M. E. Peskin and D. V. Schroeder, “An Introduction to quantum field theory,” Reading, USA: Addison-Wesley (1995) 842 p.
- [4] L. D. Faddeev and V. N. Popov, “Feynman Diagrams for the Yang-Mills Field,” *Phys. Lett.* **B25** (1967) 29.
- [5] M. Kobayashi and T. Maskawa, “CP violation in the renormalizable theory of weak interaction,” *Prog. Theor. Phys.* **49** (1973) 652.
- [6] T. Tait, *Signals for the Electroweak Symmetry Breaking Associated with the Top Quark*. PhD thesis, Michigan State University, 1999.
- [7] **Super-Kamiokande** Collaboration, Y. Fukuda *et al.*, “Evidence for oscillation of atmospheric neutrinos,” *Phys. Rev. Lett.* **81** (1998) 1562–1567, hep-ex/9807003.
- [8] **D0** Collaboration, S. Abachi *et al.*, “Observation of the top quark,” *Phys. Rev. Lett.* **74** (1995) 2632–2637, hep-ex/9503003.

- [9] **CDF** Collaboration, F. Abe *et al.*, “Evidence for top quark production in anti-p p collisions at $s^{*}(1/2) = 1.8\text{-TeV}$,” *Phys. Rev. Lett.* **73** (1994) 225–231, hep-ex/9405005.
- [10] J. F. Gunion, H. E. Haber, G. L. Kane, and S. Dawson, “The Higgs Hunter’S Guide,” . SCIPP-89/13.
- [11] K. G. Wilson, “Renormalization group and critical phenomena. 2. Phase space cell analysis of critical behavior,” *Phys. Rev.* **B4** (1971) 3184–3205.
- [12] **LEP Higgs Working Group for Higgs boson searches** Collaboration, “Search for the standard model Higgs boson at LEP,” hep-ex/0107029.
- [13] A. Djouadi, J. Kalinowski, and M. Spira, “HDECAY: A program for Higgs boson decays in the standard model and its supersymmetric extension,” *Comput. Phys. Commun.* **108** (1998) 56, hep-ph/9704448.
- [14] M. Spira, “QCD effects in Higgs physics,” *Fortsch. Phys.* **46** (1998) 203, hep-ph/9705337.
- [15] C. Balazs and C. P. Yuan, “Higgs boson production at the LHC with soft gluon effects,” *Phys. Lett.* **B478** (2000) 192–198, hep-ph/0001103.
- [16] M. Carena *et al.*, “Report of the Tevatron Higgs working group,” hep-ph/0010338.
- [17] G. ’t Hooft and M. Veltman, “Combinatorics of gauge fields,” *Nucl. Phys.* **B50** (1972) 318–353.
- [18] J. Amundson, C. Schmidt, W.-K. Tung, and X. Wang, “Charm production in deep inelastic scattering from threshold to high Q^{*2} ,” *JHEP* **10** (2000) 031, hep-ph/0005221.

- [19] M. Mangano and S. Parke, “Multi-Parton Amplitudes in Gauge Theories,” *Phys.Rep.* **200** (1991) 301–367.
- [20] Z. Bern, L. Dixon, D. Kosower, and A. Signer, “Multiparton Loop Amplitudes and Next-to-Leading Order Jet Cross-Sections,” in *International Symposium on QCD Corrections and New Physics*. Hiroshima Japan, Oct., 1997.
- [21] R. Kleiss and W. J. Stirling, “Spinor Techniques for Calculating p anti- $p \rightarrow W^{+-} / Z^0 + \text{Jets}$,” *Nucl. Phys.* **B262** (1985) 235–262.
- [22] Z. Xu, D.-H. Zhang, and L. Chang, “Helicity Amplitudes for Multiple Bremsstrahlung in Massless Nonabelian Gauge Theories,” *Nucl. Phys.* **B291** (1987) 392.
- [23] Z. Kunszt, S. Moretti, and W. J. Stirling, “Higgs production at the LHC: An update on cross sections and branching ratios,” *Z. Phys.* **C74** (1997) 479–491, [hep-ph/9611397](#).
- [24] S. Dawson, “The standard model intermediate mass Higgs boson,” [hep-ph/9703387](#).
- [25] F. Wilczek, “Decays of Heavy Vector Mesons into Higgs Particles,” *Phys. Rev. Lett.* **39** (1977) 1304.
- [26] S. Dawson, “Radiative corrections to Higgs boson production,” *Nucl. Phys.* **B359** (1991) 283–300.
- [27] M. Spira, A. Djouadi, D. Graudenz, and P. M. Zerwas, “Higgs boson production at the LHC,” *Nucl. Phys.* **B453** (1995) 17–82, [hep-ph/9504378](#).
- [28] D. Graudenz, M. Spira, and P. M. Zerwas, “QCD corrections to Higgs boson production at proton-proton colliders,” *Phys. Rev. Lett.* **70** (1993) 1372–1375.

- [29] M. A. Shifman, A. I. Vainshtein, M. B. Voloshin, and V. I. Zakharov, “Low-Energy Theorems for Higgs Boson Couplings To Photons,” *Sov. J. Nucl. Phys.* **30** (1979) 711–716.
- [30] A. Djouadi, M. Spira, and P. M. Zerwas, “Production of Higgs bosons in proton colliders: QCD corrections,” *Phys. Lett.* **B264** (1991) 440–446.
- [31] R. V. Harlander and W. B. Kilgore, “Soft and virtual corrections to $p p$ to $H + X$ at NNLO,” *Phys. Rev.* **D64** (2001) 013015, [hep-ph/0102241](#).
- [32] R. V. Harlander, “Virtual corrections to $g g$ to H to two loops in the heavy top limit,” *Phys. Lett.* **B492** (2000) 74–80, [hep-ph/0007289](#).
- [33] R. K. Ellis, I. Hinchliffe, M. Soldate, and J. J. van der Bij, “Higgs Decay to $\tau^+ \tau^-$: A Possible Signature of Intermediate Mass Higgs Bosons at the SSC,” *Nucl. Phys.* **B297** (1988) 221.
- [34] **CTEQ** Collaboration, H. L. Lai *et al.*, “Global QCD analysis of parton structure of the nucleon: CTEQ5 parton distributions,” *Eur. Phys. J.* **C12** (2000) 375, [hep-ph/9903282](#).
- [35] S. Catani and M. H. Seymour, “A general algorithm for calculating jet cross sections in NLO QCD,” *Nucl. Phys.* **B485** (1997) 291–419, [hep-ph/9605323](#).
- [36] D. de Florian, M. Grazzini, and Z. Kunszt, “Higgs production with large transverse momentum in hadronic collisions at next-to-leading order,” *Phys. Rev. Lett.* **82** (1999) 5209–5212, [hep-ph/9902483](#).
- [37] D. de Florian and M. Grazzini, “Next-to-next-to-leading logarithmic corrections at small transverse momentum in hadronic collisions,” *Phys. Rev. Lett.* **85** (2000) 4678–4681, [hep-ph/0008152](#).

- [38] R. P. Kauffman, “Higher order corrections to Higgs boson $p(T)$,” *Phys. Rev.* **D45** (1992) 1512–1517.
- [39] R. P. Kauffman, “Higgs boson $p(T)$ in gluon fusion,” *Phys. Rev.* **D44** (1991) 1415–1425.
- [40] C. P. Yuan, “Kinematics of the Higgs boson at hadron colliders: NLO QCD gluon resummation,” *Phys. Lett.* **B283** (1992) 395–402.
- [41] I. Hinchliffe and S. F. Novaes, “On the Mean Transverse Momentum of Higgs Bosons at the SSC,” *Phys. Rev.* **D38** (1988) 3475–3480.
- [42] C. Schmidt, “ $H \rightarrow ggg(gq\bar{q})$ at two loops in the large- M_t limit,” *Phys. Lett.* **B413** (1997) 391–395.
- [43] R. P. Kauffman, S. V. Desai, and D. Risal, “Production of a Higgs boson plus two jets in hadronic collisions,” *Phys. Rev.* **D55** (1997) 4005–4015, hep-ph/9610541.
- [44] S. T. W. Press, B. Flannery and W. Vetterling, *Numerical Recipes in C*. Cambridge University Press, 1988.
- [45] J. C. Collins and D. E. Soper, “Back to Back Jets in QCD: Comparison With Experiment,” *Phys. Rev. Lett.* **48** (1982) 655.
- [46] J. C. Collins, D. E. Soper, and G. Sterman, “Transverse Momentum Distribution In Drell-Yan Pair and W And Z Boson Production,” *Nucl. Phys.* **B250** (1985) 199.
- [47] S. Dawson and R. P. Kauffman, “Higgs boson plus multi - jet rates at the SSC,” *Phys. Rev. Lett.* **68** (1992) 2273.

- [48] W. L. van Neerven, “Dimensional Regularization of Mass and Infrared Singularities in Two Loop On-Shell Vertex Functions,” *Nucl. Phys.* **B268** (1986) 453.
- [49] C. Davies and W. Stirling, “Non-Leading Corrections to the Drell-Yan Cross Section at Small Transverse Momentum,” *Nuc.Phys.* **B244** (1994) 337–348.
- [50] R. K. Ellis, G. Martinelli, and R. Petronzio, “Lepton Pair Production at Large Transverse Momentum in Second Order QCD,” *Nucl. Phys.* **B211** (1983) 106.